秋田県立大学大学院博士学位論文

Development of Poly(N-phenylglycine)-Based Adsorbent for Precious Metals Recovery and Study on Adsorption Mechanism

（ポリ-N-フェニルグリシン吸着剤の開発及び吸着メカニズムと貴金属のリサイクルに関する研究）

Tingting Wu

呉 婷婷

2023 年 3 月

Abstract

Today's global society is economically and socially dependent on minerals and metals. Terrestrial mineral deposits are by definition ‘non-renewable’ over human timescales, and their stocks are thus finite. Due to the large-quantity mining and consumption of metal resources, the decreasing grade of metal resources in the earth's crust greatly increases the mining difficulty and cost. Precious metals, such as gold and silver, are rare with high economic value, and also widely used in many fields. The imbalance between metal supply and demand is a major concern worldwide. At the same time, the increasing waste generated by electrical and electronic equipment has drawn more and more attention. The sustainable utilization of metal resources urgently requires the metal recovery from the urban mine—e-waste.

The main methods of metal recovery start with a physical pretreatment, followed by pyrometallurgy, hydrometallurgy. For precious metals, hydrometallurgy has advantages of less release of hazardous substances, more suitability for the treatment of low-grade raw material. In the final step of hydrometallurgy, an appropriate method is essential for the recovery of precious metals from leaching solutions.

Great effort has been devoted to the recycling of precious metals from leaching liquid, and many methods have been developed. Among them, adsorption method offers advantages, because they are simple in process without secondary pollutants. Conventional adsorbents, such as activated carbons, shows limited adsorption capacity and selectivity. In the past few years, nanomaterials, including inorganic nanomaterials, organic polymer-support nano composites, and metal-organic frameworks (MOFs) nanomaterials, have been applied in the capture and isolation of precious metals ions due to their unique physical and chemical properties, including large surface area, high reactivity, developed porosity, and diverse functional groups. Conductive polymer, Poly-N-phenylglycine (PNPG), is an emerging polymer adsorbent used in adsorption studies, but its adsorption study on precious metals has not been reported so far.

Therefore, the purpose of this study is to develop PNPG-based adsorbent materials,

study the adsorption mechanism towards representative precious metals ions (gold and silver), and recover them from the leaching solutions of waste electronic substrate, etc. Firstly, it has been proved that the nanoscale PNPG particles have a good adsorption ability towards gold ions, but their nanoscale structure will bring about the separation problem after adsorption. To reduce the separation burden, we proposed a strategy making PNPG particles into PNPG membrane, so that it can be rapidly separated after adsorption. Subsequently, the adsorption mechanism towards gold and silver ions was elaborated with the aid of a series of characterization techniques. Besides, the adsorption studies related to composite membranes showed the improved adsorption performance as well as membrane stability, providing a theoretical basis for the actual metal recovery application in the future. Finally, the selectivity of gold and silver was investigated by adsorption experiments from both experimental mixed solutions and real leaching solution of printed circuit boards, and the results indicated the possibility of metals recovery by PNPG-based adsorbents.

The main contents of the paper are arranged as follows.

Chapter 1 showed the research background, research significance, and research topic studying the PNPG-based adsorbent for precious metals recovery and providing the basic theory for practical application.

Chapter 2 summarized and presented the detail information about materials and equipment, as well as the preparation method of PNPG particles, PNPG membranes, and composite membranes of PNPG and multi-walled carbon nanotube.

In chapter 3, PNPG particles were first used to capture gold with adsorption capacity (1356.78 $mg \cdot g^{-1}$) and good sensitivity to Au(III) in low-concentration solutions at pH 1. The mechanism of Au(III) adsorption by PNPG mainly involved chemisorption and monolayer adsorption, as evidenced by the well-fitting pseudo-second-order model (PSO) and Langmuir isotherm model. Electrostatic interactions and redox reactions occurred during adsorption, as characterized by zeta potential, XRD, TEM, FT-IR, and XPS. To solve the problem of removing the adsorbent after adsorption, the PNPG membrane was prepared in advance by vacuum filtration, and corresponding stability test experiments were conducted. SEM characterization revealed that the

support layer did not participate in the adsorption process. The PNPG membrane remained active for a minimum of three cycles and could selectively capture Au(III) from uneven-concentration polymetallic solutions. Approximately 80% of the gold in the leaching solution of waste printed circuit boards of computers was selectively recovered using the prepared 2-mg PNPG membrane, proving the possibility of practical application of PNPG membranes for the recovery of gold from e-waste.

Chapter 4 is about the Ag(I) adsorption by PNPG membrane. In this chapter, the PNPG membrane was prepared by the same method as before. The characterization studies were also performed to elucidate the reaction mechanism between the PNPG membrane and Ag(I). It was found that most benzenoid diamine structures undergo a redox reaction with Ag(I), while a minority undergoes chelation which was different from the mechanism of Au(III) adsorption by PNPG. Through studies on the pH influence, adsorption kinetics, and adsorption isotherms, the maximum adsorption capacity was 366 $mg \cdot g^{-1}$ at pH 6, and this Ag(I) adsorption process also fit well with PSO and Langmuir models. In particular, the PNPG membrane showed potential for the recovery of Ag from real solutions when leaching solutions of e-waste and municipal solid waste incineration fly ash were subjected to adsorption experiments.

Chapter 5 introduced the preparation and characterization of PNPG-based composite membrane, and the adsorption performance towards gold ions. PNPG decorated with multi-walled carbon nanotube (MWCNT) composite membranes (PNPG@MWCNT) was easily prepared using ultrasound-aided vacuum-assisted filtration and showed high stability. The results showed that MWCNT bound to PNPG through non-covalent interactions. The PNPG@MWCNT composite membrane with a mass composition of P3.5M0.5 showed an approximately 20% higher adsorption efficiency than the pure PNPG membrane after 24 h adsorption in acidic Au(III) solution with pH = 1. The Au(III) adsorption capacity was up to 1262.6 $mg \cdot g^{-1}$ at pH 1, and the well-fitted pseudo-second-order kinetic and Langmuir isothermal models indicated that the adsorption process was mainly chemisorption and monolayer adsorption. More importantly, the characterization data confirmed that the adsorption mechanism between composite membrane and Au(III) included electrostatic

interactions and redox reactions, and the electron transfer from PNPG to MWCNT promoted the adsorption capacity. Furthermore, the results of all competitive adsorption, repeatability, and gold recovery experiments in the leaching solution of waste printed circuit boards also demonstrated the potential of the PNPG@MWCNT composite membrane in practical applications of gold recovery.

In chapter 6, the general conclusions outlook of this thesis was presented.

Contents

Chapter 1

Introduction

1.1. Metal resources

Archaeologists believe that the use of metals, such as gold, dates back as early as 7,000 BC, because it sometimes exists as pure metallic elements which can be easily picked up and beaten to the desired form due to their malleability. As man learned to extract them by smelting ores, more and more metals were discovered and used. With the development of civilization, especially since the Industrial Revolution of 1750, the production and employment of metals have expanded explosively, generating a series of thinking and research on metal resources.

1.1.1. About metal resources

Before metal resources, the term ‘minerals’ should be understood. Minerals are such lifeless substances that occur naturally in or on the earth's crust and can be extracted and used for specific purposes in a variety of commodities and products because of the special physical and chemical properties of their components. Minerals play an important role in economic development, social functioning, and life quality maintenance. Minerals can be classified into four categories, based on their primary uses: (1) Construction minerals, including sand, gravel, and clay, which provide the foundation and strength for buildings, roads, and other infrastructure. (2) Industrial minerals, such as salt, gypsum, fluorspar, and kaolin, are non-metallic minerals and widely used in industry and consumer goods. (3) Energy minerals, including gas, coal, and oil, are used to generate energy when burned. (4) Metals [1].

Metal generally refers to a class of ductile and conductive substances with unique luster (that is, a strong reflection of visible light) but not transparent. In a narrow sense, the concept of metal is a simple substance composed of metallic elements. Metals have unique chemical and physical properties, such as high electrical conductivity, thermal conductivity,

malleability, as well as the ability to form alloys with other elements. Thus, metals are widely used. For example, iron is a bulk commodity with huge production quantities and mainly for industrial purposes [2]; copper has been highly used in both electrical and electronic applications; gold has been used in jewelry, investment and banks, and technology. However, metal resources are unsustainable. It is estimated that mineral deposits take up to even millions of years to form, but the average life of a viable mine is as short as about 30–50 years and the existing deposits will be used up before new deposits can be formed. This makes metal resources inherently unsustainable on a human time scale [3].

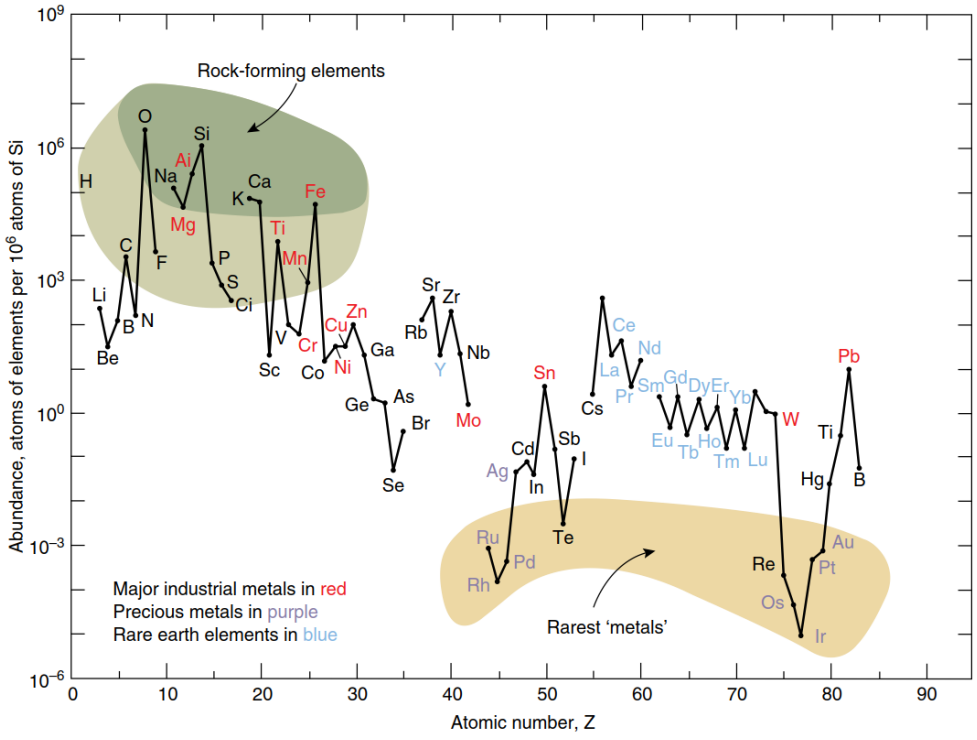

Fig. 1.1. The abundance of the chemical elements in the earth's upper continental crust as a function of atomic number [1]. © 2014 John Wiley & Sons

The existing forms of metals in nature are different. Except for a few inert metals (e.g. gold, silver) which exist in the form of elemental, the rest exist in the form of compounds widely distributed in the crust and the ocean [1]. Besides, the abundance of each metal in the earth's crust is quite different (**Fig. 1.1**). Some major industrial metals (e.g. iron, aluminum) have a similar abundance to major rock-forming elements (e.g. calcium,

potassium), and also show several orders of magnitude higher than that of many widely used base metals (e.g. copper, lead, and zinc). Many other precious metals, such as gold and platinum, are very rare [1].

1.1.2. Metal production

Metals are produced through a series of actions after exploration: mining, crushing and milling, separating, smelting, and refining [1]. The general process can be summarized as follows (**Fig. 1.2**).

Exploration: Discovering and finding out where the valuable minerals are. This is one of the most important steps in metal production. Although minerals are everywhere in the lithosphere, economic deposits of metals are rare and difficult to locate. This step involves drilling and sampling to determine the type, quantity, quality of the mineral, and grade of the metal (i.e. the percentage of metals in the rock) [1]. Considering profit, mining will proceed if the metal concentrations are evaluated to be high enough.

Mining: Getting the ores out of the ground. There are two main methods—surface mining and underground mining, the combination of both methods is also used in some locations. Surface mining is the way that digging rocks out from the surface, forming a hole or pit. When minerals are found far from the earth's surface or deeper down, underground mining will proceed. In addition, the selection of mining method is the result of sufficient consideration of physical structure, location, grade or value of the ore body, and geological characteristics of the adjacent area [4].

Crushing and milling: The process of reducing particle size. Huge ores need to be broken into smaller and smaller pieces, and the mineral monomers are fully dissociated after milling. If the particles are too large, no monomers are not fully dissociated; Conversely, over small particles are not easily separated in the next. These will affect the economic indicators of production. Therefore, the mineral monomers with target scale are usually sorted out in time by classification.

Separating the minerals from the waste rock. There are many different separation techniques to use based on the mineral’s properties, such as hand sorting, magnetic separation, density separation, and flotation. The methods mentioned above are all

physical separation methods. Different minerals are often found together, for example copper and zinc, gold and silver or other precious metals, so the combination of separation techniques is used to separate them from the waste rock and then from each other.

Smelting and refining: The target element is more often found as a chemical compound, so it needs to be separated from other atoms by chemical methods. There are many different methods used to extract the target metal from the compound or remove impurities from the final product. And the produced metal will be distributed to where they are needed.

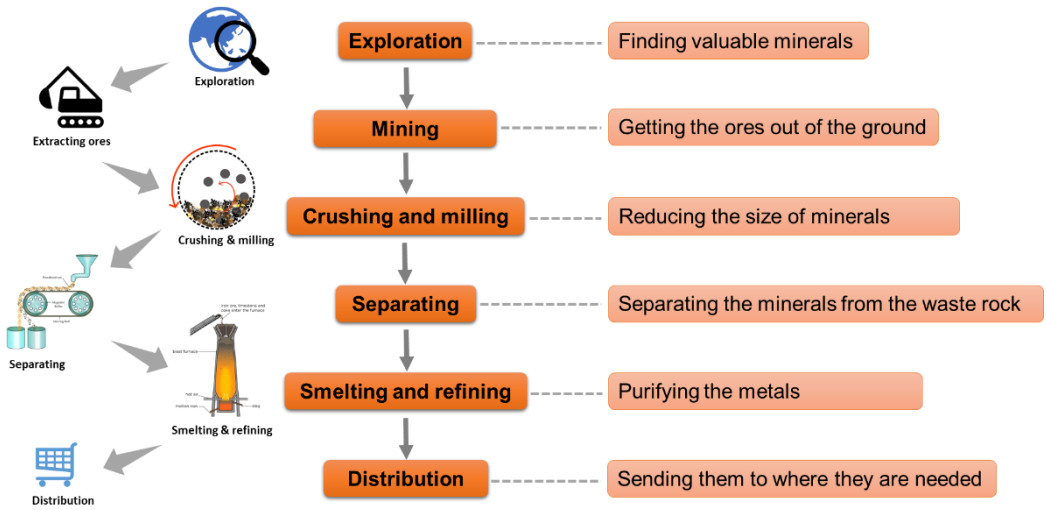

Fig. 1.2. Brief process of metal production.

1.1.3. Precious metals

Precious metals (PMs) (e.g. gold, silver, and platinum group metals) are rare and high-value metallic elements. Most PMs have outstanding physical and chemical properties. In addition to good electrical and thermal conductivity, they have strong chemical stability, high coordination ability, outstanding wear resistance and fading resistance, and good catalytic performance [5, 6]. PMs are widely used in the manufacture of numerous products, such as jewelry, aircraft turbines, industrial catalysts, and electronic and electric equipment [6-8].

(1) Gold

Gold is often found in the elemental form in nature. This metal is dense, soft, bright,

malleable, and resistant to corrosion. Since ancient times, gold has been treasured for its beauty and permanence. Today, gold is not only processed into jewelry, but also used in computers, communications equipment, spaceships, jet engines, and many other products, and it is one of the essential industrial metals since the late 20th century.

Gold is predominantly utilized for jewelry fabrication accounting for 44–61% from the year 2010 to 2021, followed by investment (21–38%), technology (7–11%), central banks & other inst. (2–15%) (**Fig. 1.3**). According to statistics, the total demand for gold in these 12 years was basically around 4,000 t.

Thanks to its conductivity, the utilization of gold in technology has occupied a certain proportion. Gold is mainly used in the printed circuit boards of equipment in the electronics industry, or used as the germanium-gold alloy to evaporate contacts in the semiconductor industry. It is also used as connectors, switches, relay contacts, and so on [9]. From a global perspective, gold consumption varies by country, for example in the United States, there was 35% of gold was used for electrical and electronic equipment in 2015, which was much higher than the global level [10].

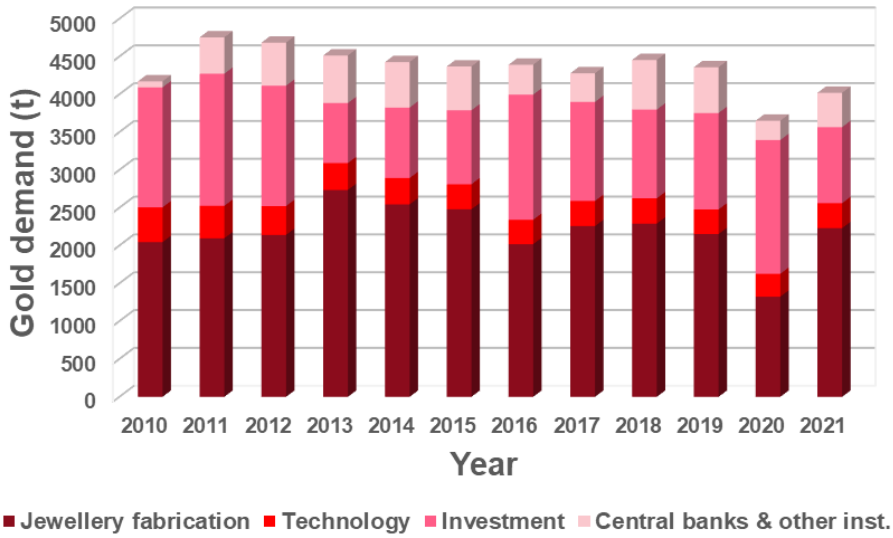

Fig. 1.3. World gold demand in diverse uses from 2010 to 2021 (t: tons). Redraw with the data from Ref. [11].

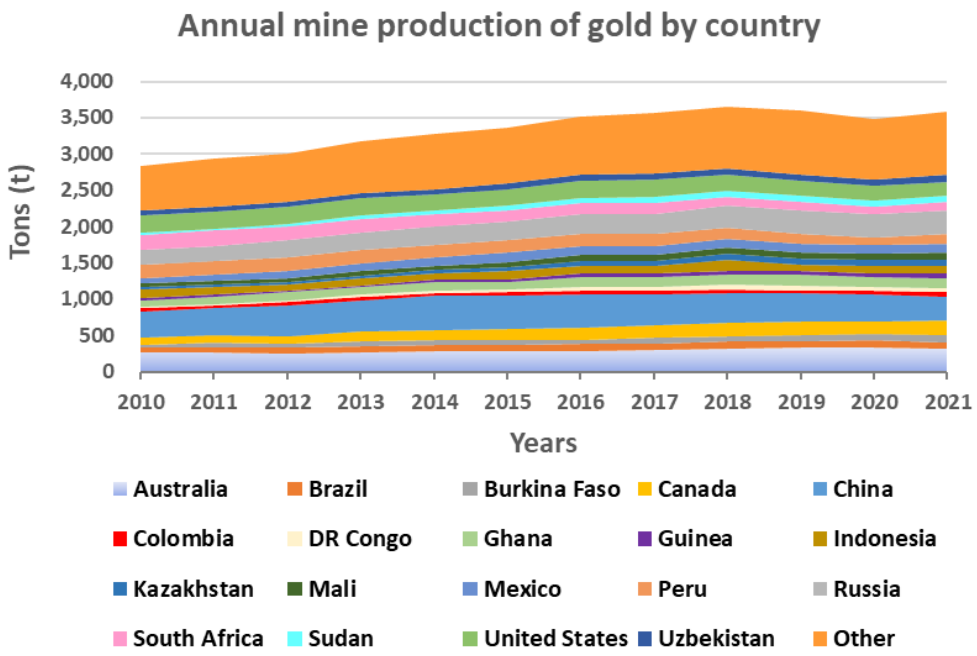

Fig. 1.4. Global mine production of gold from 2010 to 2021 in various countries. Redraw with the data from Ref. [12].

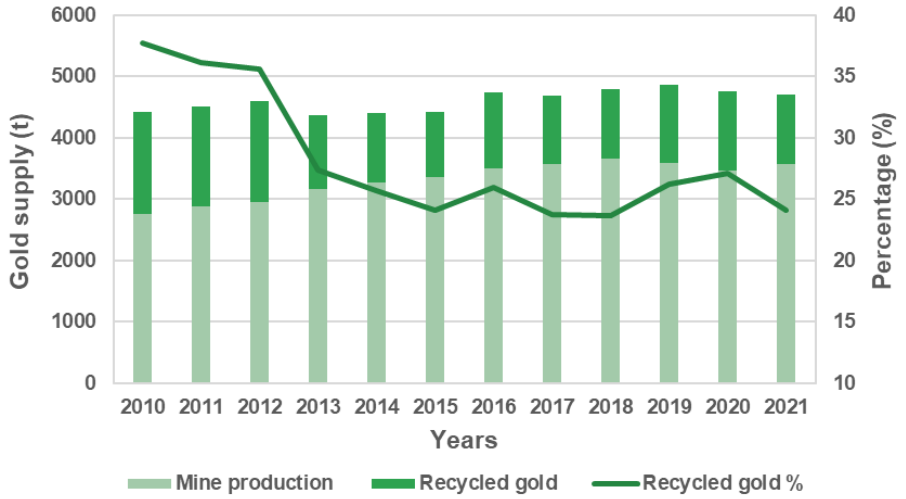

Fig.1.5. World gold supply from 2010 to 2021. Redraw with the data from Ref. [11].

Gold has a long production history dating back to 4000 BC, so its ore grades have fallen over the centuries with huge mining. However, the amount of gold mining was still on the rise in recent years. In total, the global mine production of gold increased from 2830 to 3580 t in the past twelve years (**Fig. 1.4**). The 19 major gold-producing countries accounted for more than 75% of total global production, and China was the

largest producer with 332 t in 2021 and accounted for about 9% of the total. The comparison between **Fig. 1.3** and **Fig. 1.4** shows that it is not enough to meet the global demand if all gold production comes from mining. To meet the gold demand, 23−37% of the supply came from recycled gold (**Fig. 1.5**), but more effort can be put into recycled gold whose production percentage has been declining in recent years.

(2) Silver

Silver, one of the most known and utilized metals since ancient times, is an important precious metal as well. It exists in the forms of single substances and compounds in silver ores in nature. Silver has the highest electrical conductivity than other metals, as well as excellent corrosion resistance and antibacterial properties, so it is widely used in electronics, solar cell manufacturers, pharmaceutical industries, and other applications. According to statistics (**Fig.1.6**), the total silver consumption in 2018 was calculated to be 32,141 t, about 7 times as high as that of gold in the same year. Because of silver's unique physical properties, it cannot be easily replaced. Up to 9,533 t of silver, approximately accounting for 30%, were used in the electronics industry in 2018 which ranked first.

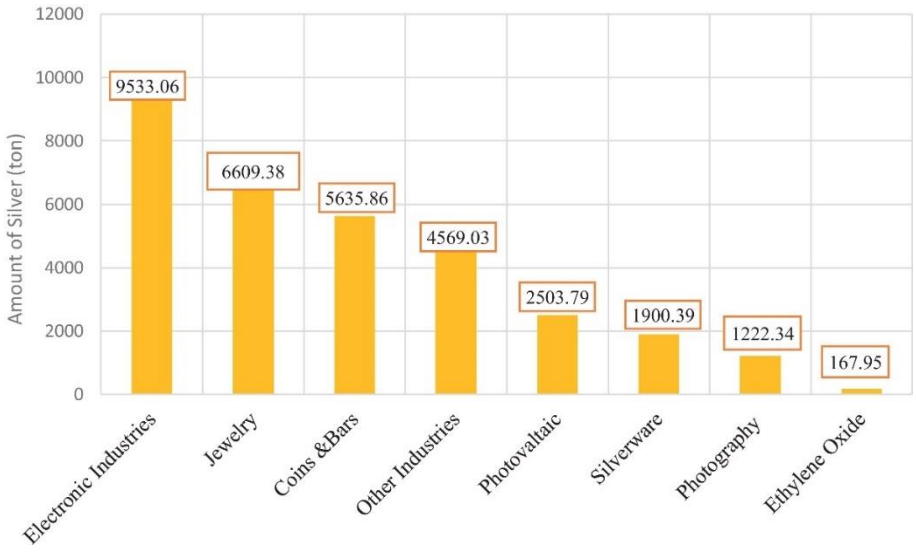

Fig. 1.6. Global silver consumption by different industries in 2018 [14]. © 2021 Elsevier

The total silver demand was basically more than 25,000 t in the past 9 years except for 2020 (**Fig. 1.7**). After the decline in 2020 caused by the COVID-19 pandemic,

global silver demand increased by 19% to 32,627 t in 2021, in which industrial section rose by 9.3% to 15,807 t. This upward trend was mainly attributable to the resumption of industrial activities and the re-opening of economic activities, and also potentially due to the increased demand for electronic products resulting from telecommuting, investment in new generation communications facilities, and increased use of photovoltaic [13].

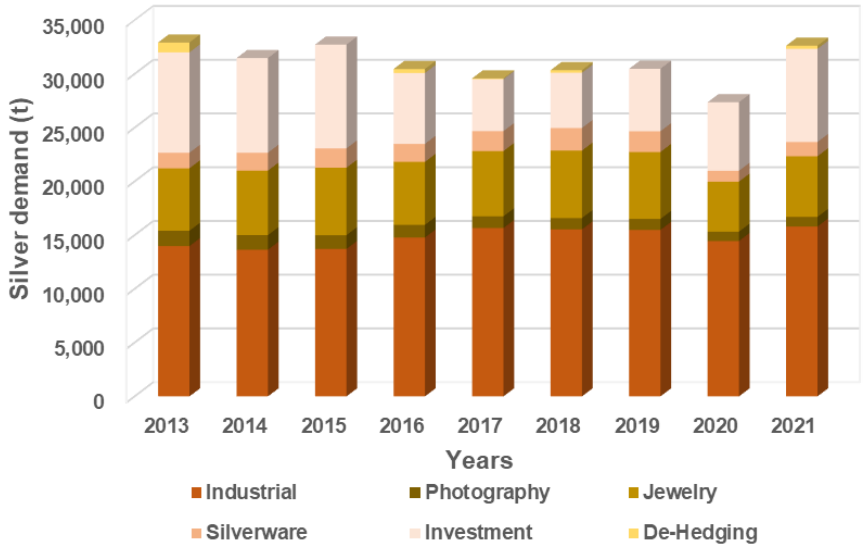

Fig. 1.7. World silver demand from 2013 to 2021. Redraw with the data from Ref. [15], and the original data has been recalculated according to 1 ton (t) = 32,151 troy ounces.

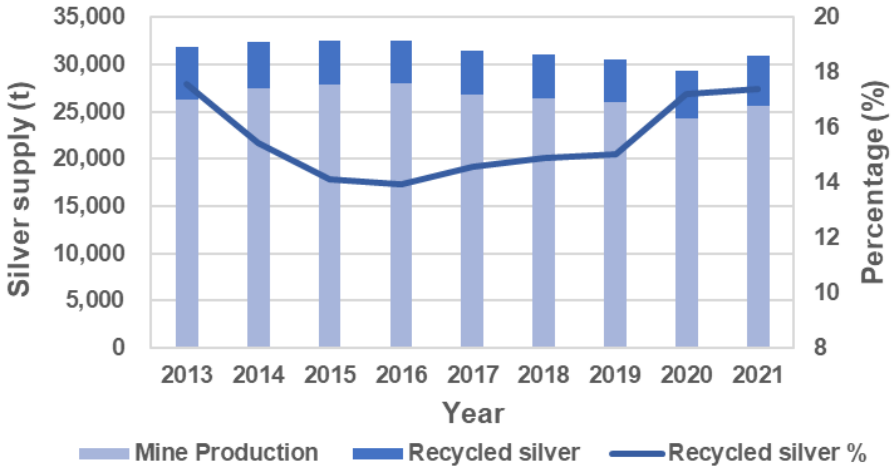

Fig. 1.8. World silver supply from 2013 to 2021. Redraw with the data from Ref. [15], and the original data has been recalculated according to 1 ton (t) = 32,151 troy ounces.

Silver mining began in approximately 3,000 BC in modern-day Turkey. After small-amounts mining, silver mining spread to other countries and its production continued to expand due to the advances in mining techniques, so that many of the high-grade ores throughout the world had been largely used up by the end of the 19th century [16]. Moreover, the mine production of silver has not escalated to match the demands, evidenced by the 24.3−28.0 kilotons of silver mine production (**Fig. 1.8**) but 27.4−33.0 kilotons of total silver demand. Although 14% of recycled silver was produced to meet consumer demand, this percentage was much lower than that of recycled gold, and recycled silver needs to be more concerned.

1.1.4. Necessity of metal recovery

With the spread and development of mining and metal-working techniques since ancient times, a close link between metals, metal pollution, and human history has been formed [17]. World soils have been increasingly polluted by heavy metals (e.g. Pb, Cd) since the industrial age [18]. Water pollution also occurs, one reason being the acid drainage caused by the oxidation of minerals in the air oxygen, and the wastewater containing high-concentration metal ions [4]. The other reason is that the acid and other chemicals produced by smelting and refining process will flow into the nearby water systems such as rivers and groundwater, if the mining process is not properly monitored. Air pollution will also occur, caused by the dust of the dew pit, and the harmful gases, for example sulfur dioxide, released from the mining process. This is toxic to plants, animals, and humans.

In addition, mining activities do harm to natural beauty. In many cases, especially in open pit mines, the shape of the landscape changes when large amounts of rock are dug out from the earth and piled up at the surface and leaving some large unsightly, and dangerous holes or pits in the ground. These mine dumps also change the landscape.

The most direct problem is the depletion of metals. As mineral reserves are finite and unsustainable, a decline in the grade of exploited mineral ores would typically be viewed as a deterioration in quality and a sign of depletion [1]. Due to the increasing global population and the development of new technologies such as modern

communication and computing, greater quantities of minerals and metals are being used than ever before. The mine production of many metals has grown by one, two, or even three orders of magnitude since 1900 [1]. Teseletso et al. showed that the ore grade steadily decreased with the increase in cumulative production. A declining trend was observed for Cu, Au, Ni, Pb, and Zn [2]. Moreover, the declining gold grade in mining deposit extremely increases the cost of mining and the consumption of water, electricity, and so on.

In light of these trends, as ore grades continue to decline, metal recovery and urban ore mining are necessary to complement archaic mining to assure supplementation of current and future increasing global demand and consumption. As can be seen from the applications mentioned above, a significant proportion of gold and silver is used in electrical and electronic equipment. Once the equipment is obsolete, it is important to recover precious metals from it.

1.2. E-waste and metal recovery

The rapid development of industries and technological innovations result in the fast increasing demand for PMs, leading to a supply crisis due to their deficiency in the earth's crust. The primary production of PMs through mining, beneficiation, and metallurgy is a quite complicated process requiring intensive capital, energy, and labor input, and poses a great challenge to the environment. In the meantime, the discharge of waste electronic and electric equipment (WEEE) is increasing dramatically since millions of people are adopting a modern lifestyle. Nowadays, recycling precious metals from electrical and electronic wastes is very crucial and has been a hot topic.

1.2.1. E-waste, the secondary metal resource

Electrical and Electronic Equipment (EEE), including a wide range of products with circuity or electrical components with a power or battery supply, is becoming increasingly used in transport, health, security systems, and generators of energy, and strongly links to widespread global economic development. It includes many household or business-use products like basic kitchen appliances, toys, tools to music, and ICT

items, such as mobile phones, laptops, etc. These kinds of equipment will become electronic waste (e-waste) once they are discarded without the intent of continued reuse. E-waste contains a range of components and materials (**Fig. 1.9**), such as electric cables, printed circuit boards (PCBs), cathode-ray tubes (CRTs), liquid crystal display (LCD) monitors, plastics, metals, and glass, some of which can be systematically recovered, thus making this waste stream a resource of raw materials [19].

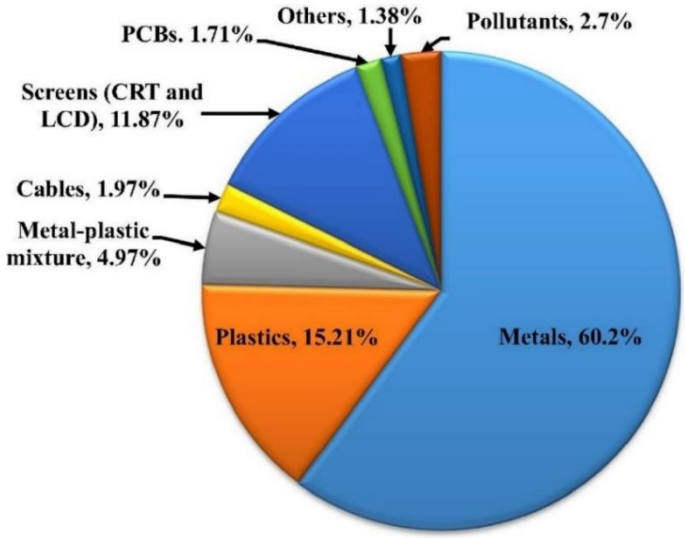

Fig. 1.9. Generalized material composition in e-waste. Note: Iron and steel (most common materials) content found in WEEE is included in the metal fraction [19]. © 2018 Elsevier

The metal content of Cu and Au in primary metal resources like ores was 0.5–1% and 1–10 g/t respectively, while in the case of e-waste, it was 20% and 250 g/t respectively. This justifies that the high content of base metal (e.g. Fe, Cu, Al, Pb, and Ni) and PMs (e.g. Ag, Au, and Pd) makes e-waste a potential source of secondary resources for metal recovery if feasible technologies can develop with environmentally friendly methods [20, 21].

From the list, the exact metal content of e-waste varies significantly with its type, age, origin, and manufacturer (**Table 1.1**). E-waste such as DVD players, portable audio, and electronic scrap has most base metals while electronic devices such as personal computers and mobile phone cards contained a higher level of precious metal compared with others [21]. For example, TV board scrap contains about 10% Cu, 280 g/t Ag, and

20 g/t Au, whilst PC board scrap and mobile phone scrap approximately contain 13–20% Cu, 1000–1380 g/t Ag, and 250–350 g/t Au. Thus, the type of e-wastes as the secondary metal resource should be chosen according to the main goal of target recovered metals (precious metals or copper) [22].

Table 1.1 Various types of e-wastes and their metal content. Redraw with the data from Ref. [21]. © 2008 Elsevier

E-Waste	Fe (wt%)	Cu (wt%)	Al (wt%)	Pb (wt%)	Ni (wt%)	Ag (ppm)	Au (ppm)	Pd (ppm)
TV board scrap	28	10	10	1	0.3	280	20	10
PC board scrap	7	20	5	1.5	1	1000	250	110
Mobile phone scrap	5	13	1	0.3	0.1	1380	350	210
Portable audio scrap	23	21	1	0.14	0.03	150	10	4
DVD player scrap	62	5	2	0.3	0.05	115	15	4
Calculator scrap	4	3	5	0.1	0.5	260	50	5
TV scrap (CRT' s removed)	–	3.4	1.2	0.2	0.038	20	<10	<10
PC scrap	20	7	14	6	0.85	189	16	3
E-scrap (1972 sample)	26.2	18.6	–	–	–	1800	220	30

Note that "–" denotes not reported.

1.2.2. Current situation of e-waste

The current situation with e-waste can be summarized in three aspects.

First, increasing production. The production of e-waste is increasing over years. The per capita production of e-waste increased by 10.7% from 6.6 kg to 7.3 kg (**Table 1.2**), which seems small, but it was numerous when multiplied by the global population. The total e-waste production rose by 15.6% from 46.35 to 53.60 Mt during this period from 2015 to 2019 (**Fig. 1.10**). It is estimated that the amount of e-waste generated will exceed 74 Mt in 2030 [23]. There are some reasons for this. The first is the increasing consumer demand and high rate of obsolescence, which has resulted in an expansion of the production of electronic equipment and the generation of e-waste. The second factor

is the short life span/replacement interval (e.g. mobile phones, personal computers) of most of the currently in-use EEE. For example, the average life cycle of new computers has reduced from 4.5 years in 1992 to 2 years in 2005 [24]. Thirdly, the difference between high production and poor recycling rates leads to the increasing e-waste inventories [19]. The above data also shows that e-waste generation varies from continent to continent. More developed countries (such as Europe and Americas) produce twice e-waste more than the global average (**Table 1.2**). Asia produces more e-waste than Europe or Americas because it has the largest population (**Fig. 1.10**).

Table. 1.2 Per capita production (kg) of e-waste from 2015 to 2019. Redraw with the data from Ref. [25].

	2015	**2016**	**2017**	**2018**	**2019**
Africa	2.3	2.4	2.4	2.5	2.5
Americas	12.5	12.7	12.9	13.1	13.3
Asia	4.7	4.9	5.1	5.4	5.6
Europe	15.5	15.7	15.9	16.1	16.2
Oceania	15.7	15.9	16	16	16.1
Global	**6.6**	**6.8**	**6.9**	**7.1**	**7.3**

Second, insufficient recycling. The statistics show that in 2019, the continent with the highest collection and recycling rate was Europe with 42.5%, Asia ranked second at 11.7%, the Americas and Oceania were similar at 9.4% and 8.8%, respectively, and Africa had the lowest rate at 0.9% (**Fig. 1.11**)[23]. In 2019, the formal documented collection and recycling was 9.3 Mt, thus 17.4% compared to e-waste generated. It grew by 1.8 Mt since 2014, an annual growth of almost 0.4 Mt. However, the total e-waste generation increased by 9.2 Mt, with an annual growth of almost 2 Mt. Therefore, more effort is needed to make the recycling activities keep pace with global growth of e-waste.

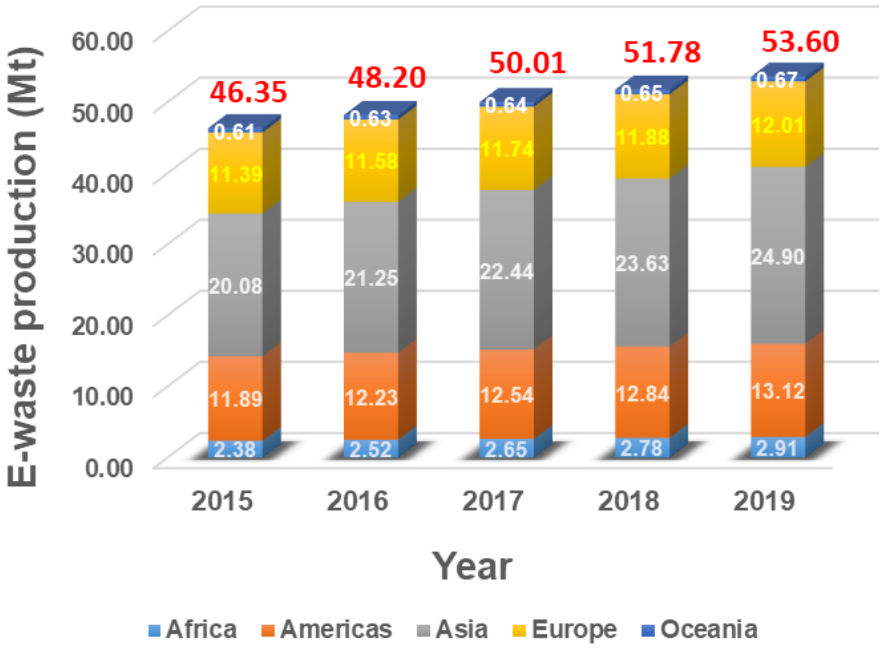

Fig. 1.10. E-waste production from 2015 to 2019 (Mt: million metric tons). Redraw with the data from Ref. [25].

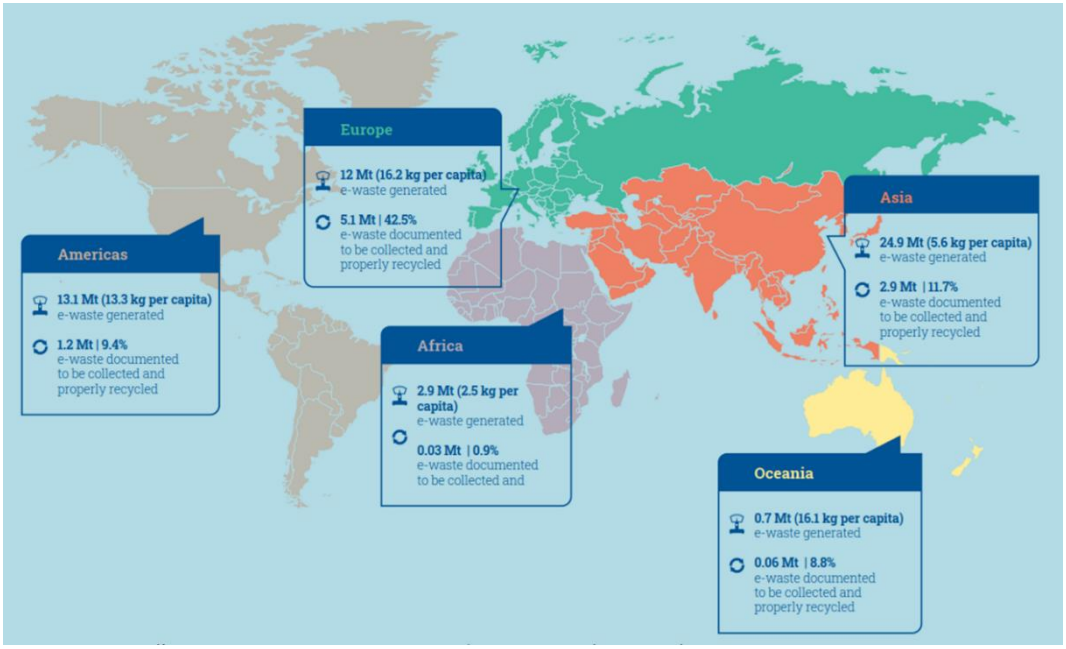

Fig. 1.11. Global e-waste production and recycling in 2019 [23].

Third, implications resulting from e-waste. The most negative impact is the waste of metal resources caused by the imbalance between e-waste production and recycling. Besides, there are also environmental problems caused by hazardous ingredients (e.g. mercury, brominated flame retardants, chlorofluorocarbons) or improper treatment [23].

For example, the large quantities of heavy metals (e.g. Cd, Hg, Pb, Cr) and organic pollutants in unofficially buried e-waste not only pollute soil, air, and water but also do harm to human health [26]. Human exposure to toxic substances in the soil will be through soil-crop-food or inhalation and skin absorption [27]. Improper treatment of e-waste also contributes to global warming. First of all, if the materials in e-waste are not recycled, they cannot substitute primary raw materials and reduce greenhouse gas emissions from the extraction and refinement of primary raw materials. Next, a total of 98 Mt of CO_2-equivalents were released into the atmosphere from discarded fridges and air-conditioners without environmental management. This is approximately 0.3% of global energy-related emissions in 2019 [23].

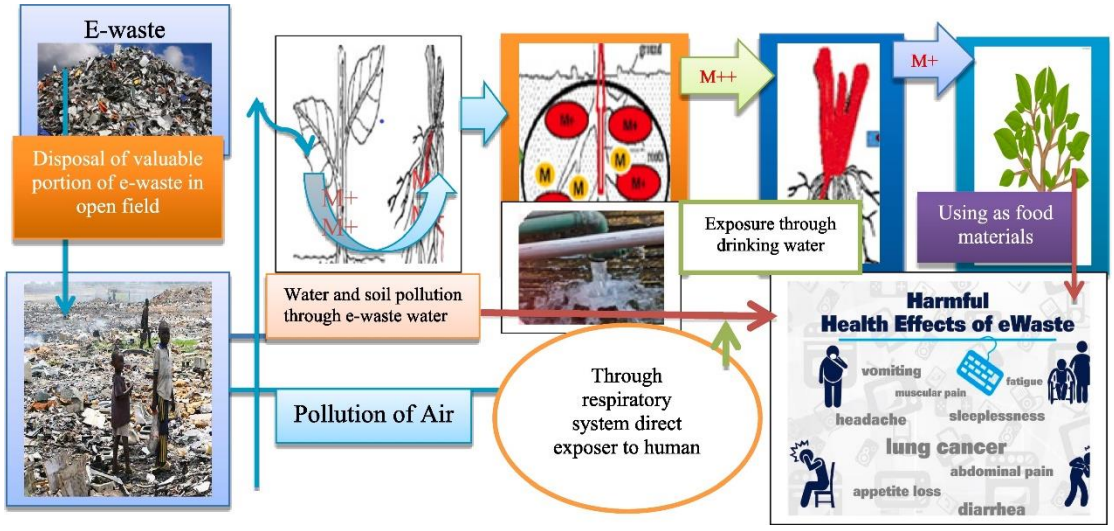

Fig. 1.12. Environmental, groundwater and health hazards of e-waste [27]. © 2019 Elsevier

1.2.3. Benefit from e-waste treatment

Considering the current situation of e-waste, there are various economic and environmental benefits from e-waste treatment and metal recovery.

(1) Contributions to SDGs

E-waste management closely relates to many Sustainable Development Goals (SDGs) identified by the United Nations and all member states. For example, such as SDG 8 on decent work and economic growth, SDG 3 on good health and well-being, SDG 6 on clean waste and sanitation, and SDG 14 on life below water. Given the high

raw material demand for the production of EEE, e-waste also closely relates to the SDG indicators, particularly the Target 12.5 of SDG 12: By 2030, substantially reduce waste generation through prevention, reduction, repair, recycling, and reuse. An increasing number of people on the Earth are consuming growing amounts of goods, and it is critical to make metal production and consumption more sustainable [23].

(2) Resource and economic benefit

As metal resources are unsustainable, properly treating e-waste and recovering metals from e-waste is an important way to protect metal resources. E-waste is an 'urban mine', as up to 69 elements can be, including PMs (e.g. Au, Ag, Pt, Pd), critical raw materials (e.g. Co, In, Ge, Bi), and non-critical metals such as Al and Fe (**Fig. 1.13.**) [26]. Besides, the contents of PMs in waste PCBs are higher than that of ores, so that it is worth recycling metals from e-waste.

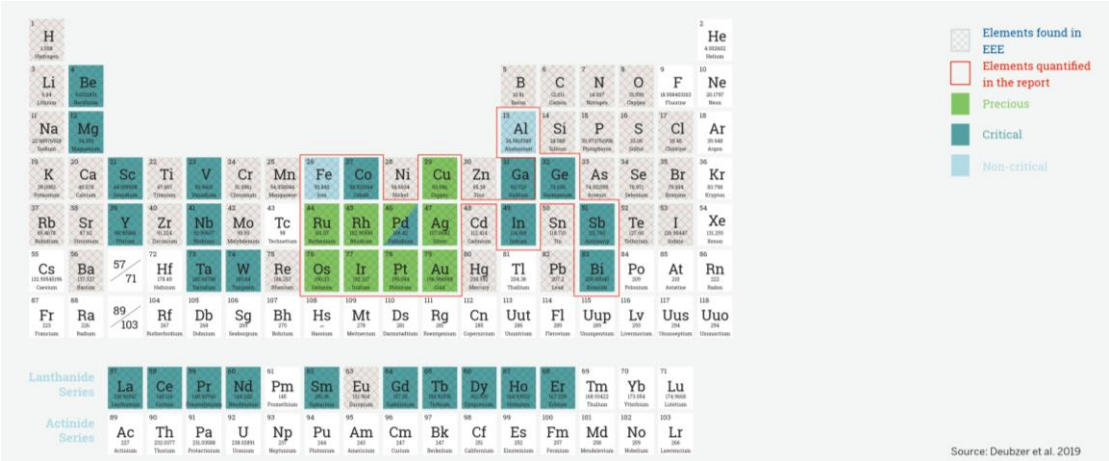

Fig. 1.13. Founded elements in EEE from the periodic table [26].

In addition, there are significant economic profits from recycling and utilizing e-waste. The metal contents in waste PCBs (**Table 1.3**) describe their economic value, for which the recovery of metal values from e-waste could be preferred in the future [28]. The PMs in PCBs represent more than 80% of the total intrinsic value even when their total concentration is less than 1 wt% [29]. The value of raw materials in the global e-waste generated in 2019 was $57 billion. Iron, copper, and gold contribute mostly to this value. With the current documented formal collection and recycling rate of 17.4%,

a potential raw material value of $10 billion can be recovered from e-waste, and 4 Mt of secondary raw materials would become available for recycling [23].

Table 1.3 Metal content economic value of waste PCBs (per ton) [28]. © 2009 IEEE

Metal	Content (%)[b]	Metal price ($/kg)[a]	Potential value	Value (%)
Cu	9.7	3.6	349.2	4.8
Al	5.8	1.7	98.6	1.35
Fe	9.2	0.4	36.8	0.51
Ni	0.69	10.5	72.5	0.99
Pb	2.24	1.2	27	0.37
Sn	2.15	13	279.5	3.84
Ag	0.06	315	189	2.6
Au	0.023	24434	5620	77.17
Pd	0.01	6100	610	8.38
Total	29.87	–	7282	–

a London Metal Exchange, November, 2008.

b Chris et al. (2003) [30].

(3) Environmental benefit

Due to the negative impacts of mining activities and the environmental implications resulting from e-waste, recovering PMs from the secondary resource with proper treatment has the advantages of less difficulty, less capital and energy cost, less emission of waste solid and gas, and less pollution on water, soil and air. For example, in 2019 the recycling of iron, aluminum, and copper has helped save up to 15 Mt of CO_2 equivalent emissions by comparing the emissions results between their use as virgin raw materials and secondary raw materials [23].

1.2.4. Recovery methods

Systematic recovery of metals from e-waste has similar steps to that of metal production mentioned above, involving e-waste collection, preparation (including

disassembly and sorting out valuable parts from e-waste), separation (including mechanical crushing or crusher stripping metal from sorted parts), recovering valuable metals from concentrates (similar to refining in metal production) [8]. The commonly used recovery methods in industry are pyrometallurgy and hydrometallurgy, and the products will be further refined by electrometallurgy. The potential process for recovering metals from e-waste is shown in **Fig. 1.14**.

Pyrometallurgy: A traditional technology used to thermally and physically separate metal phases. There are several treatment options, such as smelting in a plasma arc furnace or blast furnace, drossing, sintering, melting, and reactions in a gas phase at high temperatures [31]. In the case of PCBs, pyrometallurgy usually provides a sharper and faster separation [32], but requires considerable energy input. Although pyrometallurgical processing can recover certain metal components, it generally only provides the first separation step between a metallic and a (non-metallic) slag phase, while incinerating organic components. Industrial pyrometallurgical operations are therefore usually coupled with further processing methods, both pyro- and hydrometallurgical, to further separate individual metals [33].

Hydrometallurgy: A process traditionally used to extract PMs from ores and to recover metals from e-waste. The hydrometallurgical processes begin with leaching, using an appropriate acid or alkali leaching agent to dissolve the maximum metal content into solutions. This is an important step in the hydrometallurgical recovery of metal from waste PCBs [20]. Solvent extraction, adsorption, ion exchange, or other methods and then used to further refine and concentrate the metal [34]. The brief process of using hydrometallurgy to recover metal from e-waste is shown in **Fig. 1.15**. In recent years, there has been an increase in literature on the hydrometallurgical treatment of waste PCBs.

Compared to pyrometallurgical operation, the hydrometallurgical process is technically simpler, operates at lower temperatures, does not require high energy inputs, and does not release harmful substances such as furans and dioxins. Thus, hydrometallurgy is generally considered to be more "environmentally friendly", which is its major advantage [19]. Additionally, hydrometallurgy is suitable for small-scale

applications and the processing of low-grade samples, making it attractive from an economic point [35].

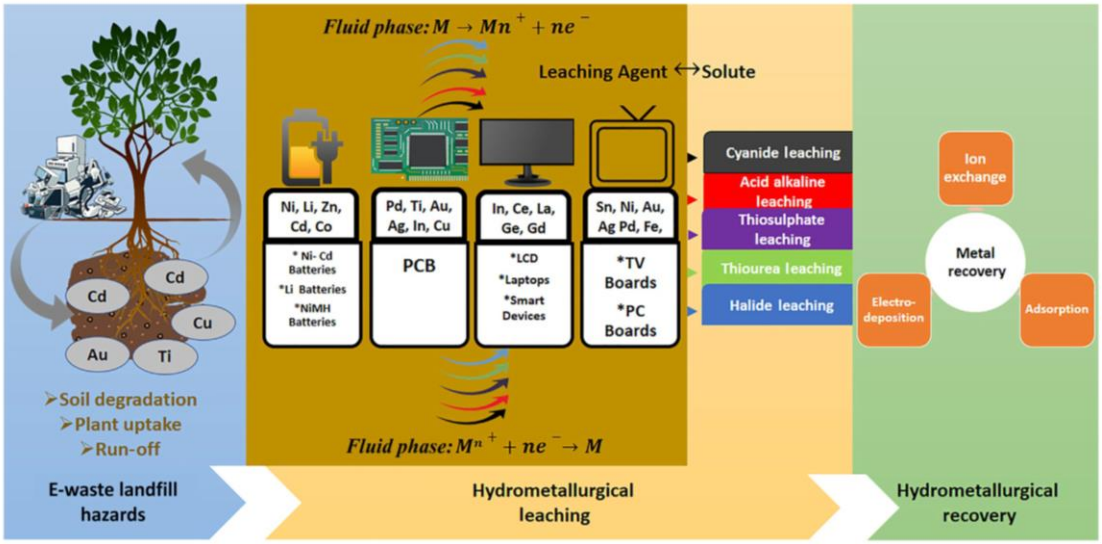

Fig. 1.15. A brief process used in hydrometallurgy to recover metals from e-waste, rather than landfill which is harmful to the environment [34]. © 2019 Elsevier

In the final step for PMs recovery in hydrometallurgy, the metals need to be recovered from the leaching solutions by precipitation, solvent extraction, adsorption, and electrorefining [34]. Precipitation has the advantages of low cost and easy operation, but it will produce secondary pollutants during the chemical reaction. Electrorefining is mature, but with high energy consumption. When employing solvent extraction, the processes including extraction and stripping steps require more volume of extraction reagent, thus increasing the processing cost [36]. In general, the concentration of PMs (e.g., Au) in leaching solutions is much lower than that of other co-leached metals (e.g., Cu), which lowers the efficiency of gold separation and purification [37]. Considering this, adsorption is a more suitable recovery method in such low-concentration leaching solutions, and it has the advantages of low cost and high efficiency from a technical and economic standpoint, without secondary pollution [7].

1.3. Adsorption

Due to the increasing demand for PMs and the decrease in natural metal resources,

metal recovery has great economic benefits and environmental significance. Adsorption is one of the most economical and effective methods for recovering PMs ions in hydrometallurgy.

1.3.1. Adsorption mechanism

The adsorption process is a phenomenon of the accumulation of soluble adsorbates on the surface of the adsorbent. The adsorption mechanism can be classified into two main categories: physical adsorption (physisorption) and chemical adsorption (chemisorption), based on the type of interactions between PMs ions and adsorbents [38]. Physical adsorption, including electrostatic interaction and diffusion, is weak and reversible with small energy changes, while chemical adsorption such as coordination, acid-base interactions, and redox reactions is strong, irreversible, and involves large energy changes [38]. Generally, the adsorption of metal ions onto adsorbents is a complicated process involving more than one interaction, and this can be proved by a variety of characterization and experimental methods.

Physical adsorption: Including electrostatic interaction and diffusion. The electrostatic interaction depends on the surface charge of adsorbents and the state of PMs species, which is indicated by the change of PMs uptakes with changing pH. Diffusion refers to the transport of ions or molecules from a high concentration (or high chemical potential) area to the low through Brownian motion during the adsorption process by porous adsorbents [38].

Chemical adsorption: Being further subdivided into six modes of action. Coordination interactions occur between PMs ions and adsorbents modified with functional groups such as amino group (–NH_2), thiol group (–SH), and carboxyl group (–COOH), usually resulting in better adsorption performance. The importance of functional groups may override the surface area of materials in determining the adsorption capacity. New chemical bonds formed between PMs ions and adsorbents are another predominant mechanism for PMs adsorption. Ion exchange usually happens in the adsorption of PMs chloride anions (e.g. $AuCl_4^-$, $PtCl_6^{2-}$ and $PdCl_4^{2-}$) by amino-functionalized adsorbents in chloride solution. Acid-base interactions have been

occasionally reported as the mechanism, based on the hard-soft-acid-base (HSAB) theory, i.e. soft acids react strongly with soft bases while hard acids react strongly with hard bases when other factors are controlled. Reduction is extensively reported, wherein the PMs ions are reduced to lower valance and metallic states during the adsorption, as high valance PMs ions with high electronegativity tend to acquire electrons from low electronegativity groups such as amino groups and thiol groups. Reduction is crucial to determining the adsorption capacity of PMs [38].

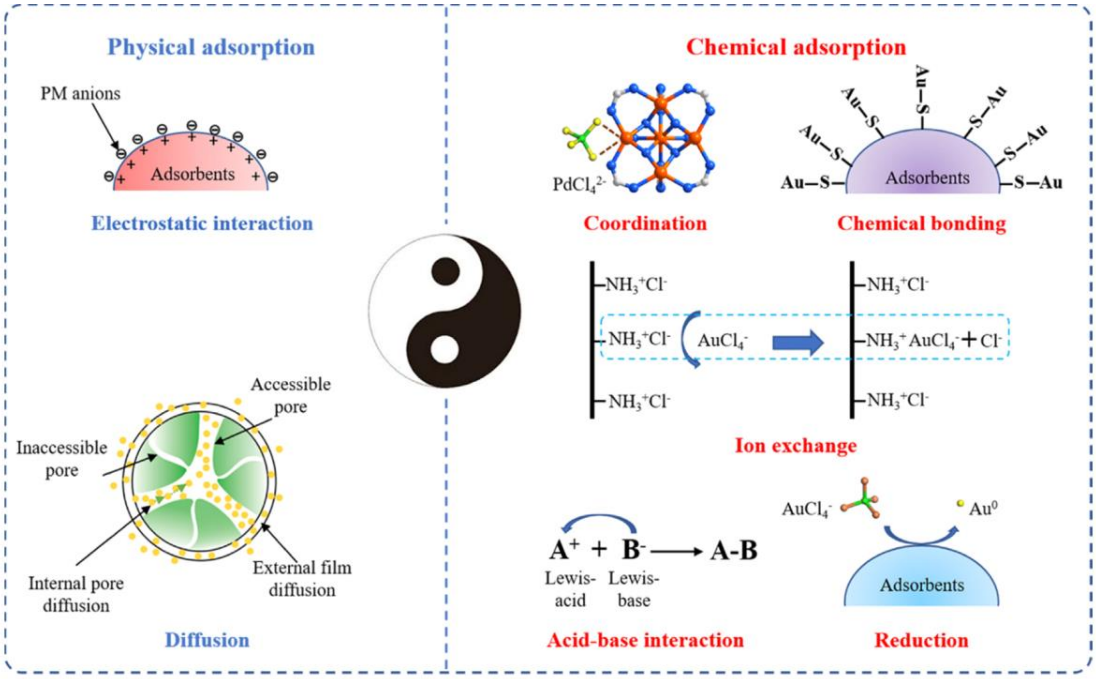

Fig. 1.16. Adsorption mechanisms between PMs ions and adsorbents [38]. © 2021 Elsevier

1.3.2. Adsorption kinetic models

Studying the kinetics of adsorption is a routine experimental method to investigate the adsorption behavior of PMs and explore the possible adsorption mechanisms.

Adsorption is a mass transfer process in which adsorbates move from the liquid phase to the solid adsorbent. The adsorption mass transfer kinetic consists of three steps (**Fig. 1.17**). The first step is external diffusion, wherein the adsorbate transfers through the liquid film around the adsorbent. The concentration difference between bulk solution and adsorbent surface is the driving force of the external diffusion. The second

step is internal diffusion, which describes the diffusion of the adsorbate in the pores of the adsorbent. The third step is the adsorption of adsorbate on active sites of adsorbent [39]. Adsorption kinetics models have been used to evaluate the properties of adsorbents and study the mechanism of adsorption mass transfer, and Wang and Guo summarized and elaborated on 16 adsorption kinetic models [39]. Among various adsorption kinetics models, the pseudo-first-order (PFO) model and pseudo-second-order (PSO) model, which fit the relationship between adsorbate uptakes and contact time, are the most widely used empirical models to estimate whether the rate-determining step is physical adsorption or chemical adsorption [38].

Pseudo-first-order (PFO) model. The PFO model has been considered as an empirical model for a long time. This kinetic model assumes that the adsorption process is limited by physical adsorption, and a diffusion step restricts the movement of adsorbed substance from liquid to adsorbent surface. The nonlinear and linear formulars of PFO model are respectively presented as Eq. (1) and (2), respectively:

$$q_t = q_e\left(1-e^{-k_1 t}\right) \tag{1}$$

$$\ln\left(q_e - q_t\right) = \ln q_e - k_1 t \tag{2}$$

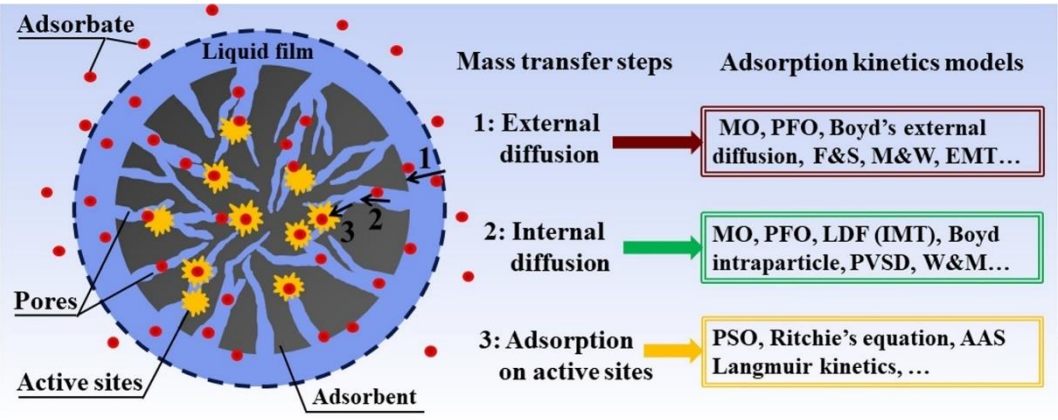

Fig. 1.17. Mass transfer steps and corresponding adsorption kinetic models [39]. © 2020 Elsevier

Pseudo-second-order (PSO) model. The PSO model was first applied to model the adsorption of lead onto peat (Ho et al., 1996). Since then, the PSO model has been

widely adopted to describe the adsorption processes. Most published papers have used the PSO model to predict the adsorption experimental data and to calculate adsorption rate constants. The PSO kinetic model assumes that the adsorption process is controlled by chemical adsorption, involving the sharing or transfer of electrons between adsorbed substances and adsorbent materials. The nonlinear and linear formulars of PSO model are respectively presented as Eq. (3) and (4):

$$q_t = \frac{tk_2q_e^2}{1+k_2q_et} \tag{3}$$

$$\frac{t}{q_t} = \frac{1}{k_2q_e^2} + \frac{t}{q_e} \tag{4}$$

In the above four formulas, t (h) is the contact time and q_e is the equilibrium adsorption capacity, and constants k_1 (h^{-1}) and k_2 ($g \cdot mg^{-1} \cdot h^{-1}$) of PFO and PSO models respectively are used to describe the rate of adsorption equilibrium [39]. The reliabilities of PFO and PSO models can be analyzed by comparing the values of the adjusted coefficient of determination (R^2). The higher R^2 means the better-fitting model and its theoretical value of equilibrium adsorption capacity q_e is closer to the experimental value [38].

In addition, there are other kinetic models, such as the intraparticle diffusion model, Mixed-order (MO) model, and Elovich model, which are not introduced here due to the length of the thesis. The specific models used will be introduced in the corresponding chapters.

1.3.3. Adsorption isotherm models

Studying isotherms of adsorption is a routine experimental method to investigate the adsorption behavior as well. An isotherm refers to the relationship between the equilibrium adsorbate concentrations in liquid phase and the equilibrium adsorption amount in solid phase at a certain temperature. Modeling of adsorption data by isotherm models (**Fig. 1.18**) can provide information about the adsorption mechanisms, the maximum adsorption capacity, and the properties of adsorbents by the isotherms [40].

For example, in chemical adsorption, a monolayer formation of adsorbate occurs on the adsorbent, while in physical adsorption a multi-layer formation appears [40, 41].

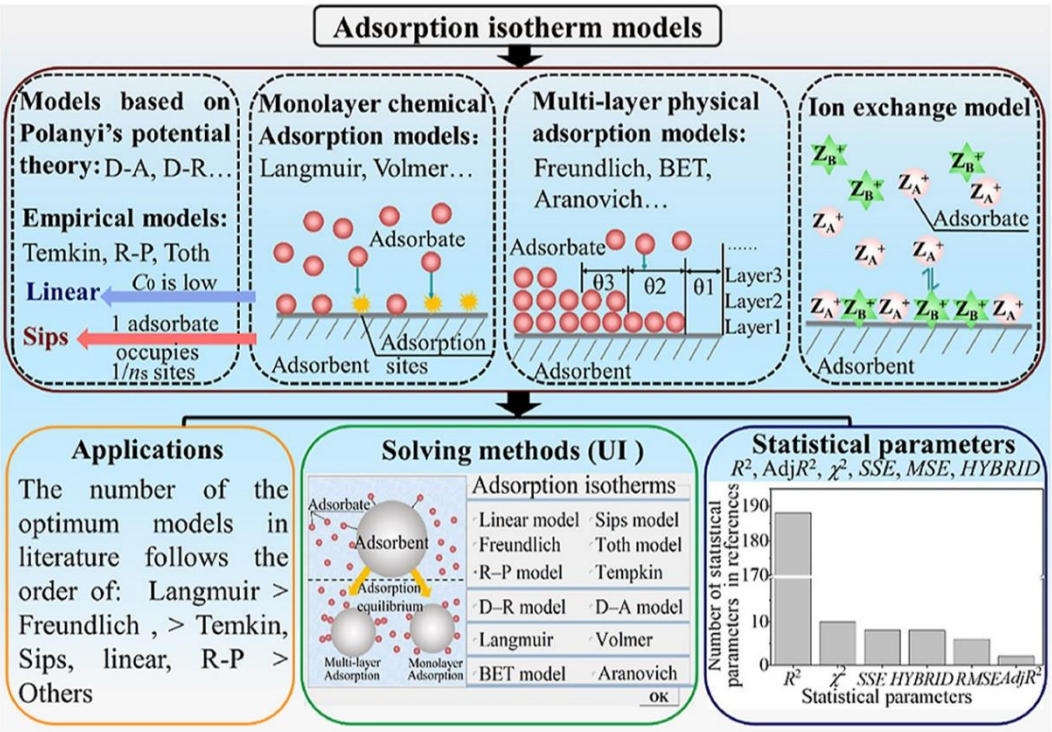

Fig. 1.18. Types of adsorption isotherm models [40]. © 2020 Elsevier

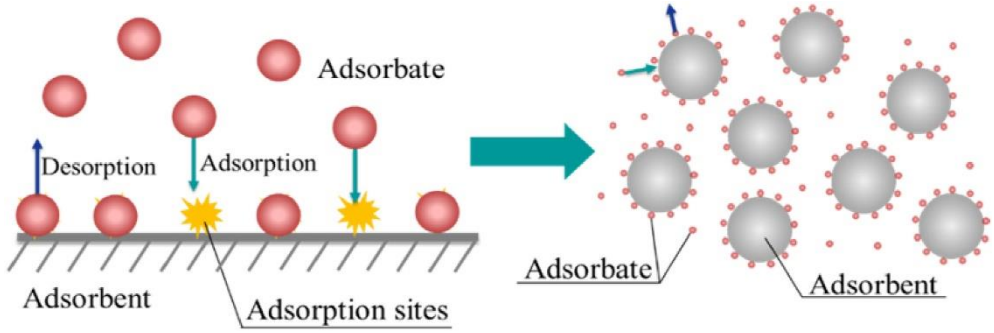

Fig. 1.19. The adsorption mechanisms revealed by the Langmuir isotherm model [40]. © 2020 Elsevier

Langmuir isotherm model. The most commonly applied Langmuir isotherm model was raised to represent gas-solid adsorption [42, 43]. It describes the equilibrium condition of monolayer homogeneous adsorption (**Fig. 1.19**). The basic assumptions of the Langmuir isotherm model are: (1) monolayer adsorption; (2) the distribution of adsorption sites is homogeneous; (3) the adsorption energy is constant; (4) the

interaction between adsorbate molecules is negligible [40]. The term "homogeneous" means macroscopic homogeneous adsorption. For most adsorption processes, the adsorbent materials are homogeneous in the macroscopic view, and the solutions are homogeneous with agitation. Therefore, even though the adsorbent materials (such as microplastics, activated carbons from natural sources, modified mineral, and shale) have irregular shapes and non-uniform surfaces in the microscope, the adsorption can still be represented by the Langmuir isotherm model [40]. The nonlinear and linear equations of Langmuir isotherm model are presented as Eq. (5) and (6), respectively:

$$q_e = \frac{q_m K_L c_e}{1 + q_m c_e} \tag{5}$$

$$\frac{c_e}{q_e} = \frac{c_e}{q_m} + \frac{1}{K_L \times q_m} \tag{6}$$

where c_e (mg·L^{-1}) and q_e (mg·g^{-1}) are the equilibrium concentration and equilibrium adsorption capacity, respectively, and q_m (mg·g^{-1}) is the maximum adsorption capacity estimated by Langmuir isotherm model. K_L (L·mg^{-1}), the isotherm equilibrium binding constants, is the ratio of the adsorption rate and desorption rate.

Freundlich isotherm model. The Freundlich isotherm model is also one of the most widely used isotherm in adsorption. Unlike the Langmuir isotherm model, the Freundlich model describes the reversible and non-ideal adsorption process and is used to represent the multi-layer adsorption on heterogamous surfaces [40]. The equation of Freundlich isotherm model is empirical and was originally obtained by assuming the heterogeneous distribution of adsorption energy and the patchwise topography of surface [41]. Freundlich isotherm model expression defines the heterogeneity of surface as well as the exponential distribution of the active sites and their energies. Its nonlinear and linear forms are given by Eq. (7) and (8):

$$q_e = K_F c_e^{1/n} \tag{7}$$

$$\log q_e = \log K_F + \frac{1}{n} \times \log c_e \tag{8}$$

where K_F (L$^{1/n}$·mg$^{1-1/n}$·g^{-1}) is the isotherm equilibrium binding constants. The value of

$1/n$ determines the availability of the adsorption process. $1/n$ is the characteristic constant related to adsorption intensity, which can be explained as the smaller $1/n$, the greater the heterogeneity, and the adsorption is favorable on the scale of 0–1 [44]. The nonlinear Freundlich model (Eq. (7)) can be solved by nonlinear regression analysis. Eq. (8) is easy to be solved by plotting $\log q_e$ vs. $\log C_e$.

In addition to the above two isotherm models commonly used in judging monolayer or multi-layer adsorption in many works of literature, other isotherms, such as the Sips model, the Temkin model, and the Brunauer, Emmett, and Teller (BET) model, have been also applied in adsorption systems. These models are not introduced here due to the length of the thesis. The specific models used will be introduced in the corresponding chapters.

1.4. Adsorbents

Adsorption is an effective and promising method for isolating and separating PMs ions from aqueous solutions. In addition to conventional adsorbents (e.g. activated carbons, biosorbent), nanostructured materials are being rapidly developed to enhance the adsorption capacity and rate of adsorbents.

1.4.1. Conventional adsorbents

Activated carbons (ACs): Activated carbons is a kind of carbonaceous material. Due to its great capacity to adsorbates, commercial ACs is the most effective adsorbent, and it can give a good quality output if the adsorption system is properly designed. The adsorption capacity is mainly due to its distinct porous structure and large surface area, and its chemical nature which can be easily modified by chemical treatment. The processes that use these usual adsorbents are often carried out in a batch mode, by adding ACs to a vessel containing the contaminated solution, or by feeding the solution continuously through a packed bed of carbon [45]. There are numerous studies on the application of ACs for the separation/purification of gold from the leaching liquor of e-waste [46, 47]. ACs exhibit good performance in the adsorption and recovery of PMs through physical/chemical adsorption [48, 49]. The main limitations of ACs are low

adsorption capacity and poor selectivity [50].

Biosorbent: Biosorption has been aimed at the removal or recovery of organic and inorganic substances from solutions by biological materials which can include living or dead microorganisms and their components, seaweeds, plant materials, industrial and agricultural wastes, and natural residues [51]. The commonly used biosorbents include bacteria, fungi, algae, yeasts, biopolymers (e.g. chitosan, tannin, cellulose, protein, etc.[52].)) and some biowaste materials. For example, chitosan-based bioadsorption was used for efficient and selective recovery of gold from the chlorate leachate of waste PCBs [53]. The main attractions of biosorbent are low cost, high efficiency, and minimal chemical or biological sludges [54]. However, the disadvantages of biosorbent include low stability and adsorption capacity, poor mechanics, and difficulty in realizing the solid–liquid separation [38].

1.4.2. Nano-adsorbents

In the past few years, the development and utilization of nanomaterials for PMs recycling have been attracting tremendous interest due to their unique physical and chemical properties, including large surface area, high reactivity, and developed porosity [38]. Nano-adsorbents can be categorized as inorganic nanomaterials, organic polymer-support nanocomposites, and metal-organic frameworks (**Fig. 1.20**).

(1) Inorganic nano-adsorbents

Inorganic nanomaterials have gained much interest in PMs adsorption, which can be further divided into metal oxide/sulfide nanoparticles, carbon-based nanomaterials, and silica-based nanomaterials [38].

Metal oxide/sulfide nanoparticles, such as Fe_3O_4, TiO_2, ZrO_2, and MoS_2, are widely used in PMs adsorption because of their unique properties. For example, the magnetism of Fe_3O_4 provides an easy, efficient, and convenient way to isolate adsorbents from water by external magnetic field [38]. MoS_2 was capable of capturing gold due to the strong soft–soft interactions between gold and sulfur atoms and the in-situ reduction in which gold thiosulfate complex ($[Au(S_2O_3)_2]^{3-}$) can be reduced to elemental gold particles because of the photo-generated electrons released by MoS_2 [55,

56]. Carbon-based nanomaterials, such as graphene, graphene oxide (GO), and carbon nanotubes, have been developed to recover PMs, not only for the improvement of adsorption ability but also for tracing PMs at ppb level in which the effect of ACs is limited. Carbon-based nanomaterials have the advantages of high stiffness and resilience, high electrical conductivity, large surface area, good thermal conductivity, and optical properties [38]. Silica-based nanomaterials, such as silica gel, silica nanofibers, and silica-coated magnetic particles, are promising for the separation and recovery of PMs from solutions due to their ordered pore channels and large surface area [38].

Inorganic nanoparticles have large surface areas but limited adsorption capacities towards PMs due to the lack of functional groups to chelate PM ions, so they usually act as substrates and require further modification with functional groups to interact with PMs, with the exception of metal sulfide nanomaterials, as sulfur has a strong affinity to PMs through soft–soft interaction. However, the poor stability of metal oxide nanoparticles in harsh aqueous environment also limits the application in recovering PMs, as aqua regia and concentrated hydrochloric acid are commonly used as leaching agents in hydrometallurgy [57].

(2) Organic nano-adsorbents

Organic nanomaterials, possessing abundant functional groups such as $–NH_2$, –COOH, –OH, can efficiently bind metal ions from water through ion exchange, complexation, electrostatic attraction, and reduction [38]. For example, polydopamine contains a variety of functional groups (e.g. catechol, amine, and imine), which provide active sites for covalent modification of the desired molecules and also firmly anchor transition metal ions [58]. Bashir et al. reported that Polythiophene/Prussian red nanocomposites displayed a good adsorptive tendency towards Au (III), Pd (II), and Ag (I), which was ascribed to the hard-soft-acid-base (HSAB) interaction and complexation of PMs ions with sulfur lone pairs from Polythiophene [59].

Polymers are used as not only single adsorbents to recover precious metals, but also chelating agents for inorganic adsorbents to improve their dispersion and stability, because metal oxide nanoparticles are prone to aggregate in aqueous solutions and

reduce the contacts between adsorbents and adsorbates [38].

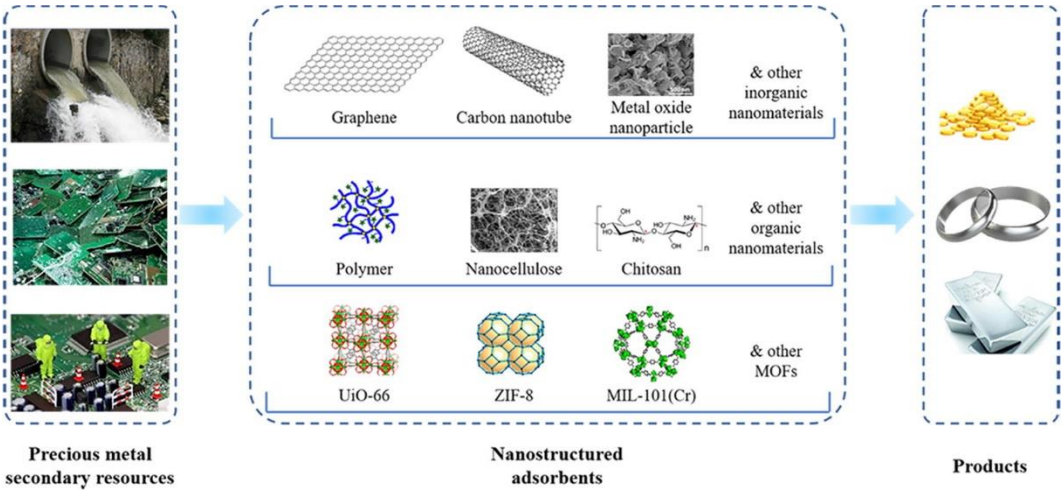

Fig. 1.20. Adsorptive recovery of PMs from aqueous solution using nanomaterials [38]. © 2021 Elsevier

(3) Metal-organic frameworks (MOFs)

MOFs have emerged as a new type of nano-porous inorganic-organic hybrid materials with one-dimensional (1D), two-dimensional (2D), or three-dimensional (3D) topology. They are constructed with inorganic metal ions or clusters as the center and organic ligands as the linker. Due to their unique structure, high porosity (about 94%), and large specific surface area (about 7140 m^2/g), MOFs have a great prospect in adsorption and other applications [60]. For example, a synthesized MOFs adsorbent (MOF-AFH) was used to separate Pd(II) and Au(III) from water due to the reduction reaction and chelation with N and O-containing functional groups, as well as the electrostatic interaction for Au(III) adsorption [61]. Zr-based MOF (DONA-MOF) was synthesized and showed an excellent removal effect on Au(III) in pH 2–9, with electrostatic attraction, chelation, and reduction being identified as the main adsorption mechanisms [62].

MOFs are superior to other nanomaterials due to their large surface area, versatile functionality, and tunable pore structure. However, the stability of MOFs in acidic aqueous solution still needs to be improved [38], and MOFs with the nano-sized powdered microcrystalline structure are prone to aggregate, which would cause pipe

blockage and reduce processing efficiency. Furthermore, the synthesis steps of multifunctional selective MOFs with controllable sizes/shapes are often complex and require significant costs for industrial-scale production [60].

1.4.3. Conductive polymers

From the perspective of the advantages of polymers, conductive polymers (CPs) are also considered as efficient adsorbents [63, 64]. In addition to the aforementioned advantages of numerous functional groups and stability, CPs also show unique conductivity characteristics originated by a small, but substantial, alteration in backbone chemistry with alternating double-single bond structures along the main chain of the polymer; overlapping the π bonds in the structure of these electroactive long-range conjugated polymers enables the electrons to be freely shifted and transferred in their bound atom space [63]. The chemical structures or repeat units of several CPs are shown below (**Fig. 1.21**). So far, CPs and their derivatives have been vastly applied in diverse fields such as biomedicine (e.g., antimicrobial therapy, drug delivery, and biosensors) [65], coating and anti-corrosion [66, 67], the charge storing (e.g., supercapacitors and batteries) [68], and more specifically for environmental engineering (e.g., water treatment and gas separation) [64].

Among CPs, polyaniline (PANI or PAn) and polypyrrole (PPy) with their ramifications are the two most commonly studied CPs in adsorption [64]. For example, the hybrid materials of PANI/Mg-Al layered double oxides were used to reduce hexavalent chromium (Cr(VI)) to Cr(III),thus enabling the detoxification treatment of Cr(VI) in water [69]. Additionally, PANI/Fe_3O_4 nanofibers exhibited magnetism and were able to remove Ag nanoparticles from wastewater [70]. Acetate cellulose composite membranes coated with PANI or PPy exhibited relevant PMs adsorption properties for bromine complexes: 72% for gold and 98% for silver with PANI; 50% for gold, and 97% for silver with PPy [71]. Composing them with other polymers or materials (e.g. carbon-based structures and bio-based materials) promotes adsorption properties, making them high-efficacy agents [63].

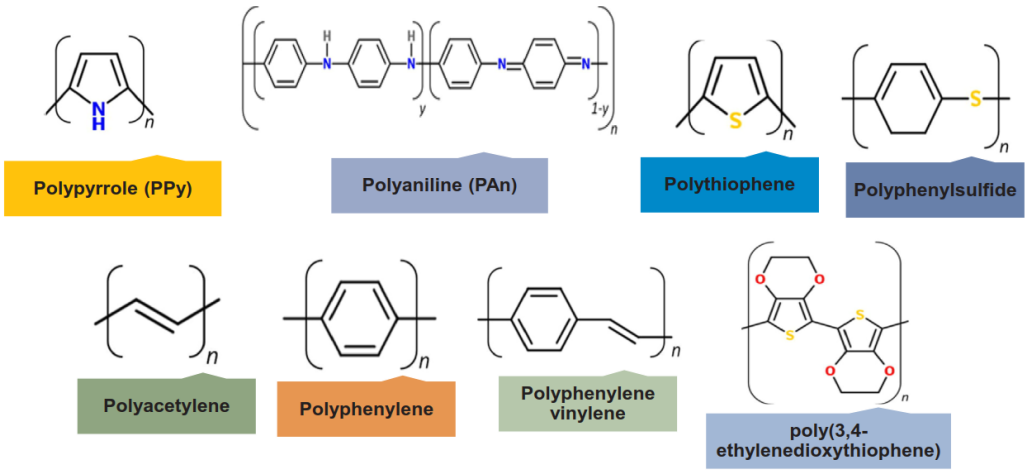

Fig. 1.21. The chemical structures or repeat units of several CPs [64]. © 2019 Elsevier

1.4.4. Poly-N-phenylglycine

Poly-N-phenylglycine (PNPG), first published in 2007 [72], is another conjugated polymer with a skeleton similar to that of PANI. It has low toxicity, which can be demonstrated by several studies in biomedical applications [73, 74]. PNPG is also a promising adsorbent with a high density of functional groups, which may provide numerous adsorption sites. For example, deprotonated PNPG can adsorb more Cu^{2+} via the ionic interaction between Cu^{2+} and the carboxylate group $–COO^-$ [75]. The adsorption of Cu^{2+}, Pb^{2+}, and Cd^{2+} by phytic acid-functionalized PNPG is mostly based on the complexation and electrostatic attraction with $H_2PO_4^-$ groups of phytic acid, which validated the idea of using the active phytic acid to enhance the capacity of PNPG [76]. A ternary nanocomposite of deprotonated PNPG, reduced graphene oxide, and Fe_3O_4 nanoparticle can capture more Cu ions due to the cationic affinity of deprotonated PNPG [77]. In the above base metal adsorption studies, PNPG was pretreated with deprotonation or functionalization. Compared with other CPs or well-studied CPs, PNPG is an emerging adsorbent material whose properties can be further discussed as its research began relatively recently. From the extensive literature investigation at the beginning of our study, it was found that there was no research about the adsorption of PNPG towards PMs from secondary metal resource such as waste PCBs.

1.5. Research topic and contribution of this dissertation

1.5.1 Research topic

To sum up, the research background can be summarized as follows.

(1) The fact that demand for metals exceeds supply and the emergence of dwindling reserves of metals as non-renewable resources make the recycling of metals increasingly important.

(2) E-waste can be considered an urban mine or a secondary metal resource, with higher metal grades than those found in natural ores. However, the current global e-waste recycling situation is not ideal, and there is still great room for improvement. Recycling metals from e-waste is of great economic and environmental importance.

(3) The steps to recover metals from e-waste are similar to those used to produce metals from ores. The commonly used recovery methods in industry include pyrometallurgy and hydrometallurgy, but hydrometallurgy is technically simpler, requires less energy input, and does not release harmful substances.

(4) There are several methods for recovering metals from leaching solutions in the final step of hydrometallurgy. Adsorption is a more suitable recovery method for such low-concentration leaching solutions, and it has the advantages of low cost and high efficiency from the technical and more economical without secondary pollution.

(5) Adsorbent is the key to the adsorption method. The development and utilization of nanomaterials for PMs recycling is consequently attracting tremendous interest due to their unique physical and chemical properties, such as large surface area, high reactivity, and developed porosity.

(6) Poly-N-phenylglycine is a relatively recently-discovered conductive polymer and an emerging adsorbent material of organic nano-adsorbents. It has abundant functional groups and low toxicity. Most importantly, its application research in the recovery of PMs has not been reported before our study.

Based on the above background and facts, we carried out the research on the adsorption of Au and Ag, and achieved the following research objectives one by one.

(1) Au and Ag as the main precious metals, their adsorption by PNPG was studied,

and their adsorption mechanism was explained in detail.

(2) Nano-sized adsorbent is not easy to separate after adsorption. To solve this problem, PNPG adsorbent or with other material was prepared into the form of membranes by a simple method.

(3) More applications of PNPG adsorbent were explored, including selectivity, reusability, stability, and the recovery of PMs from leaching solutions of e-waste.

1.5.2. Contribution of this work

From the point of view of materials, our research on the adsorption mechanism of PMs by PNPG expands the application of this material and fills its gap in PMs recovery which has actively promoted the research progress of this adsorbent, though it is not a new material discovered by us. By preparing nano-structure PNPG into membrane form or composite membrane, the separation problem of adsorbent after adsorption is effectively solved, and providing a choice for the recovery and subsequent use of adsorbent.

From the point of view of metal recovery. Recycling metals from e-waste is a multi-stakeholder task involving society, government, and individuals, and it is also a task to achieve sustainable use of resources for the benefit of future generations. Recovery of metals from e-waste is also a large and systematic process, and adsorption is important as one of the many options for the final step in hydrometallurgy (i.e. recovery of metals from solutions). Based on the adsorption mechanism of PNPG on PMs, this study extended the adsorption application to the real leaching solutions, for contributing to the basic work of PMs recovery and sustainable development.

Reference

[1] T.E. Graedel, G. Gunn, L. Tercero Espinoza, Metal resources, use and criticality, Critical metals handbook, 2014, pp. 1-19. https://doi.org/10.1002/9781118755341.ch1.

[2] L.S. Teseletso, T. Adachi, Future availability of mineral resources: Ultimate reserves and total material requirement, Mineral Economics, (2021). https://doi.org/10.1007/s13563-021-00283-2.

[3] S.M. Jowitt, G.M. Mudd, J.F.H. Thompson, Future availability of non-renewable metal resources and the influence of environmental, social, and governance conflicts on metal production, Communications Earth & Environment, 1 (2020) 13. https://doi.org/10.1038/s43247-020-0011-0.

[4] D.W. Blowes, C.J. Ptacek, J.L. Jambor, et al., 11.5 - The geochemistry of acid mine drainage, H.D. Holland, K.K. Turekian (Eds.) Treatise on geochemistry (second edition), Elsevier, Oxford, 2014, pp. 131-190. https://doi.org/10.1016/B978-0-08-095975-7.00905-0.

[5] V. Fernandez, Some facts on the platinum-group elements, International Review of Financial Analysis, 52 (2017) 333-347. https://doi.org/10.1016/j.irfa.2017.04.003.

[6] T. Bossi, J. Gediga, The environmental profile of platinum group metals, Johnson Matthey Technology Review, 61 (2017) 111-121. https://doi.org/10.1595/205651317X694713.

[7] A. Ramesh, H. Hasegawa, W. Sugimoto, et al., Adsorption of gold(III), platinum(IV) and palladium(II) onto glycine modified crosslinked chitosan resin, Bioresour. Technol., 99 (2008) 3801-3809. https://doi.org/10.1016/j.biortech.2007.07.008.

[8] S. Zhang, Y. Ding, B. Liu, et al., Supply and demand of some critical metals and present status of their recycling in weee, Waste Manag., 65 (2017) 113-127. https://doi.org/10.1016/j.wasman.2017.04.003.

[9] I. Bakas, C. Fischer, S. Haselsteiner, et al., Present and potential future recycling of critical metals in WEEE, (2014). https://epub.wupperinst.org/frontdoor/deliver/index/docId/5687/file/5687_WEEE.pdf. 10 November, 2022.

[10] P. Chancerel, C.E.M. Meskers, C. Hagelüken, et al., Assessment of precious metal flows during preprocessing of waste electrical and electronic equipment, J. Ind. Ecol., 13 (2009) 791-810. https://doi.org/10.1111/j.1530-9290.2009.00171.x.

[11] Historical demand and supply, ICE Benchmark Administration, Metals Focus, Refinitiv GFMS, World Gold Council. https://www.gold.org/goldhub/data/gold-demand-by-country. 7 January, 2023.

[12] Gold mining production volumes data, Metals Focus, World Gold Council. https://www.gold.org/goldhub/data/gold-production-by-country. 4 January, 2023

[13] World silver survey 2022, The Silver Institute. https://www.silverinstitute.org/wp-content/uploads/2022/04/World-Silver-Survey-2022.pdf.

[14] G. Mishra, R. Jha, M.D. Rao, et al., Recovery of silver from waste printed circuit boards (WPCBs) through hydrometallurgical route: A review, Environmental Challenges, 4 (2021) 100073-100081. https://doi.org/10.1016/j.envc.2021.100073.

[15] World silver survey 2022, The Silver Institute. https://www.silverinstitute.org/wp-content/uploads/2022/04/World-Silver-Survey-2022.pdf. 12 January, 2023.

[16] Silver mining in history, The Silver Institute. https://www.silverinstitute.org/silver-mining-history/. 6 January, 2023.

[17] J.O. Nriagu, A history of global metal pollution, Science, 272 (1996) 223-223. https://doi.org/10.1126/science.272.5259.223.

[18] F.X. Han, A. Banin, Y. Su, et al., Industrial age anthropogenic inputs of heavy metals into the pedosphere, Naturwissenschaften, 89 (2002) 497-504. https://doi.org/10.1007/s00114-002-0373-4.

[19] I.M.S.K. Ilankoon, Y. Ghorbani, M.N. Chong, et al., E-waste in the international context – A review of trade flows, regulations, hazards, waste management strategies and technologies for value recovery, Waste Manag., 82 (2018) 258-275. https://doi.org/10.1016/j.wasman.2018.10.018.

[20] A. Akcil, C. Erust, C.S. Gahan, et al., Precious metal recovery from waste printed circuit boards using cyanide and non-cyanide lixiviants – A review, Waste Manag., 45 (2015) 258-271. https://doi.org/10.1016/j.wasman.2015.01.017.

[21] J. Cui, L. Zhang, Metallurgical recovery of metals from electronic waste: A

review, J. Hazard. Mater., 158 (2008) 228-256. https://doi.org/10.1016/j.jhazmat.2008.02.001.

[22] L.H. Yamane, V.T. de Moraes, D.C.R. Espinosa, et al., Recycling of WEEE: Characterization of spent printed circuit boards from mobile phones and com puters, Waste Manag., 31 (2011) 2553-2558. https://doi.org/10.1016/j.wasman.2011.07.006.

[23] V. Forti, C. Baldé, R. Kuehr, et al., The global e-waste monitor 2020. Quantities, flows, and the circular economy potential, 2020. https://www.itu.int/en/ITU-D/Environment/Documents/Toolbox/GEM_2020_def.pdf.

[24] R. Widmer, H. Oswald-Krapf, D. Sinha-Khetriwal, et al., Global perspectives on e-waste, Environmental Impact Assessment Review, 25 (2005) 436-458. https://doi.org/10.1016/j.eiar.2005.04.001.

[25] Country and regional sheets, The Global E-waste Statistics Partnership. https://globalewaste.org/country-sheets/. 8 January, 2023.

[26] R.E. Ouabo, M.B. Ogundiran, A.Y. Sangodoyin, et al., Ecological risk and human health implications of heavy metals contamination of surface soil in e-waste recycling sites in douala, cameroun, Journal of Health and Pollution, 9 (2019). https://doi.org/10.5696/2156-9614-9.21.190310.

[27] A. Islam, T. Ahmed, M.R. Awual, et al., Advances in sustainable approaches to recover metals from e-waste-a review, J. Clean. Prod., 244 (2020) 118815. https://doi.org/10.1016/j.jclepro.2019.118815.

[28] Y. Jinglei, E. Williams, J. Meiting, Review and prospects of recycling methods for waste printed circuit boards, 2009 IEEE International Symposium on Sustain able Systems and Technology, 2009, pp. 1-5. https://doi.org/10.1109/ISSST.2009.5156727.

[29] Y.J. Park, D.J. Fray, Recovery of high purity precious metals from printed circuit boards, J. Hazard. Mater., 164 (2009) 1152-1158. https://doi.org/10.1016/j.jhazmat.2008.09.043.

[30] C.Y. Yuan, H.C. Zhang, G. McKenna, et al., Experimental studies on cryogenic recycling of printed circuit board, The International Journal of Advanced

Manufacturing Technology, 34 (2007) 657-666. https://doi.org/10.1007/s00170-006-0634-z.

[31] J.-C. Lee, H.T. Song, J.-M. Yoo, Present status of the recycling of waste electrical and electronic equipment in korea, Resour. Conserv. Recycl., 50 (2007) 380-397. https://doi.org/10.1016/j.resconrec.2007.01.010.

[32] A. Kumar, M. Holuszko, D.C.R. Espinosa, E-waste: An overview on generation, collection, legislation and recycling practices, Resour. Conserv. Recycl., 122 (2017) 32-42. https://doi.org/10.1016/j.resconrec.2017.01.018.

[33] A. Khaliq, M.A. Rhamdhani, G. Brooks, et al., Metal extraction processes for electronic waste and existing industrial routes: A review and australian perspective, Resources, 3 (2014) 152-179. https://doi.org/10.3390/resources3010152.

[34] A. Ashiq, J. Kulkarni, M. Vithanage, Chapter 10 - Hydrometallurgical recovery of metals from e-waste, in: M.N.V. Prasad, M. Vithanage (Eds.) Electronic waste management and treatment technology, Butterworth-Heinemann, 2019, pp. 225-246. https://doi.org/10.1016/B978-0-12-816190-6.00010-8.

[35] V. Innocenzi, I. De Michelis, B. Kopacek, et al., Yttrium recovery from primary and secondary sources: A review of main hydrometallurgical processes, Waste Manag., 34 (2014) 1237-1250. https://doi.org/10.1016/j.wasman.2014.02.010.

[36] R. Jha, M.D. Rao, A. Meshram, et al., Potential of polymer inclusion membr ane process for selective recovery of metal values from waste printed circuit boards: A review, J. Clean. Prod., 265 (2020) 121621. https://doi.org/10.1016/j.jclepro.2020.121621.

[37] M. Huy Do, G. Tien Nguyen, U. Dong Thach, et al., Advances in hydrometallurgical approaches for gold recovery from e-waste: A comprehensive review and perspectives, Miner. Eng., 191 (2023) 107977. https://doi.org/10.1016/j.mineng.2022.107977.

[38] Z. Chang, L. Zeng, C. Sun, et al., Adsorptive recovery of precious metals from aqueous solution using nanomaterials – A critical review, Coord. Chem. Rev., 445 (2021) 214072. https://doi.org/10.1016/j.ccr.2021.214072.

[39] J. Wang, X. Guo, Adsorption kinetic models: Physical meanings, applications,

and solving methods, J. Hazard. Mater., 390 (2020) 122156. https://doi.org/10.1016/j.jhazmat.2020.122156.

[40] J. Wang, X. Guo, Adsorption isotherm models: Classification, physical meaning, application and solving method, Chemosphere, 258 (2020) 127279-127303. https://doi.org/10.1016/j.chemosphere.2020.127279.

[41] M.A. Al-Ghouti, D.A. Da'ana, Guidelines for the use and interpretation of adsorption isotherm models: A review, J. Hazard. Mater., 393 (2020) 122383-122404. https://doi.org/10.1016/j.jhazmat.2020.122383.

[42] I. Langmuir, The constitution and fundamental properties of solids and liquids. Part I. Solids, JACS, 38 (1916) 2221-2295. https://doi.org/10.1021/ja02268a002.

[43] I. Langmuir, The adsorption of gases on plane surfaces of glass, mica and platinum, JACS, 40 (1918) 1361-1403. https://doi.org/10.1021/ja02242a004.

[44] X. Chen, Y. Xiang, L. Xu, et al., Recovery and reduction of Au(III) from mixed metal solution by thiourea-resorcinol-formaldehyde microspheres, J. Hazard. Mater., 397 (2020) 122812-122820. https://doi.org/10.1016/j.jhazmat.2020.122812.

[45] G. Crini, E. Lichtfouse, L.D. Wilson, et al., Conventional and non-conventional adsorbents for wastewater treatment, Environ. Chem. Lett., 17 (2019) 195-213. https://doi.org/10.1007/s10311-018-0786-8.

[46] R. Khosravi, A. Azizi, R. Ghaedrahmati, et al., Adsorption of gold from cyanide leaching solution onto activated carbon originating from coconut shell—optimization, kinetics and equilibrium studies, J. Ind. Eng. Chem., 54 (2017) 464-471. https://doi.org/10.1016/j.jiec.2017.06.036.

[47] P. Navarro, C. Vargas, M. Alonso, et al., The adsorption of gold on activated carbon from thiosulfate-ammoniacal solutions, Gold Bull., 39 (2006) 93-97. https://doi.org/10.1007/BF03215535.

[48] A. Seyedhakimi, S.A. Bastami, S. Ghassa, et al., Exploring relationships between various activations of granular activated carbon on silver and gold adsorption: A kinetic and equilibrium study, Sep. Sci. Technol., 54 (2019) 1710-1721. https://doi.org/10.1080/01496395.2018.1540635.

[49] C.N. Mpinga, S.M. Bradshaw, G. Akdogan, et al., The extraction of Pt, Pd and Au from an alkaline cyanide simulated heap leachate by granular activated carbon, Miner. Eng., 55 (2014) 11-17. https://doi.org/10.1016/j.mineng.2013.09.001.

[50] C. Liu, Q. Wang, F. Jia, et al., Adsorption of heavy metals on molybdenum disulfide in water: A critical review, J. Mol. Liq., 292 (2019) 111390. https://doi.org/10.1016/j.molliq.2019.111390.

[51] M. Fomina, G.M. Gadd, Biosorption: Current perspectives on concept, definition and application, Bioresour. Technol., 160 (2014) 3-14. https://doi.org/10.1016/j.biortech.2013.12.102.

[52] R. Fan, F. Xie, X. Guan, et al., Selective adsorption and recovery of Au(III) from three kinds of acidic systems by persimmon residual based bio-sorbent: A method for gold recycling from e-wastes, Bioresour. Technol., 163 (2014) 167-171. https://doi.org/10.1016/j.biortech.2014.03.164.

[53] T.H. Bui, S. Jeon, Y. Lee, Facile recovery of gold from e-waste by integrating chlorate leaching and selective adsorption using chitosan-based bioadsorbent, J. Environ. Chem. Eng., (2020) 104661-104669. https://doi.org/10.1016/j.jece.2020.104661.

[54] Y. Göksungur, S. Üren, U. Güvenç, Biosorption of cadmium and lead ions by ethanol treated waste baker's yeast biomass, Bioresour. Technol., 96 (2005) 103-109. https://doi.org/10.1016/j.biortech.2003.04.002.

[55] B. Feng, C. Yao, S. Chen, et al., Highly efficient and selective recovery of Au(III) from a complex system by molybdenum disulfide nanoflakes, Chem. Eng. J., 350 (2018) 692-702. https://doi.org/10.1016/j.cej.2018.05.130.

[56] S. Zeng, F. Jia, B. Yang, et al., In-situ reduction of gold thiosulfate complex on molybdenum disulfide nanosheets for a highly-efficient recovery of gold from thiosulfate solutions, Hydrometallurgy, 195 (2020) 105369. https://doi.org/10.1016/j.hydromet.2020.105369.

[57] M.K. Jha, J.-C. Lee, M.-S. Kim, et al., Hydrometallurgical recovery/recycling of platinum by the leaching of spent catalysts: A review, Hydrometallurgy, 133 (2013) 23-32. https://doi.org/10.1016/j.hydromet.2012.11.012.

[58] R. Chen, B. Lin, R. Luo, Recent progress in polydopamine-based composites for the adsorption and degradation of industrial wastewater treatment, Heliyon, 8 (2022) e12105. https://doi.org/10.1016/j.heliyon.2022.e12105.

[59] S. Bashir, S.K. Moosvi, T. Jan, et al., Development of polythiophene/prussian red nanocomposite with dielectric, photocatalytic and metal scavenging properties, J. Electron. Mater., 49 (2020) 4018-4027. https://doi.org/10.1007/s11664-020-08117-7.

[60] H. Lin, B. Jie, J. Ye, et al., Recent advance of macroscopic metal-organic frameworks for water treatment: A review, Surfaces and Interfaces, 36 (2023) 102564. https://doi.org/10.1016/j.surfin.2022.102564.

[61] J. Tang, Y. Chen, S. Wang, et al., Highly efficient metal-organic frameworks adsorbent for Pd(II) and Au(III) recovery from solutions: Experiment and mechanism, Environ. Res., 210 (2022) 112870. https://doi.org/10.1016/j.envres.2022.112870.

[62] Y. Chen, J. Tang, S. Wang, et al., Facile preparation of a remarkable MOF adsorbent for Au(III) selective separation from wastewater: Adsorption, rege neration and mechanism, J. Mol. Liq., 349 (2022) 118137. https://doi.org/10.1016/j.molliq.2021.118137.

[63] A. Taghizadeh, M. Taghizadeh, M. Jouyandeh, et al., Conductive polymers in water treatment: A review, J. Mol. Liq., 312 (2020) 113447. https://doi.org/10.1016/j.molliq.2020.113447.

[64] E. Eskandari, M. Kosari, M.H. Davood Abadi Farahani, et al., A review on polyaniline-based materials applications in heavy metals removal and catalytic processes, Sep. Purif. Technol., 231 (2020) 115901. https://doi.org/10.1016/j.seppur.2019.115901.

[65] E.N. Zare, P. Makvandi, B. Ashtari, et al., Progress in conductive polyaniline-based nanocomposites for biomedical applications: A review, J. Med. Chem., 63 (2020) 1-22. https://doi.org/10.1021/acs.jmedchem.9b00803.

[66] F. Gao, J. Mu, Z. Bi, et al., Recent advances of polyaniline composites in anticorrosive coatings: A review, Prog. Org. Coat., 151 (2021) 106071. https:

//doi.org/10.1016/j.porgcoat.2020.106071.

[67] H. Chen, H. Fan, N. Su, et al., Highly hydrophobic polyaniline nanoparticles for anti-corrosion epoxy coatings, Chem. Eng. J., 420 (2021) 130540. https://doi.org/10.1016/j.cej.2021.130540.

[68] H. Zhuo, Y. Hu, Z. Chen, et al., Cellulose carbon aerogel/PPy composites for high-performance supercapacitor, Carbohydr. Polym., 215 (2019) 322-329. https://doi.org/10.1016/j.carbpol.2019.03.101.

[69] F.-L. Long, C.-G. Niu, N. Tang, et al., Highly efficient removal of hexavalent chromium from aqueous solution by calcined Mg/Al-layered double hydroxides /polyaniline composites, Chem. Eng. J., 404 (2021) 127084. https://doi.org/10.1016/j.cej.2020.127084.

[70] Q. Yang, Removal and reuse of Ag nanoparticles by magnetic polyaniline/Fe_3O_4 nanofibers, J. Mater. Sci., 53 (2018) 8901-8908. https://doi.org/10.1007/s10853-018-2181-z.

[71] S. Rascón-Leon, M.M. Castillo-Ortega, I. Santos-Sauceda, et al., Selective adsorption of gold and silver in bromine solutions by acetate cellulose composite membranes coated with polyaniline or polypyrrole, Polym. Bull., 75 (2018) 3241-3265. https://doi.org/10.1007/s00289-017-2206-9.

[72] X. Lei, Z. Su, Novel conducting polyaniline copolymers of aniline and N-phenylglycine, Mater. Lett., 61 (2007) 1158-1161. https://doi.org/10.1016/j.matlet.2006.06.076.

[73] B.-P. Jiang, L. Zhang, X.-L. Guo, et al., Poly(N-phenylglycine)-based nanoparticles as highly effective and targeted near-infrared photothermal therapy/photodynamic therapeutic agents for malignant melanoma, Small, 13 (2017) 1602496-1602510. https://doi.org/10.1002/smll.201602496.

[74] C. Ruan, C. Liu, H. Hu, et al., NIR-II light-modulated thermosensitive hydrogel for light-triggered cisplatin release and repeatable chemo-photothermal therapy, Chemical Science, 10 (2019) 4699-4706. https://doi.org/10.1039/C9SC00375D.

[75] J.H. Doh, J.H. Kim, H.J. Kim, et al., Enhanced adsorption of aqueous copper(II) ions using dedoped poly-N-phenylglycine nanofibers, Chem. Eng. J., 277 (2015)

352-359. http://dx.doi.org/10.1016/j.cej.2015.04.120.

[76] M. Ben Ali, F. Wang, R. Boukherroub, et al., High performance of phytic acid-functionalized spherical poly-phenylglycine particles for removal of heavy metal ions, Appl. Surf. Sci., 518 (2020) 146206-146213. https://doi.org/10.1016/j.apsusc.2020.146206.

[77] H.J. Kim, H. Choi, A.K. Sharma, et al., Recyclable aqueous metal adsorbent: Synthesis and Cu(II) sorption characteristics of ternary nanocomposites of Fe_3O_4 nanoparticles@graphene-poly-N-phenylglycine nanofibers, J. Hazard. Mater., 401 (2021) 123283. https://doi.org/10.1016/j.jhazmat.2020.123283.

Chapter 2

Materials, methods, equipment and characterization

This chapter mainly introduces the detailed information of chemical reagents, synthesis methods, experimental devices and characterization equipment used in the research of this thesis. If relevant contents are involved in the subsequent chapters, only a brief mention will be given instead of a detailed description.

2.1. Materials

The detailed information of materials used in this research was listed in **Table 2.1**. Except for the standard solution, which is analytically pure, all other chemical reagents were chemically pure or even more. Target-concentration acid or base solutions were prepared by diluting or dissolving the corresponding reagent.

2.2. General synthesis methods

The preparation methods of the main samples will be shown as follows. The detailed procedure will not be redescribed in the following chapters if relevant contents are involved, but the dosage of chemical reagents will be clearly described if necessary.

2.2.1. Synthesis of PNPG

PNPG can be synthesized by polymerization of the N-Phenylglycine (NPG) monomer, where ammonium peroxodisulfate (APS) acts as an oxidant and dilute sulfuric acid provides the necessary acidic environment [1, 2]. First, NPG (2.0 g) was completely dissolved in 100 mL H_2SO_4 (0.1 mol·L^{-1}) by ultrasound to form the NPG–H_2SO_4 mixture, and then it was poured into a flask. The others, APS–H_2SO_4 mixture, was prepared by completely dissolving 3.2 g APS in 100 mL H_2SO_4 (0.1 mol·L^{-1}) by ultrasound, and then it was transferred to a separator funnel. This acidic APS solution was slowly added to the as-prepared NPG acid solution at a rate of approximately one drop in every 4 s. Constant stirring at 700 rpm was provided to avoid local overheating,

Table 2.1 Information of materials

Materials	**Maker**
N-Phenylglycine ($C_6H_5NHCH_2COOH$)	Kanto Chemical Co., Inc. (Japan)
ammonium peroxodisulfate $(NH_4)_2S_2O_8$)	Kanto Chemical Co., Inc. (Japan)
Multi-walled carbon nanotubes (60–100 nm (diameter), >5 mm (length))	Tokyo Chemical Industry Co. Ltd. (Japan)
Mixed cellulose ester membranes (pore size: 0.2 μm, diameter: 47 mm)	Toyo Roshi Kaisha, Ltd. (Japan)
Standard solutions (1000 $mg \cdot L^{-1}$) of Au(III), Pb(II), Co(II), Ni(II), Cu(II), Zn(II), Al(III), and Fe(III), Ag(I), Cd(II), Pt(IV), Sn(II), Ca(II), Mg(II)	Kanto Chemical Co., Inc. (Japan)
$CS(NH_2)_2$ (thiourea)	Kanto Chemical Co., Inc. (Japan)
H_2SO_4 (98%)	Fujifilm Wako Pure Chemical Corporation (Japan)
HNO_3 (69%)	Fujifilm Wako Pure Chemical Corporation (Japan)
HCl (35–37%)	Fujifilm Wako Pure Chemical Corporation (Japan)
NaOH	Kanto Chemical Co., Inc. (Japan)
Na_2SO_4	Kanto Chemical Co., Inc. (Japan)
NaCl	Fujifilm Wako Pure Chemical Corporation (Japan)
$NaNO_3$	Nacalai Tesque (Japan)
Waste PCBs from end-of-life computers	Kosaka Smelting & Refining Co., Ltd. (Japan)
MSWI fly ash	Akita City Environment Center (Japan)

and an ice-water bath environment (approximately 0°C) was set up to facilitate polymerization. After the reaction, the mixture was kept at the same stirring speed for 24 h. Subsequently, the mixture was filtered to collect the solid product; and then the solid product was washed with deionized (DI) water at least five times until the filtrate

was colorless, and the no-impurities PNPG will be obtained.

One part of the PNPG was dried at 60 °C for 24 h to obtain the PNPG particles. The other part was immediately dispersed in a certain amount of DI water by ultrasound to form a PNPG suspension which used to prepare membrane samples, as shown in the following section.

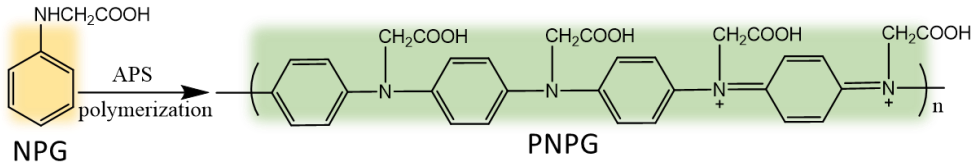

Fig. 2.1. The polymerization of NPG to form PNPG.

2.2.2. Preparation of PNPG membranes

PNPG suspension, obtained in the above section, was performed by vacuum filtration to form PNPG membranes. Firstly, the concentration of the PNPG suspension was calculated by carefully vacuum filtering a given volume (1.0 mL) of the dispersion and weighing the dried solid (dried at 60 °C for 24 h). Subsequently, the target-mass PNPG membranes (e.g. 2 mg, 4 mg, or 5 mg) were prepared from a certain amount of the PNPG suspension through vacuum filtration, in which the mixed cellulose ester membrane acted as the supporting layer. The PNPG membranes were then dried at 60 °C for 24 h before experiment.

2.2.3. Preparation of the PNPG@MWCNT membranes

The sum of the masses of the multi-walled carbon nanotubes (MWCNT) and PNPG was fixed at 4 mg. First, x mg of MWCNT (solid) was added to DI water and subjected to ultrasonic irradiation at 20 kHz for 4 min, in which the probe of the ultrasonic horn was directly immersed. Subsequently, a certain volume of PNPG suspension was added to the MWCNT dispersion and sonicated for another 4 min. Note that the required volume of PNPG suspension is equal to the quotient of $(4-x)$ mg and concentration. To prepare the PNPG, PNPG@MWCNT, and MWCNT membranes (marked as P$(4-x)$Mx according to the composition), the solutions after ultrasonic

treatment were immediately filtered onto the MCE membrane by vacuum filtration, followed by drying at 60 ℃ for 12 h.

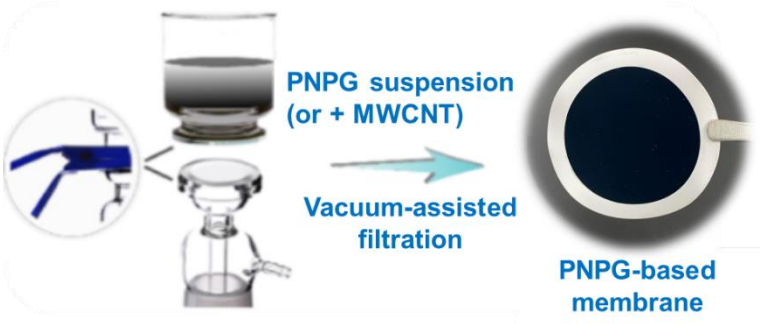

Fig. 2.2. The Preparation of PNPG-based membrane by vacuum filtration while mixed cellulose ester membrane act as the supporting layer.

2.3. Equipment

This section lists the detailed information of equipment and instruments used in this thesis. It will not be redescribed in the following sections except necessary.

2.3.1. Equipment for adsorption experiments

Yamato WG250 (Japan) water purification equipment was used to produce deionized water (DI water) whose conductivity is less than 0.06×10^{-4} S/m.

Branson Ultrasonics Sonifier 250 (USA) was used to disperse samples in DI water.

TOA-DKK HM-41X pH meter (Japan) was used to evaluate the pH of solutions.

Sartorius BP211D (Germany), a five-digit electrical balance, was used to measure the mass of the materials

Laboratory shaker Adolf Kühner AG LSR-V-50 (Switzerland), and Thomas T-3SJ (Japan), provided the shaking environment in the adsorption experiment.

2.3.2. Equipment for characterization

A zeta potential analyzer (Zeta Plus, Brookhaven, USA) was used to measure the zeta potential of the samples in an electrolyte of 1 $mmol \cdot L^{-1}$ KCl.

Fourier transform infrared (FTIR) analysis (FTIR-6600, Jasco, Japan) was used to obtain the functional groups information of the samples through using an IRT-5200

accessory with a KBr tablet on which a few milligrams of the sample were homogeneously dispersed. The FTIR spectra, obtained in the transmittance mode, were recorded from 3600 cm^{-1} to 600 cm^{-1} and scanned 20 times with a resolution of 4 cm^{-1}.

X-ray powder diffraction (XRD) patterns were obtained using the X'Pert PRO (PANalytical, Netherlands) with Cu-Kα radiation of wavelength 1.5406 Å (generator voltage = 45 kV, tube current = 40 mA, fixed divergence slit size = 0.76 mm). All XRD patterns were recorded at 2θ from 10° to 80° with a step size of 0.017°.

X-ray photoelectron spectroscopy (XPS) was utilized to characterize the chemical composition using a PHI Quantera II (Ulvac-Phi, Japan) with Mg Kα radiation (powered at 150 W). The pass energies were 160 eV and 40 eV for the wide spectra and individual spectra, respectively, and each measured element was scanned 10 times. The XPS profiles were calibrated by setting the C 1s binding energy at 284.8 eV, and the characteristic peaks were fitted using the software XPSPEAK41.

Scanning electron microscopy (SEM) was employed to observe the morphology of all the dried samples using the device S-4300 (Hitachi, Japan) at an accelerating voltage of 5 kV. The equipped energy dispersion spectroscopy (EDS), in conjunction with SEM, was used to characterize the distribution of elements. Prior to SEM characterization, all the membrane samples were dried at 60 ℃ for 24 h, cut into small pieces, and mounted on the conductive adhesive, and then platinum spraying was performed to enhance the conductivity of the sample surface for more clear observation.

Transmission electron microscopy (TEM) images were obtained using a Hitachi HT7830 microscope (Japan) and showed the microstructures of the adsorbents.

Outgassed samples were characterized by N_2 adsorption–desorption method at 77 K using the Autosorb IQ instrument (ASIQM0V002-5, Quantachrome, USA), where Brunauer–Emmett–Teller (BET) surface areas were determined using the multi-point BET method under a relative pressure of 0.05–0.35, and the pore volume and pore diameter were calculated by the Barrett–Joyner–Halenda (BJH) method.

The plasma atomic emission spectrometer (ICPE-9000, Shimadzu, Japan; ICPE-9820, Shimadzu, Japan) was used to determine the concentrations of metal ions before and after adsorption.

UV-vis spectroscopy (V-560, Jasco, Japan) was used to verify the presence of gold nanoparticles in the post-adsorption solution.

A portable X-ray fluorescence analyzer (S1 TITAN, Bruker, USA) was operated to quickly analyze the elemental composition of the MSWI fly ash.

Reference

[1] M.R. Nabid, S.S. Taheri, R. Sedghi, et al., Chemical synthesis and characterization of water-soluble, conducting poly(N-phenylglycine), Iran. Polym. J., 17 (2008) 365-371. https://www.sid.ir/en/Journal/ViewPaper.aspx?ID=107888.

[2] Z. Lin, T. Wu, J. Shi, et al., Poly(N-phenylglycine)-based bioinspired system for stably and efficiently enhancing solar evaporation, ACS Sustainable Chem. Eng., 9 (2021) 448-457. https://doi.org/10.1021/acssuschemeng.0c07608.

Chapter 3

Selective and sensitive adsorption of Au(III) by poly(N-phenylglycine)

3.1. Introduction

Population growth, economic development, changing lifestyles, and the faster update and widespread use of electronic devices have all contributed to an increase in electronic waste (e-waste) in recent years [1, 2]. On the other hand, the current recycling of e-waste cannot keep up with its generation, as shown by the fact that in the past decade (2010–2019), the global e-waste generation has increased by nearly 38%, while the recycling of e-waste has increased by less than 20% [3]. Therefore, considerable effort needs to be devoted to recycling activities for achieving one of the targets of the Sustainable Development Goals 12: "by 2030, waste generation should be substantially reduced through prevention, reduction, recycling, and reuse" [4].

E-waste can be considered an "urban mine", since the components of e-waste reportedly contain a higher concentration of metallic materials than commonly found in primary ores [5, 6]. According to published data, at a current recycling rate of less than 20%, 4 million metric tons of raw materials valued at $10 billion can be recycled environmentally from global e-waste [7]. In reality, the idea of using metals from recyclable e-waste to make medals for the 2020 Tokyo Olympic Games has gone from proposal to practice, and this success has gradually drawn international attention to issues related to e-waste treatment and the great economic value of this urban mine [8, 9]. Printed circuit boards (PCBs) are an indispensable part of all electronics, consisting of metals, organics, and refractories in a ratio of 4:3:3 [10]. PCBs account for approximately 4–7% of the total mass of global e-waste [6]. Hsu et al. highlighted that PCBs had the highest contents of precious metals (e.g., Au, Ag, Pd, etc.) and showed the highest monetary value of gold [10]. Gold is a precious metal with limited reserves but is widely used in jewelry, dentistry, catalysts, the electronics industry, and other

fields [11-13]. Therefore, it is worthwhile to study the recycling of gold from PCBs for economic and environmental benefits.

Precious metals can be recovered by pyrometallurgy and hydrometallurgy. The low quantity and low purity of gold found in e-waste make pyrometallurgy an inefficient method to melt and recover gold from e-waste. Traditionally, gold is recovered by hydrometallurgical methods, which have the advantages of less air pollution, full utilization of leachate, etc. [14-16]. In leaching or aqueous solutions, gold is normally extracted by metal displacement. However, the adsorption method is more suitable for enrichment or recovery at very low concentrations. The adsorption method is easy to operate, does not generate secondary pollutants, and is apparently more economically and environmentally friendly [17]. However, traditional adsorbents, such as activated carbon, suffer from poor selectivity and low adsorption capacity. To maximize the adsorption performance, new adsorbents with excellent adsorption efficiencies, such as graphene oxide [18], carbon nanotubes [19], MoS_2 nanosheet [20], and polymers [21, 22], have been developed and have become a focal point in research.

The advantages of polymers include large surface area, adjustable surface chemical properties, good mechanical rigidity, uniform pore size distribution, and easy regeneration under mild conditions. Therefore, polymers can be considered as highly efficient metal adsorption materials [17, 23]. Poly-N-phenylglycine (PNPG), formed by the polymerization of N-phenylglycine (NPG) monomer [24], is a promising adsorbent with a high density of functional groups, which may provide numerous adsorption sites. It has been reported that deprotonated PNPG can adsorb more Cu^{2+} via ionic attraction which was evidenced by the increase of maximum adsorption capacity from 9.2 to 12.8 $mg \cdot g^{-1}$ [25]. The adsorption of Cu^{2+}, Pb^{2+}, and Cd^{2+} by phytic acid-functionalized PNPG mostly based on the complexation and electrostatic attraction with $H_2PO_4^-$ groups of phytic acid, which validated the idea of using the active phytic acid to enhance the capacity of PNPG [26]. A ternary nanocomposite of deprotonated PNPG, reduced graphene oxide, and Fe_3O_4 nanoparticle could be captured more Cu ions due to the cationic affinity of deprotonated PNPG [27]. To date, there have been no studies on the other adsorption mechanisms of PNPG, or the recovery

performance of original PNPG on gold ions. When talking about Au(III) adsorption, some polymer-based adsorbents have been reported with good adsorption capacity of Au [28, 29]. However, it is still technically challenging because of the low concentration of gold ions and the burden of rapid adsorbent separation after adsorption. Based on this consideration, it is more attractive to study the adsorption sensitivity of Au(III) by PNPG through use of a PNPG membrane, which can potentially uncomplicate the separation of nano-adsorbents during gold recovery.

In this study, the effect of pH, time, and concentration on the Au adsorption behavior of PNPG particles, as well as the kinetics, isotherms, and adsorption mechanisms of this polymer adsorbent, were investigated. The stability, selectivity, and reusability of the PNPG membrane were evaluated to explore its potential for practical applications. Finally, the recovery performance of the leaching solutions of real waste PCBs was investigated.

3.2. Experimental section

3.2.1. Materials

Used materials were N-Phenylglycine (NPG), ammonium peroxodisulfate (APS), thiourea, mixed cellulose ester (MCE) membranes, H_2SO_4, HNO_3, HCl, NaOH, Na_2SO_4, NaCl, $NaNO_3$, and standard solutions (1000 $mg \cdot L^{-1}$) of Au(III), Pb(II), Co(II), Ni(II), Cu(II), Zn(II), Al(III), and Fe(III). Samples of waste PCBs from end-of-life computers was pre-broken into 20 mm.

3.2.2. Synthesis of PNPG particles and PNPG membranes

PNPG can be prepared according to the reported polymerization method using ammonium peroxodisulfate (APS) as an oxidant under acidic conditions [30, 31]. Please refer to Section 2.2.1 for the specific preparation of PNPG particles and Section 2.2.2 for the detailed procedure of preparing 2-mg PNPG membranes.

3.2.3. Characterization

Fourier-transform infrared (FT-IR) spectroscopy with KBr pellets was used to

characterize the functional groups of the adsorbent, and the spectra were recorded in the wavenumber range of 500–4000 cm^{-1} using a Spectrum Two™ N system (PerkinElmer, USA). X-ray powder diffraction (XRD) patterns with 2θ = 10−80° were obtained using a Rigaku 18VB3-450 (Japan) diffractometer with Cu-Kα radiation. The concentrations of ions before and after adsorption were determined using ICPE-9000 (Shimadzu, Japan)

Other characterization methods, such as zeta potential analysis, SEM, EDS, TEM, XPS, UV-vis, BET surface areas were the same as shown in Section 2.3.2.

3.2.4. Adsorption experiments of PNPG particles

The working solutions of Au(III) were prepared by diluting the standard solution for target concentrations and adjusting with 0.1 $mol \cdot L^{-1}$ HCl or NaOH to obtain the target pH. PNPG (2.0 mg) was added to 30 mL of Au(III) solution. The entire adsorption process was kept static and maintained at 25 °C in a constant-temperature water bath. After adsorption, the samples were independently filtered through mixed cellulose ester syringe filters (pore size = 0.2 μm).

After a period (t (h)) of contact, the adsorption capacity q_t ($mg \cdot g^{-1}$) and adsorption efficiency E_t (%) were used to quantify the adsorption behavior of Au(III) on PNPG. The abovementioned parameters can be calculated using Eqs. (1) and (2), respectively:

$$q_t = \frac{(c_0 - c_t)V}{m} \tag{1}$$

$$E_t = \frac{(c_0 - c_t)}{c_0} \times 100 \tag{2}$$

where V (L) is the volume of the Au(III) solution, m (g) is the mass of adsorbent, c_0 ($mg \cdot L^{-1}$) is the initial concentration, and c_t ($mg \cdot L^{-1}$) is the residual concentration at time t. When equilibrium is reached, the residual concentration c_t is equal to the equilibrium concentration c_e, and the equilibrium adsorption capacity q_e, and

equilibrium adsorption efficiency E_e can be calculated.

3.2.5. Adsorption experiments of PNPG membrane

To explore the actual adsorption performance of the PNPG membrane, it was directly immersed in the working solution at a pH of 1. After adsorption, the PNPG membrane was removed promptly, and the remaining concentration of gold ions was determined using ICPE-9000.

The working solutions include a single Au(III) solution, a mixed solution containing multiple metal ions, and a real leaching solution of waste PCBs. The first two solutions were prepared by diluting the standard solutions, and the leaching solution was obtained using the method shown as follow.

Waste printed circuit boards (PCBs) were shredded and treated by the method shown in **Fig. 3.1**, and the samples of 1–2 mm were chosen for the subsequent preparation experiment of the leaching solution of waste PCBs (**Fig. 3.2**). The 1–2 mm samples were treated with supercritical water, and the resin part was dissolved while the insoluble part was separated. This insoluble part, including metals and other residues, was ground with a mortar, and then gravity separation was carried out and the obtained concentrates were for subsequent use. 3.0 g concentrates were leached with 30 ml 69% HNO_3 (heated to 100 ℃, stirred at 300 rpm for 20 min), and most of the metals such as Cu, Pb, and Zn were dissolved at this time. After the reaction, the solid obtained by filtration was leached with 40 mL fresh aqua regia (heated to 100 ℃, stirred at 300 rpm for 30 min), and the filtrate was adjusted to attain the leaching solution containing Au with pH = 1.

Fig. 3.1. The pre-treatment of waste PCBs.

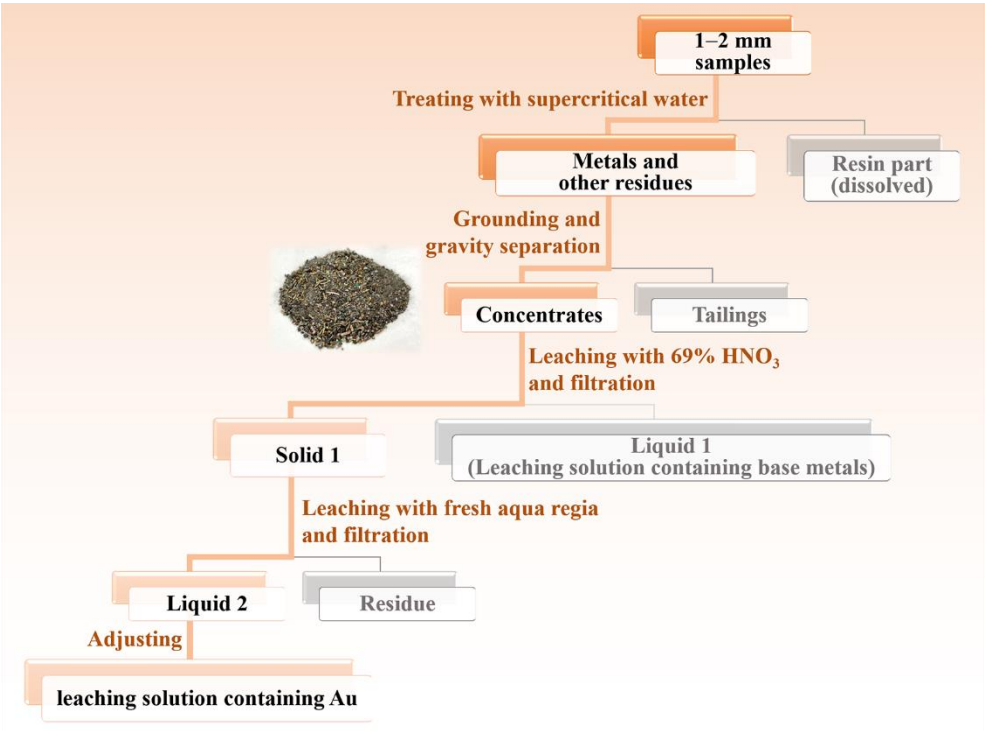

Fig. 3.2. The preparation of leaching solution containing Au.

3.3. Results and discussion

3.3.1. Characterization of PNPG particles

As we mentioned in the synthesis step, the PNPG particles were prepared by the polymerization of NPG using APS as an oxidant. The industrial price of used chemicals was derived from the chemical e-commence platforms MOLBASE and ChemAnalyst, and shown below: NPG (US$ 2.84×10^3/ton), APS (US$ 2.64×10^3/ton), H_2SO_4 (US$ 0.124×10^3/ton). According to the synthetic ratio, the approximate production cost of PNPG is $\$7.185\times10^3$ /ton, which is relatively lower than that of modified cellulose adsorbent (US$ 8.7×10^3/ton) [32], single-walled or multi-wall carbon nanotubes (US$ 4.4×10^8/ton, 4.8×10^7/ton) [33]. The cost analysis indicates that PNPG is a relatively cost-effective adsorbent with potential for real applications.

The Tyndall scattering effect, in which a clear laser beam pathway appears in the colloid, is easily observed in the as-prepared dark-green PNPG suspension (**Fig. 3.3a**), indicating the presence of nanoscale PNPG particles and good dispersion in water. The TEM image (**Fig. 3.3b**) shows that the microscopic morphology of PNPG consists of several tiny parts aggregating to form a spherical PNPG particle, similar to the report by Ben et al. [26]. but unlike the previously reported deprotonated PNPG nanofibers synthesized by immersion in NH_4OH aqueous solution [25, 27]. Using Brunauer-Emmett-Teller model (BET) and the Barrett-Joyner-Halenda model (BJH) to analyze the surface area and porous diameter separately, and PNPG nanoparticles has a surface area of 36.48 $m^2 \cdot g^{-1}$ and an average pore diameter of 1.368 nm.

The chemical functional groups of PNPG were determined by FT-IR spectroscopy (**Fig. 3.3c**). The characteristic peak at 817 cm^{-1} is due to the presence of 1,4 (para)-substituted phenyl rings, proving the synthesis of PNPG [25, 30]. The peak at 1165 cm^{-1} is attributed to the vibrational mode of the quinoid ring, which further confirms the formation of PNPG [30]. The C–N stretching vibration of the benzenoid amine was found at 1311 cm^{-1} [26]. The characteristic peaks at 1496 and 1573 cm^{-1} correspond to the C=C stretching vibration of the benzenoid ring and quinonoid ring of PNPG, respectively [26, 34, 35]. Additionally, the stretching vibration absorption of C=O was

observed at 1651 cm^{-1} [34].

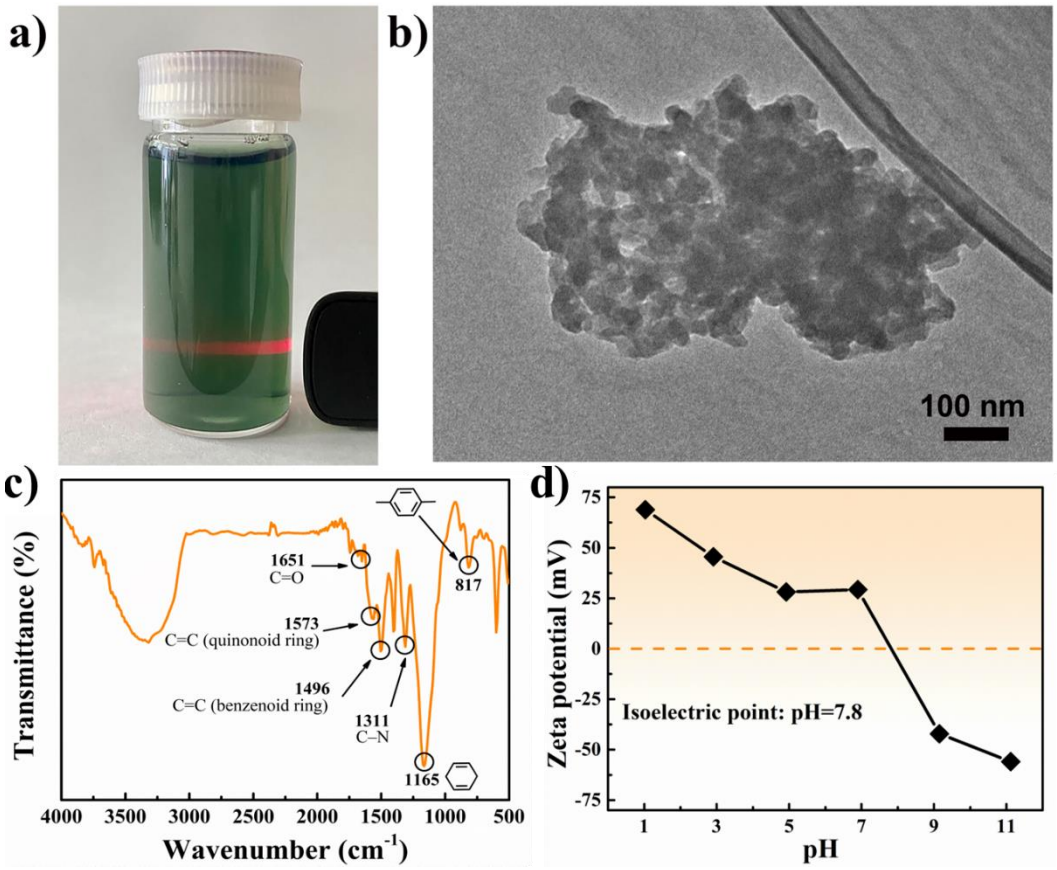

Fig. 3.3. (a) Photograph of PNPG suspension. (b) TEM image of a PNPG particle. (c) FT-IR spectra of PNPG. (d) Zeta potentials of PNPG at different pH levels (0.001 $mol \cdot L^{-1}$ KCl was used as the electrolyte).

As shown in **Fig. 3.3d**, PNPG has a positive zeta potential under acidic conditions due to a large amount of H^+ that accumulates around the PNPG particles, which protonates functional groups like carboxylic groups [27]. Under alkaline conditions, the –COOH groups of PNPG are deprotonated to form $–COO^-$ groups due to the lack of H^+, and the zeta potential of PNPG becomes negative [25, 27]. From these zeta potential data, the isoelectric point of PNPG was calculated to be at pH 7.8.

3.3.2. Adsorption performance of PNPG particles at different pH and anion concentrations

It is known that pH, time, and concentration are the three essential factors governing adsorption behavior. The influence of pH on adsorption behavior was

measured by q_t and E_t in the 24-h immersion adsorption experiment with a 50 mg·L^{-1} Au(III) solution. The pH of the solution ranged from 1 to 11. **Fig. 3.4a** shows an obvious difference in adsorption behavior at different pH levels. In general, while pH increases from 1 to 11, q_t decreases from 597.07 mg·g^{-1} to 13.24 mg·g^{-1}, and E_t also shows a downward trend from 80.3% to single digits. When pH ≤ 7, q_t and E_t are higher than that obtained under alkaline conditions, indicating that it is more favorable for PNPG to adsorb Au(III) under acidic conditions. Particularly, q_t reaches its maximum at pH 1. This is also true for the adsorption efficiency, reaching a maximum of 80.3%.

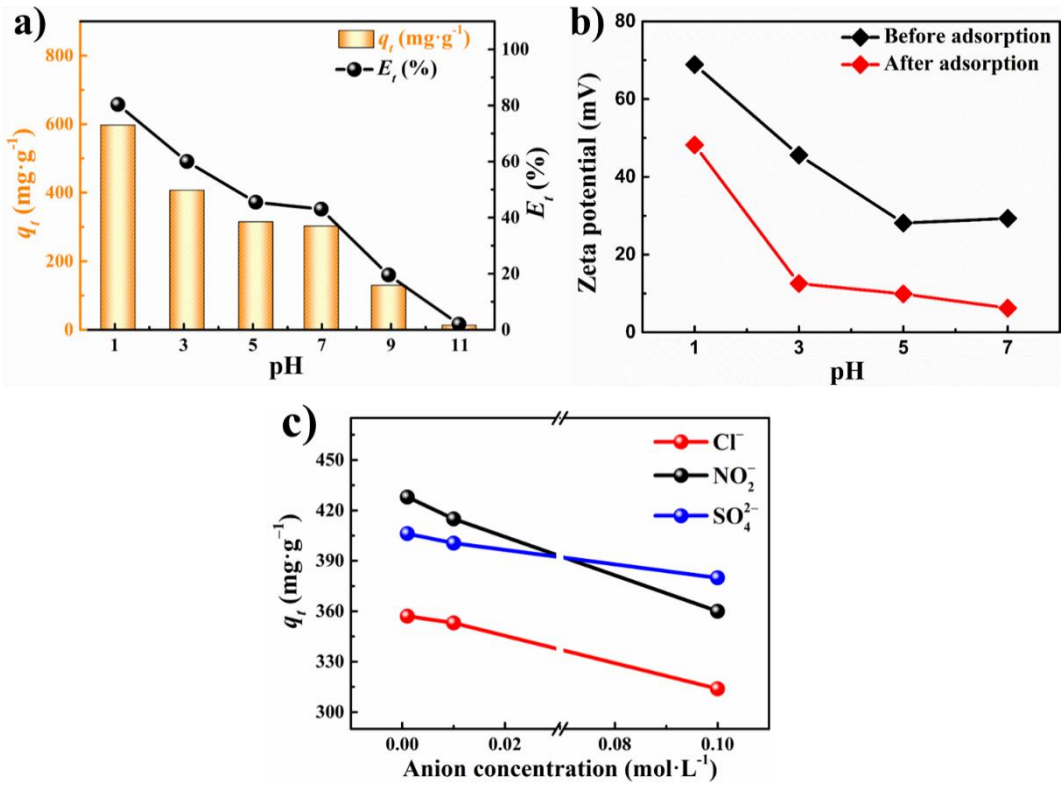

Fig. 3.4. (a) The relationship between adsorption behavior and pH. (b) The change of zeta potential before and after adsorption. (c) The relationship between adsorption behavior and anion concentration (c_0 = 50 mg·L^{-1}, pH = 2, t = 24 h).

The excellent adsorption behavior at pH 1 is presumably due to the cooperation of positive PNPG and negative $[AuCl_4]^-$ [27, 36]. As mentioned previously (**Fig. 3.3d**),

PNPG has a positive zeta potential in acidic solutions and a negative zeta potential in alkaline solutions. At low pH, Au(III) mainly exists in the negatively charged form as $[AuCl_4]^-$, which is easily attracted and adsorbed by the positive PNPG particles due to electrostatic interactions, thus improving the probability of capture and recovery of gold. The drop in potential of PNPG after adsorption (**Fig. 3.4b**) also indicates the occurrence of electrostatic interactions. With an increase in pH, PNPG becomes negative, and $[AuCl_4]^-$ undergoes a series of hydrolysis reactions to form other negatively charged gold complexes, which are difficult to capture by PNPG since similarly charged species repel each other [36].

The influence of anions on the Au adsorption behavior was tested by using NaCl, $NaNO_3$, and Na_2SO_4 in different concentrations (0.001, 0.01, and 0.1 mol·L^{-1}). As can be seen from **Fig. 3.4c**, these three kinds of anions all have negative effects on Au(III) adsorption. The higher the anion concentration is, the lower the q_t is, implying that Cl^-, NO_3^-, and SO_4^{2-} compete with Au(III) for some positively-charged adsorption sites.

3.3.3. Time-dependent adsorption of PNPG particles and kinetics study

The time-dependent adsorption experiment was performed from 0.25 h to 96 h in 100 mg·L^{-1} Au(III) solution of pH 1. The results are shown in **Fig. 3.5a**. Both adsorption capacity and adsorption efficiency increased with time. The adsorption of gold occurs quicker during the first 24 h has compared to the following hours, due to the high availability of adsorption sites at the start of adsorption. As adsorption sites become gradually occupied, the increase of q_t slows down and tends to reach equilibrium (1085.85 mg·g^{-1}) after 96 h.

To explore the adsorption process of gold on PNPG, three adsorption kinetic models were used: pseudo-first-order model (PFO), pseudo-second-order model (PSO), and intraparticle diffusion model (ID). The three models are mathematically shown in Equations (3), (4), and (5), respectively [37, 38]:

$$q_t = q_e\left(1 - e^{-k_1 t}\right) \tag{3}$$

$$q_t = \frac{tk_2q_e^2}{1+k_2q_et} \tag{4}$$

$$q_t = k_3\sqrt{t} + C \tag{5}$$

where k_1, k_2, and k_3 are the rate constants of the three models, respectively. q_t and q_e are the adsorption capacity at time t and equilibrium, respectively. The value of C is the intercept of the line and is related to the boundary thickness, where a larger value of C indicates a stronger boundary layer effect in intraparticle diffusion.

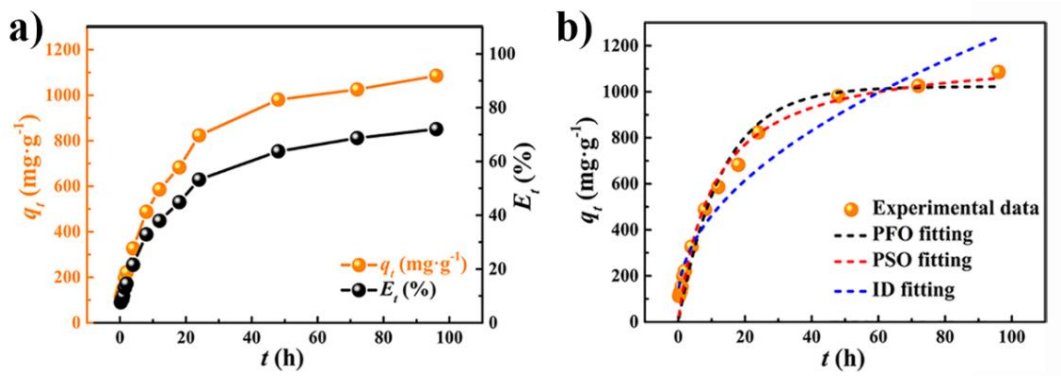

Fig. 3.5. (a) The relationship between adsorption behavior and time. (b) The fitting curves of three adsorption kinetic models.

Table 3.1 Kinetic parameters of the gold adsorption by PNPG

Model	**Parameters**	**Value**
PFO kinetic model	q_e (mg·g^{-1})	1009.71
	k_1 (h^{-1})	0.08
	R^2	0.9672
PSO kinetic model	q_e (mg·g^{-1})	1146.15
	k_2 (g·mg^{-1}·h^{-1})	1.3×10^{-5}
	R^2	0.9904
ID model	k_i (mg·g^{-1}·h$^{-1/2}$)	116.70
	C_i (mg·g^{-1})	92.90
	R^2	0.9425

Fig. 3.5b and **Table 3.1** show the fitting of the different kinetic models on the experimental time-dependent data. Compared to the PFO model, the PSO model has a higher correlation coefficient ($R^2 = 0.9904$), which indicates that mainly chemisorption occurs between PNPG and Au(III) during the extended time adsorption process. Moreover, the theoretical equilibrium adsorption capacity (1146.15 $mg \cdot g^{-1}$) fitted by the PSO model is closer to the experimental value (1085.85 $mg \cdot g^{-1}$), which also indicates that the adsorption process occurs mainly by chemisorption. As seen in the results of the ID model, the value of C is not equal to 0, indicating that intraparticle diffusion is not the speed-limiting step [37].

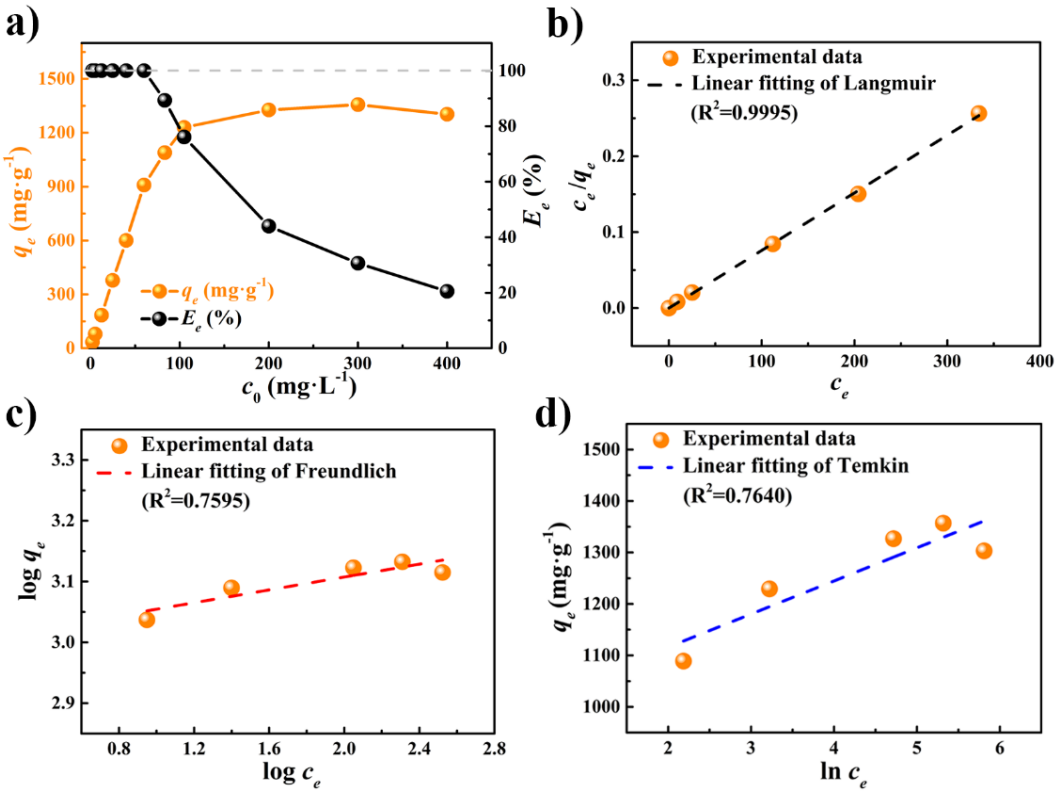

Fig. 3.6. (a) The relationship between adsorption behavior and concentration. The linear fitting of (b) Langmuir, (c) Freundlich, and (d) Temkin isotherm model.

3.3.4. Concentration-dependent adsorption of PNPG particles and isotherm study

The initial concentrations of Au(III) in the solution were selected to be 2, 5, 10, 20, 40, 60, 80, 100, 200, 300, and 400 $mg \cdot L^{-1}$ (pH 1). This adsorption experiment lasted for 120 h until equilibrium was reached. **Fig. 3.6a** reveals that q_e increases with

increasing c_0 (from 2 to 100 mg·L^{-1}), then gradually rises to a maximum of 1356.78 mg·g^{-1} and remains at this high level. This is because the increased concentration of metal ions curtails the mass transfer limitations between the solid and liquid [39]. Instead, E_e decreases from 100 % to 20.47 % due to the available adsorption sites that become limited and occupied at high concentrations. It is well worth noting that PNPG is a sensitive and efficient adsorbent when adsorbing trace quantities of Au(III) in solutions (e.g., 2 mg·L^{-1} and 5 mg·L^{-1}). From the comparison of some reported polymer-based adsorbents (**Table 3.2**), it can be said that PNPG has a better adsorption effect on gold than that of several adsorbents. Although PGMA-NH_2 and AT-S have higher adsorption capacities for gold, PNPG has optimal adsorption at more acidic conditions than PGMA-NH_2 and an easier synthesis method than AT-S [40, 41].

Table 3.2 Comparison with other polymer adsorbents

Material	q_m**(mg·g^{-1})**	**Optimum pH**	**Ref.**
N-containing polymer	1073	3.23	[28]
PANF-TETA-PT	801.2	2	[29]
AT-S	4215.2	1 mol·L^{-1} HCl	[40]
Amino-modified PGMA	1625.0	4.05	[41]
Fe_3O_4@CPTES@PEG	83	1	[42]
N-(3-aminopropyl)imidazole-based poly(ionic liquid)	236.68	1	[43]
CMPS-IL	516.5	2	[44]
PE-PGMA	601.34	3	[45]
Crosslinked polyethyleneimine resin	943.5	2	[46]
Poly(glycidyl methacrylate)	459.29	4	[47]
Metal-organic polymer (Cu-TFT-Him)	775.0	2	[48]
PNPG	1356.78	1	This work

Table 3.3 Isotherm parameters of the Au(III) adsorption by PNPG

Model	**Parameters**	**Value**
Langmuir model	q_m (mg·g^{-1})	1317.86
	K_L (L·mg^{-1})	12.38
	R^2	0.9995
Freundlich model	$1/n$	0.053
	K_F (L$^{1/n}$·mg$^{1-1/n}$·g^{-1})	1003.90
	R^2	0.7595
Temkin model	B	64.35
	K_T (L·g^{-1})	15.34
	R^2	0.7640

Langmuir, Freundlich, and Temkin isotherm models were used to explain the correlation between the adsorption behavior and concentration at a constant temperature [37, 49, 50]. The Langmuir and Freundlich isotherm models depict monolayer and multilayer adsorption, respectively, and their linear formulas are separately shown in Equations (6) and (7). The Temkin isotherm model assumes that the heat of adsorption reduces with increasing coverage and its formula is given by Eq (8):

$$\text{Langmuir isotherm model: } \frac{c_e}{q_e} = \frac{c_e}{q_m} + \frac{1}{K_L \times q_m} \tag{6}$$

$$\text{Freundlich isotherm mode: } \log q_e = \log K_F + \frac{1}{n} \times \log c_e \tag{7}$$

$$\text{Temkin isotherm model: } q_e = B \ln K_T + B \ln c_e \tag{8}$$

where c_e (mg·L^{-1}), q_e (mg·g^{-1}), and q_m (mg·g^{-1}) are the equilibrium concentration, equilibrium adsorption capacity, and theoretical maximum adsorption capacity, respectively. K_L (L·mg^{-1}), K_F (L$^{1/n}$·mg$^{1-1/n}$·g^{-1}), and K_T (L·g^{-1}) are the Langmuir constant, Freundlich constant, and Temkin isotherm equilibrium binding constants, respectively. $1/n$ is the characteristic constant related to adsorption intensity, which can

be explained as the smaller 1/n, the greater the heterogeneity, and the adsorption is favorable on the scale of 0–1 [38]. B can be expressed as $B = RT / b$, where R, T, and b are the gas constant (8.314 J·mol^{-1}·K^{-1}), temperature (298 K), and Temkin isotherm constant, respectively.

As seen in **Figs. 3.6b–d** and **Table 3.3**, compared with the Freundlich and Temkin isotherm models, the Langmuir isotherm model has a stronger correlation ($R^2 = 0.995$), indicating that monolayer adsorption plays a dominant role in the adsorption progress of Au(III) by PNPG. From the Langmuir isotherm model, the q_m (1317.86 mg·g^{-1}) is close to the experimental value of 1356.78 mg·g^{-1}.

3.3.5. Adsorption mechanism

The reported mechanisms of conductive polymers adsorbing heavy metals include electrostatic interactions and redox reactions [17]. In this section, some analyses were performed to explore the mechanism of Au(III) adsorption by PNPG, which is classified as a conductive polymers [51].

There is an electrostatic interaction during the Au(III) adsorption by PNPG. As previously mentioned, protonated functional groups make PNPG particles positively charged and thereby attracts negatively charged $[AuCl_4]^-$. Likewise, the lower zeta potential after adsorption (**Fig. 3.4b**) also proves the electrostatic interaction due to the charge decrease after electrostatic bonding.

The redox reaction can be confirmed by XRD, TEM, and UV-vis characterization methods. From the XRD results (**Fig. 3.7a**), four peaks can be seen after adsorption. The peaks at 2θ = 38.1°, 44.4°, 64.6°, and 77.6 °correspond to the crystal faces of elemental gold (1 1 1), (2 0 0), (2 2 0), and (3 1 1), which is in good agreement with the gold standard card (JCPDS No. 04−0784) [38]. It can be argued that the reduction reaction occurs during the adsorption process, and PNPG reduces gold ions to elemental gold. The TEM image of the PNPG after adsorption is shown in **Fig. 3.7b**. An ample amount of reduced gold nanoparticles are dispersed throughout the PNPG particle, also seen outside the PNPG particle, which verifies the redox reaction between PNPG and gold ions. The filtrates obtained after adsorption were analyzed. In **Fig. 3.7c**, as the

adsorption time increased, the yellow color gradually faded and a pale red colored filtrate appeared. UV-vis characterization of these colored solutions (**Fig. 3.7d**) showed no peak when the initial yellow colored solution was analyzed, while the samples subjected to adsorption for 48 and 72 h, clearly showed a peak characteristic of gold nanoparticles, in the range of 500–600 nm [52]. This validates not only the redox reaction between PNPG and the gold ions but also that some of the reduced gold nanoparticles dislodged and dispersed in the adsorbed solution. This redox reaction between PNPG and gold ions may provide a new strategy for the preparation of colloidal solutions of gold nanoparticles (AuNPs).

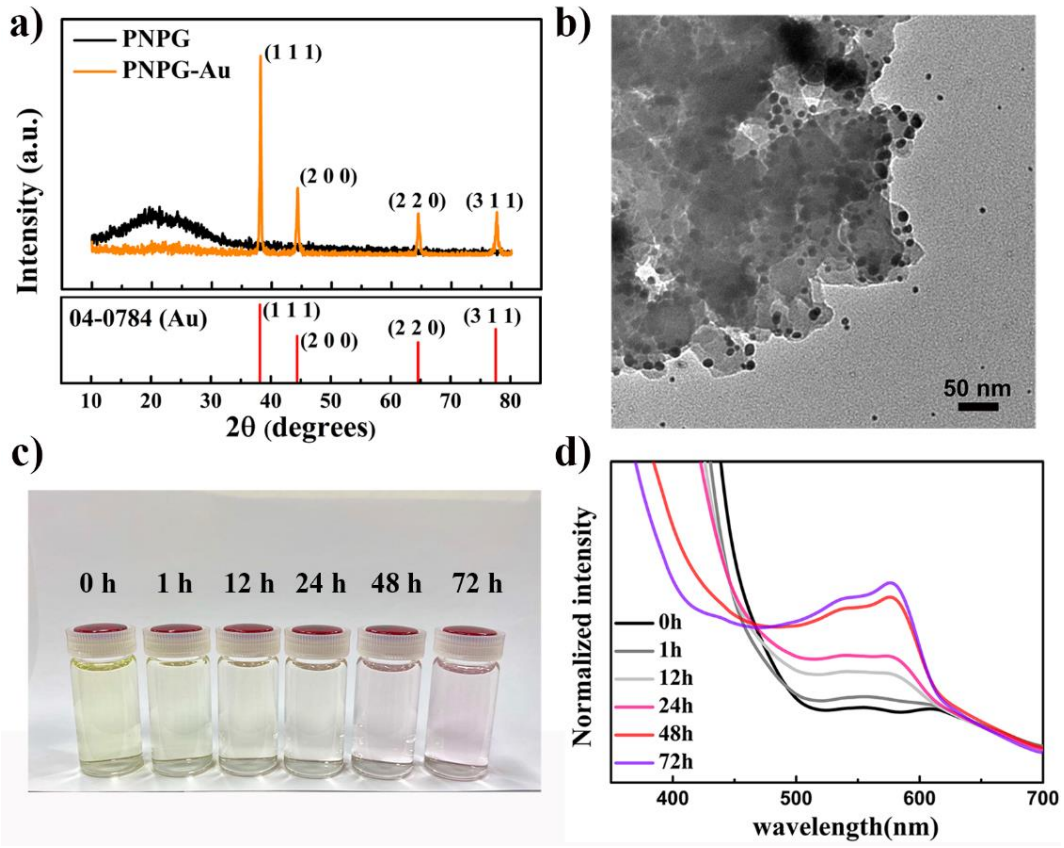

Fig. 3.7. (a) XRD patterns of PNPG, PNPG-Au, and the characteristic peaks of the gold standard card. (b) TEM image of the PNPG particle after adsorption (1 h). (c) Photograph showing changing filtrate colors with adsorption time, and (d) UV-vis absorbance spectra of the post-adsorption filtrate.

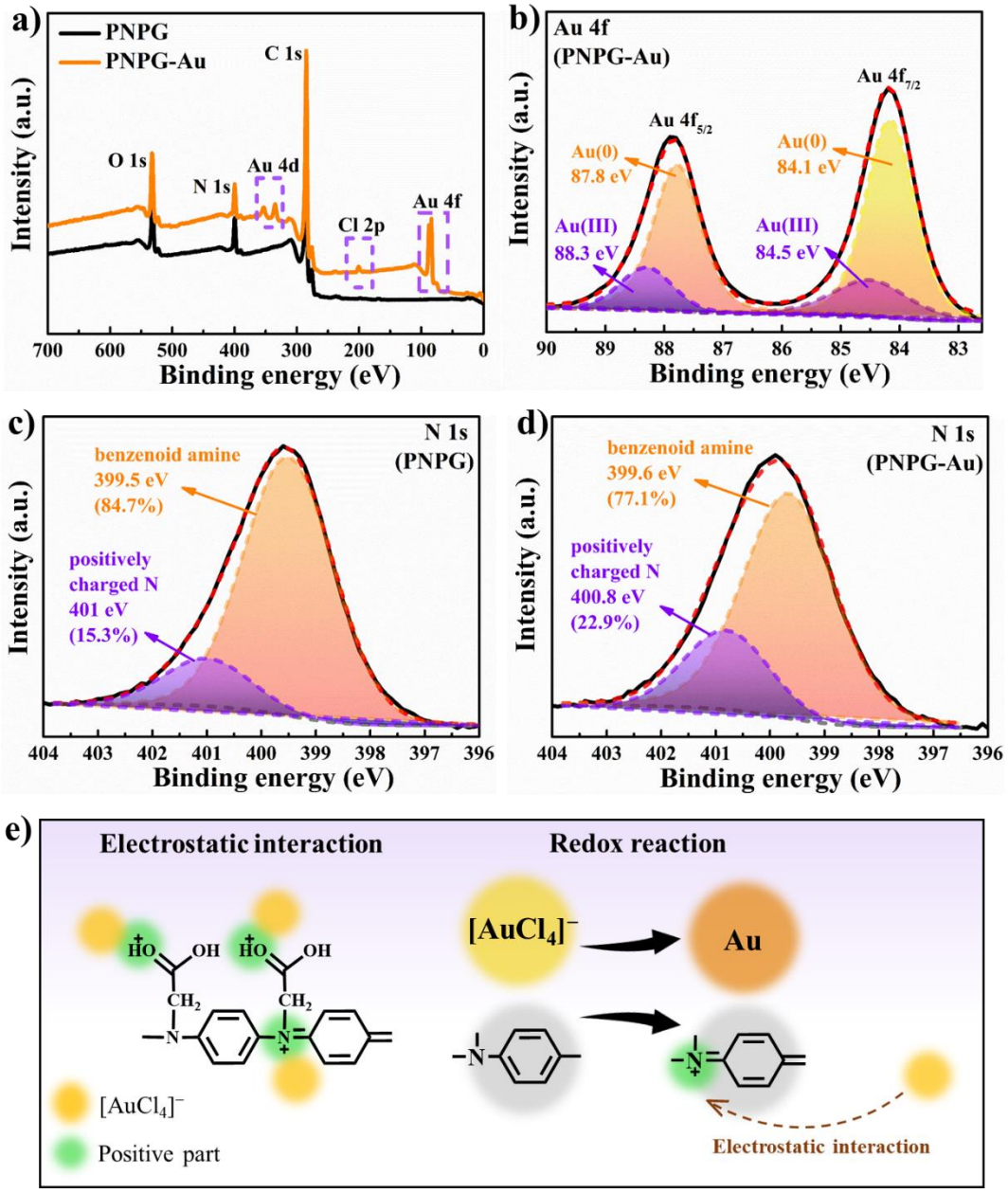

Fig. 3.8. (a) The wide-scan XPS spectra of PNPG and PNPG-Au. (b) The XPS Au 4f spectrum of PNPG-Au. The XPS N 1s spectra of (c) PNPG and (d) PNPG-Au. (e) Schematic diagram of Au adsorption by PNPG through XPS analyses.

The XPS results for PNPG and PNPG-Au are shown in **Fig. 3.8a**. Both have three dominant peaks, whose binding energies are approximately centered at 531, 399, and 284 eV because of O 1s, N 1s, and C 1s peaks, respectively [25]. After adsorption, PNPG-Au has additional characteristic peaks of Cl 2p (200.7 eV), Au 4d (353 and 334 eV), and Au 4f (87.7 and 83.7 eV) [48, 53]. In brief, the wide-scan XPS spectra

indicated that gold ions were adsorbed onto the PNPG. In detail, as seen in **Fig. 3.8b**, the fitted XPS spectra of Au 4f display Au(0) peaks (84.1 eV and 87.8 eV) and Au(III) peaks (84.5 eV and 88.3 eV), which are consistent with Au $4f_{7/2}$ and Au $4f_{5/2}$ binding energies [38, 54]. The presence of characteristic peaks of Cl and Au(III) indicates that a part of the gold is adsorbed by PNPG in the form of $[AuCl_4]^-$. Furthermore, the peak intensity of Au(0) is perceptibly stronger than that of Au(III), since most of the gold ions are reduced to elemental gold by PNPG, indicating that the oxidation-reduction reaction does occur and plays a dominant role.

Since the reducibility of PNPG is reflected in benzenoid amine structure [42], the N 1s XPS spectra of PNPG before adsorption are characterized and the results are shown in **Fig. 3.8c**. The main peak at 399.5 eV corresponds to the N in benzenoid amine [51], while the distinctive peak at 401 eV is ascribed to the positively charged N linked to the quinonoid ring [51, 55], and these two peaks account for 84.7% and 15.3% of the N content, respectively. After adsorption (**Fig. 3.8d**), the content of benzenoid nitrogen decreased to 77.1%, indicating benzenoid nitrogen units were oxidized into positive quinonoid nitrogen units, which was consistent with the oxidation process of PNPG reported by Muniraj et al. [51]. Meanwhile, the content of quinoid nitrogen increased to 22.9% due to the oxidation of benzenoid nitrogen [55], the difference being equal to the content loss of benzenoid nitrogen. The increase in positively charged quinoid nitrogen facilitates the combination with anionic $[AuCl_4]^-$ through electrostatic interactions in acidic solutions [51, 56].

The adsorption mechanism of PNPG for gold can be summarized as follows (**Fig. 3.8e**): a part of $[AuCl_4]^-$ is bound by protonated functional groups through electrostatic interactions, the other is reduced to elemental gold via the redox reaction with benzenoid nitrogen, and the generated positive quinoid nitrogen can further adsorb $[AuCl_4]^-$ through electrostatic interactions.

3.3.6. Characterization of PNPG membrane

In practice, it is difficult to separate adsorbents from the post-adsorption solution. To reduce the separation burden after adsorption, the nano-adsorbent can be made into

a film using a simple and effective method as shown above. The prepared membrane was black (**Fig. 3.9a**), and the PNPG particles were retained on the MCE substrate even after bending the membrane (**Fig. 3.9b**), demonstrating good flexibility. The membrane samples were placed in beakers with different pH solutions to investigate their stability in solution. As can be observed from the photographs in **Fig. 3.9c**, the membrane remained close to its original state for at least seven days without flaking.

Fig. 3.10 shows the SEM characterization of the pre-adsorption and post-adsorption PNPG membrane. The surface of the PNPG membrane is visibly uneven (**Figs. 3.10a–c**), and the many tiny gullies slightly increase the contact area between PNPG and the solution. Comparing **Fig. 3.10a** with **Fig. 3.10d** many reduced gold spheres on the PNPG membrane after 24-hour adsorption is evident, confirming the occurrence of the redox reaction. Elemental mapping analyses were carried out on the selected area in **Fig. 3.10g**. According to the results in **Figs. 3.10i–j**, the presence of Cl and Au confirm that some $[AuCl_4]^-$ was captured through electrostatic interaction, which is consistent with the results from zeta potential and XPS analyses. Furthermore, the existence of Au on the upper layer means that the lower layer—MCE filter membrane—as a supporting layer does not participate in the adsorption of gold.

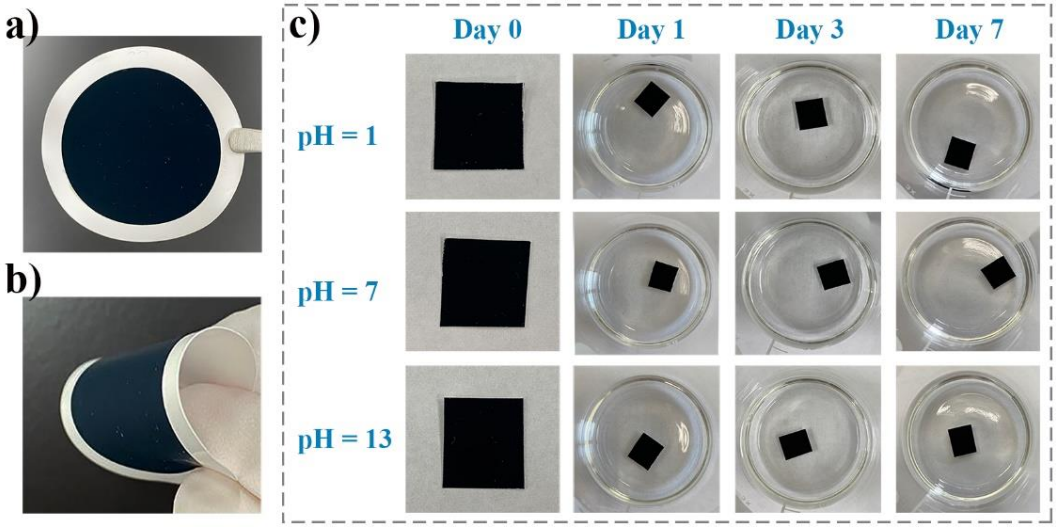

Fig. 3.9. Digital photos of the (a) complete PNPG membrane and (b) bending PNPG membrane. (c) Stability evaluation of PNPG membrane under different pH solutions.

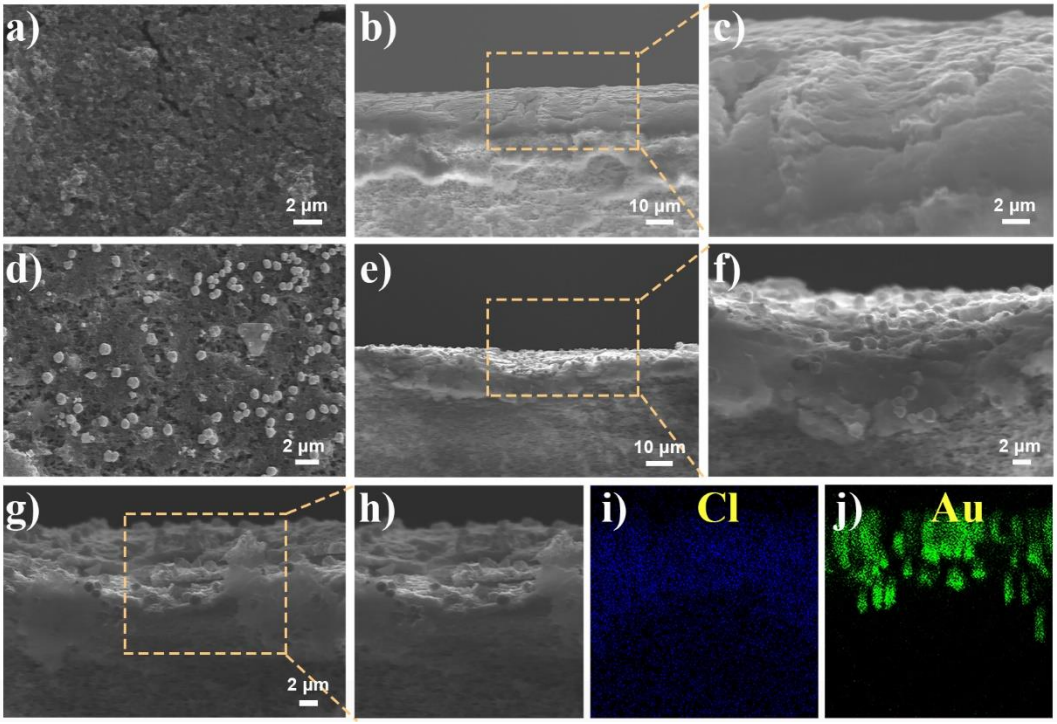

Fig. 3.10. SEM images of (a) top view and (b) (c) section view of the PNPG membrane before adsorption. SEM images of (d) top view and (e) (f) (g) (h) section view of the PNPG membrane after adsorption (24 h). The corresponding elemental maps of (i) Cl and (j) Au in (h). Note: (c), (f), (h) are the partially enlarged views of yellow boxes.

3.3.7. Reusability and selectivity of PNPG Membrane

To study the reusability, the prepared PNPG membrane was immersed in 20 $mg{\cdot}L^{-1}$ Au(III) solution with a pH of 1. The desorption experiment with the post-adsorption PNPG membrane was conducted using a fresh desorption agent to leach gold. The desorption agent contained 1.0 $mol{\cdot}L^{-1}$ $CS(NH_2)_2$ and 1.0 $mol{\cdot}L^{-1}$ HCl [34]. These reusability experiments were carried out at 25 °C, and an oscillation of 100 rpm was applied to ensure complete adsorption and desorption. After each adsorption-desorption cycle, the PNPG membrane was removed from the desorption agent, cleaned with deionized water three times, and dried at 60 °C for 24 h before the next round. **Fig. 3.11a** illustrates that the PNPG membrane can be recycled three times with a slight decrease in adsorption efficiency, which can be attributed to certain sites that were not successfully desorbed. The first desorption round did not have 100% desorption efficiency, due to a small number of nano-gold particles that were not on the membrane,

but were found in the adsorbed solution, as analyzed in **Figs. 3.7c–d**. However, the adsorption efficiency remained above 90% after three cycles, suggesting good reusability of the PNPG membrane.

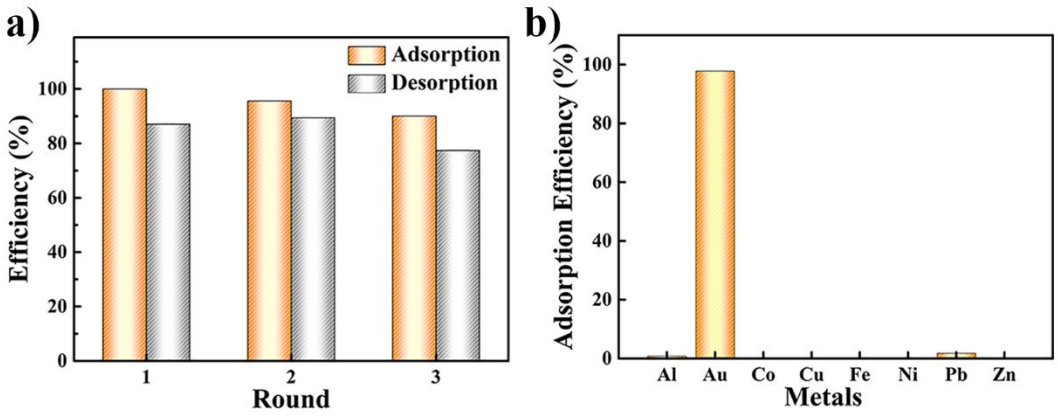

Fig. 3.11. (a) Adsorption and desorption efficiencies in successive cycles (each adsorption time or desorption time was 24 h). (b) Selective adsorption of Au(III) by PNPG membrane from a mixed solution (t = 24 h).

Selectivity is an important index when evaluating adsorption performance in a multi-substance liquid, such as wastewater and industrial wastewater, due to the diversity of ions and variation in concentrations. The selectivity of the PNPG membrane to adsorb gold was tested with the following coexisting ions: Al(III) Co(II), Cu(II), Fe(III), Ni(II), Pb(II), and Zn(II). In the multi-metal solution (pH=1), the initial concentration of gold ions was prepared at 10 mg·L^{-1}, while the other ions had a collective concentration of 100 mg·L^{-1}. This experiment was conducted at 25 °C and 100 rpm. Based on the results presented in **Fig. 3.11b**, PNPG adsorbed a small amount of Pb, which can be attributed to the N atom of the -N=C- groups possibly forming a complex binding with Pb [17]. However, the PNPG membrane shows high selectivity towards Au in acidic mixed solutions, even though the concentration of Au is very low. As previously discussed, under acidic conditions protonated functional groups make PNPG particles positively charged and thereby attract the negative form of Au(III), while repelling other positively charged metal ions. Another reason for the high selectivity can be explained from the aspect of redox potential. According to the standard electrode potential table, $[AuCl_4]^-$/Au pair is the only one whose redox

potential (1.002 V) is higher than 0.4 V which was measured as the potential of PNPG pairs by Muniraj et al. [51]. Thus, PNPG is very sensitive to Au(III) and preferentially reduces Au(III) although at such unfavorable condition of low concentration.

3.3.8. Recovery of Au from the leaching solution

Au was recovered from real e-waste samples using a waste PCB leaching solution, the preparation of which is shown in **Fig. 3.2**. The concentrations ($mg \cdot L^{-1}$) of other metals in the leaching solution (**Fig. 3.12b**) were determined as: Al(III), 12.80; Au(III), 1.83; Co(II), 0.96; Cu(II), 27.30; Fe(III), 97.60; Ni(II), 23.00; Pb(II), 4.50; Zn(II), 6.58. Although concentrated HNO_3 leaching removed most of the Cu, Fe, Pb, etc., a small part of the residue was found to be leached by aqua regia.

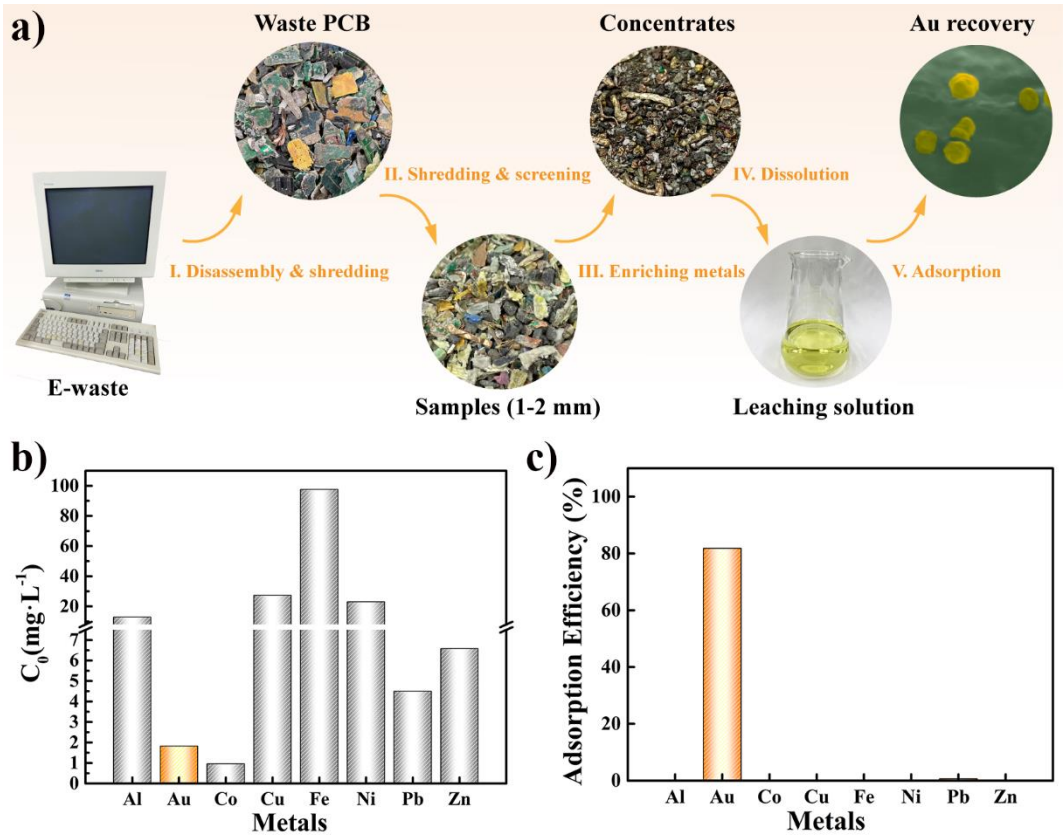

Fig. 3.12. (a) The process of gold recovery from e-waste. (b) The concentrations of metals in the leaching solution. (c) Adsorption efficiency of various metals by PNPG membrane in the leaching solution of waste PCBs.

The PNPG membrane was soaked in a 20 mL PCB leaching solution for the

adsorption experiment. Based on the results shown in **Fig. 3.12c**, other coexisting metal ions have little effect on gold adsorption by PNPG, due to their low concentration when compared to the concentrations listed in Section 3.3.7. Perhaps the use of aqua regia causes high-concentration of Cl^- ions to compete for occupancy of adsorption sites through electrostatic interaction, lowering the adsorption efficiency of Au to below 100%. However, the concentration of gold ions (1.83 $mg \cdot L^{-1}$) is much lower than that of other base metals, and the PNPG membrane still demonstrates outstanding sensitivity and good adsorption efficiency (~80%) for the selective adsorption of Au(III). Therefore, PNPG is promising and has the potential to be a selective and sensitive adsorbent for capturing gold ions from e-waste.

3.4. Conclusion

PNPG obtained by polymerization of NPG monomers can successfully capture and recover gold from solution, showing excellent adsorption capacity (1356.78 $mg \cdot g^{-1}$) and outstanding sensitivity to Au(III) in low-concentration solutions. The adsorption results of Au(III) by PNPG showed a good correlation with the PSO and Langmuir isotherm model, indicating that chemisorption and monolayer adsorption are the dominant adsorption mechanisms. Zeta potential, XRD, TEM, FT-IR, and XPS analysis showed that PNPG adsorbed gold ions through electrostatic interactions and redox reactions. UV-vis characterization revealed the presence of gold nanoparticles in the filtrate after adsorption, suggesting that the redox reaction between PNPG and gold ions may provide a new strategy for the preparation of colloidal solutions of AuNPs. In addition, the PNPG membrane formed by vacuum filtration was stable in solution and could be used as an effective way to easily separate the nano-adsorbent from the solutions. The PNPG membrane remained active for a minimum of three cycles. Additionally, PNPG selectively adsorbs gold in a multi-metal solution. More importantly, approximately 80% of the gold was selectively adsorbed from the leaching solution of waste PCBs, which also demonstrated the practical application of the PNPG membrane in recovering gold from e-waste. Therefore, PNPG is promising and sensitive to Au adsorption and has the potential to selectively recover gold from e-waste.

Reference

[1] E.R. Rene, M. Sethurajan, V. Kumar Ponnusamy, et al., Electronic waste generation, recycling and resource recovery: Technological perspectives and trends, J. Hazard. Mater., 416 (2021) 125664-125674. https://doi.org/10.1016/j.jhazmat.2021.125664.

[2] A. Kumar, M. Holuszko, D.C.R. Espinosa, E-waste: An overview on generation, collection, legislation and recycling practices, Resour. Conserv. Recycl., 122 (2017) 32-42. https://doi.org/10.1016/j.resconrec.2017.01.018.

[3] S. Marinello, R. Gamberini, Multi-criteria decision making approaches applied to waste electrical and electronic equipment (WEEE): A comprehensive literature review, Toxics, 9 (2021) 13-32. https://doi.org/10.3390/toxics9010013.

[4] A. Pires, G. Martinho, Waste hierarchy index for circular economy in waste management, Waste Manag., 95 (2019) 298-305. https://doi.org/10.1016/j.wasman.2019.06.014.

[5] F. Kubota, R. Kono, W. Yoshida, et al., Recovery of gold ions from discarded mobile phone leachate by solvent extraction and polymer inclusion membrane (PIM) based separation using an amic acid extractant, Sep. Purif. Technol., 214 (2019) 156-161. https://doi.org/10.1016/j.seppur.2018.04.031.

[6] S. Zhang, Y. Gu, A. Tang, et al., Forecast of future yield for printed circuit board resin waste generated from major household electrical and electronic equipment in china, J. Clean. Prod., 283 (2021) 124575-124587. https://doi.org/10.1016/j.jclepro.2020.124575.

[7] V. Forti, C. Baldé, R. Kuehr, et al., The global e-waste monitor 2020. Quantities, flows, and the circular economy potential, 2020. https://www.itu.int/en/ITU-D/Environment/Documents/Toolbox/GEM_2020_def.pdf.

[8] A.M. Leader, X. Wang, G. Gaustad, Creating the 2020 tokyo olympic medals from electronic scrap: Sustainability analysis, JOM, 69 (2017) 1539-1545. https://doi.org/10.1007/s11837-017-2441-4.

[9] A. Senthilselvi, V. Sellam, S.A. Alahmari, et al., Accuracy enhancement in mobile

phone recycling process using machine learning technique and meph process, Environ. Technol. Innov., 20 (2020) 101137-101147. https://doi.org/10.1016/j.eti.2020.101137.

[10] E. Hsu, K. Barmak, A.C. West, et al., Advancements in the treatment and processing of electronic waste with sustainability: A review of metal extraction and recovery technologies, Green Chem., 21 (2019) 919-936. https://doi.org/10.1039/C8GC03688H.

[11] T.S. Nguyen, Y. Hong, N.A. Dogan, et al., Gold recovery from e-waste by porous porphyrin–phenazine network polymers, Chem. Mater., 32 (2020) 5343-5349. https://doi.org/10.1021/acs.chemmater.0c01734.

[12] X. Zhao, Z. Yang, A.V. Kuklin, et al., Potassium ions promote electrochemical nitrogen reduction on nano-Au catalysts triggered by bifunctional boron supramolecular assembly, J. Mater. Chem. A, 8 (2020) 13086-13094. https://doi.org/10.1039/D0TA04580B.

[13] K. Yu, X. Hai, S. Yue, et al., Glutathione-activated DNA-Au nanomachine as targeted drug delivery platform for imaging-guided combinational cancer therapy, Chem. Eng. J., 419 (2021) 129535-129546. https://doi.org/10.1016/j.cej.2021.129535.

[14] M.K.M.Z. Hyder, B. Ochiai, Selective recovery of Au(III), Pd(II), and Ag(I) from printed circuit boards using cellulose filter paper grafted with polymer chains bearing thiocarbamate moieties, Microsyst. Technol., 24 (2018) 683-690. https://doi.org/10.1007/s00542-017-3277-0.

[15] T.H. Bui, S. Jeon, Y. Lee, Facile recovery of gold from e-waste by integrating chlorate leaching and selective adsorption using chitosan-based bioadsorbent, J. Environ. Chem. Eng., (2020) 104661-104669. https://doi.org/10.1016/j.jece.2020.104661.

[16] M.D. Rao, K.K. Singh, C.A. Morrison, et al., Recycling copper and gold from e-waste by a two-stage leaching and solvent extraction process, Sep. Purif. Technol., 263 (2021) 118400-118406. https://doi.org/10.1016/j.seppur.2021.118400.

[17] E.N. Zare, A. Motahari, M. Sillanpää, Nanoadsorbents based on conducting

polymer nanocomposites with main focus on polyaniline and its derivatives for removal of heavy metal ions/dyes: A review, Environ. Res., 162 (2018) 173-195. https://doi.org/10.1016/j.envres.2017.12.025.

[18] R. Sitko, E. Turek, B. Zawisza, et al., Adsorption of divalent metal ions from aqueous solutions using graphene oxide, Dalton Trans., 42 (2013) 5682-5689. https://doi.org/10.1039/C3DT33097D.

[19] F. Sadeghfar, M. Ghaedi, A. Asfaram, et al., Polyvinyl alcohol/Fe_3O_4@carbon nanotubes nanocomposite: Electrochemical-assisted synthesis, physicochemical characterization, optical properties, cytotoxicity effects and ultrasound-assisted treatment of aqueous based organic compound, J. Ind. Eng. Chem., 65 (2018) 349-362. https://doi.org/10.1016/j.jiec.2018.05.006.

[20] Z. Wang, B. Mi, Environmental applications of 2D molybdenum disulfide (MoS_2) nanosheets, Environ. Sci. Technol., 51 (2017) 8229-8244. https://doi.org/10.1021/acs.est.7b01466.

[21] J. Kim, K.R. Kim, Y. Hong, et al., Photochemically enhanced selective adsorption of gold ions on tannin-coated porous polymer microspheres, ACS Appl. Mater. Interfaces, 11 (2019) 21915-21925. https://doi.org/10.1021/acsami.9b05197.

[22] S. Ullah, M. Hashmi, N. Hussain, et al., Stabilized nanofibers of polyvinyl alcohol (PVA) crosslinked by unique method for efficient removal of heavy metal ions, J. Water Process. Eng., 33 (2020) 101111-101118. https://doi.org/10.1016/j.jwpe.2019.101111.

[23] A. Taghizadeh, M. Taghizadeh, M. Jouyandeh, et al., Conductive polymers in water treatment: A review, J. Mol. Liq., 312 (2020) 113447. https://doi.org/10.1016/j.molliq.2020.113447.

[24] X. Lei, Z. Su, Novel conducting polyaniline copolymers of aniline and N-phenylglycine, Mater. Lett., 61 (2007) 1158-1161. https://doi.org/10.1016/j.matlet.2006.06.076.

[25] J.H. Doh, J.H. Kim, H.J. Kim, et al., Enhanced adsorption of aqueous copper(II) ions using dedoped poly-N-phenylglycine nanofibers, Chem. Eng. J., 277 (2015) 352-359. http://dx.doi.org/10.1016/j.cej.2015.04.120.

[26] M. Ben Ali, F. Wang, R. Boukherroub, et al., High performance of phytic acid-functionalized spherical poly-phenylglycine particles for removal of heavy metal ions, Appl. Surf. Sci., 518 (2020) 146206-146213. https://doi.org/10.1016/j.apsusc.2020.146206.

[27] H.J. Kim, H. Choi, A.K. Sharma, et al., Recyclable aqueous metal adsorbent: Synthesis and Cu(II) sorption characteristics of ternary nanocomposites of Fe_3O_4 nanoparticles@graphene-poly-N-phenylglycine nanofibers, J. Hazard. Mater., 401 (2021) 123283. https://doi.org/10.1016/j.jhazmat.2020.123283.

[28] S. Zhou, W. Xu, C. Hu, et al., Fast and effective recovery of Au(III) from aqueous solution by a N-containing polymer, Chemosphere, 260 (2020) 127615-127624. https://doi.org/10.1016/j.chemosphere.2020.127615.

[29] F. Liu, Z. Zhou, G. Li, Persimmon tannin functionalized polyacrylonitrile fiber for highly efficient and selective recovery of Au(III) from aqueous solution, Chemosphere, 264 (2021) 128469. https://doi.org/10.1016/j.chemosphere.2020.128469.

[30] M.R. Nabid, S.S. Taheri, R. Sedghi, et al., Chemical synthesis and characterization of water-soluble, conducting poly(N-phenylglycine), Iran. Polym. J., 17 (2008) 365-371. https://www.sid.ir/en/Journal/ViewPaper.aspx?ID=107888.

[31] Z. Lin, T. Wu, Y.-F. Feng, et al., Poly(N-phenylglycine)/MoS_2 nanohybrid with synergistic solar-thermal conversion for efficient water purification and thermoelectric power generation, ACS Appl. Mater. Interfaces, 14 (2022) 1034-1044. https://doi.org/10.1021/acsami.1c20393.

[32] J. Ma, Y. Liu, O. Ali, et al., Fast adsorption of heavy metal ions by waste cotton fabrics based double network hydrogel and influencing factors insight, J. Hazard. Mater., 344 (2018) 1034-1042. https://doi.org/10.1016/j.jhazmat.2017.11.041.

[33] H.A. Shawky, A.H.M. El-Aassar, D.E. Abo-Zeid, Chitosan/carbon nanotube composite beads: Preparation, characterization, and cost evaluation for mercury removal from wastewater of some industrial cities in egypt, J. Appl. Polym. Sci., 125 (2012) E93-E101. https://doi.org/10.1002/app.35628.

[34] Z. Lin, T. Wu, J. Shi, et al., Poly(N-phenylglycine)-based bioinspired system for

stably and efficiently enhancing solar evaporation, ACS Sustainable Chem. Eng., 9 (2021) 448-457. https://doi.org/10.1021/acssuschemeng.0c07608.

[35] C. Lei, C. Wang, W. Chen, et al., Polyaniline@magnetic chitosan nanomaterials for highly efficient simultaneous adsorption and in-situ chemical reduction of hexavalent chromium: Removal efficacy and mechanisms, Sci. Total Environ., 733 (2020) 139316-139328. https://doi.org/10.1016/j.scitotenv.2020.139316.

[36] M. Zhao, Z. Huang, S. Wang, et al., Ultrahigh efficient and selective adsorption of Au(III) from water by novel chitosan-coated mos2 biosorbents: Performance and mechanisms, Chem. Eng. J., 401 (2020) 126006. https://doi.org/10.1016/j.cej.2020.126006.

[37] F.B. Biswas, I.M.M. Rahman, K. Nakakubo, et al., Highly selective and straightforward recovery of gold and platinum from acidic waste effluents using cellulose-based bio-adsorbent, J. Hazard. Mater., 410 (2021) 124569. https://doi.org/10.1016/j.jhazmat.2020.124569.

[38] X. Chen, Y. Xiang, L. Xu, et al., Recovery and reduction of Au(III) from mixed metal solution by thiourea-resorcinol-formaldehyde microspheres, J. Hazard. Mater., 397 (2020) 122812-122820. https://doi.org/10.1016/j.jhazmat.2020.122812.

[39] X. Hu, L. Yan, Y. Wang, et al., Self-assembly of binary oppositely charged polysaccharides into polyelectrolyte complex hydrogel film for facile and efficient Pb^{2+} removal, Chem. Eng. J., 388 (2020) 124189-124200. https://doi.org/10.1016/j.cej.2020.124189.

[40] F.-C. Wang, J.-M. Zhao, W.-K. Wang, et al., Superior au-adsorption performance of aminothiourea-modified waste cellulosic biomass, J. Cent. South Univ., 25 (2018) 2992-3003. https://doi.org/10.1007/s11771-018-3969-3.

[41] F.-C. Wang, J.-M. Zhao, W.-K. Wang, et al., Adsorption of Au(III) by amino-modified monodispersed pgma microspheres and deposition of gold nanoparticles, Rare Met., 37 (2018) 196-203. https://doi.org/10.1007/s12598-017-0992-8.

[42] X. Yang, K. Yang, L. Wu, et al., Fe_3O_4 nanoparticles functionalized with poly(ethylene glycol) for the selective separation and enrichment of Au(III), New

J. Chem., 44 (2020) 1313-1319. http://dx.doi.org/10.1039/C9NJ05551G.

[43] W. Gui, Y. Shi, J. Wei, et al., Synthesis of N-(3-aminopropyl)imidazole-based poly(ionic liquid) as an adsorbent for the selective recovery of Au(III) ions from aqueous solutions, New J. Chem., 44 (2020) 20387-20395. http://dx.doi.org/10.1039/D0NJ04420B.

[44] X. Kou, B. Ma, R. Zhang, et al., Properties and mechanism for selective adsorption of Au(III) on an ionic liquid adsorbent by grafting N-methyl imidazole onto chloromethylated polystyrene beads, RSC Advances, 10 (2020) 20338-20348. http://dx.doi.org/10.1039/D0RA03504A.

[45] C. Xiong, S. Wang, L. Zhang, Selective recovery mechanism of Au(III) from an aqueous solution by trimethyl phosphate modified poly(glycidyl methacrylate), J. Taiwan Inst. Chem. Eng., 95 (2019) 55-64. https://doi.org/10.1016/j.jtice.2018.09.035.

[46] F. Liu, L. Zhou, W. Wang, et al., Adsorptive recovery of Au(III) from aqueous solution using crosslinked polyethyleneimine resins, Chemosphere, 241 (2020) 125122-125129. https://doi.org/10.1016/j.chemosphere.2019.125122.

[47] B. Zhang, S. Wang, L. Fu, et al., Selective high capacity adsorption of Au(III) from aqueous solution by poly(glycidyl methacrylate) functionalized with 2,6-diaminopyridine, Polym. Bull., 76 (2019) 4017-4033. https://doi.org/10.1007/s00289-018-2594-5.

[48] S. Zhou, X. Mo, W. Zhu, et al., Selective adsorption of Au(III) with ultra-fast kinetics by a new metal-organic polymer, J. Mol. Liq., (2020) 114125-114133. https://doi.org/10.1016/j.molliq.2020.114125.

[49] B. Feng, C. Yao, S. Chen, et al., Highly efficient and selective recovery of Au(III) from a complex system by molybdenum disulfide nanoflakes, Chem. Eng. J., 350 (2018) 692-702. https://doi.org/10.1016/j.cej.2018.05.130.

[50] P. Samaddar, S. Kumar, K.-H. Kim, Polymer hydrogels and their applications toward sorptive removal of potential aqueous pollutants, Polym. Rev. (Philadelphia, PA, U. S.), 59 (2019) 418-464. https://doi.org/10.1080/15583724.2018.1548477.

[51] V.K.A. Muniraj, R. Boukherroub, M.V. Shelke, Flexible energy storage device

based on poly(N-phenylglycine), an incentive-energy pseudocapacitive conducting polymer, and electrochemically exfoliated graphite sheets, ACS Sustainable Chem. Eng., 8 (2020) 6433-6441. https://doi.org/10.1021/acssuschemeng.0c00880.

[52] Q. Ruan, L. Shao, Y. Shu, et al., Growth of monodisperse gold nanospheres with diameters from 20 nm to 220 nm and their core/satellite nanostructures, Adv. Opt. Mater., 2 (2014) 65-73. https://doi.org/10.1002/adom.201300359.

[53] P. Chen, Y. Liang, B. Yang, et al., In situ reduction of Au(I) for efficient recovery of gold from thiosulfate solution by the 3D MoS_2/chitosan aerogel, ACS Sustainable Chem. Eng., 8 (2020) 3673-3680. https://dx.doi.org/10.1021/acssuschemeng.9b06639.

[54] J. Guo, X. Fan, J. Wang, et al., Highly efficient and selective recovery of Au(III) from aqueous solution by bisthiourea immobilized uio-66-nh2: Performance and mechanisms, Chem. Eng. J., 425 (2021) 130588-130599. https://doi.org/10.1016/j.cej.2021.130588.

[55] S. Bhattarai, J.S. Kim, Y.-S. Yun, et al., Preparation of polyaniline-coated polystyrene nanoparticles for the sorption of silver ions, React. Funct. Polym., 105 (2016) 52-59. https://doi.org/10.1016/j.reactfunctpolym.2016.05.013.

[56] K.Z. Elwakeel, A.S. Al-Bogami, E. Guibal, 2-mercaptobenzimidazole derivative of chitosan for silver sorption – contribution of magnetite incorporation and sonication effects on enhanced metal recovery, Chem. Eng. J., 403 (2021) 126265. https://doi.org/10.1016/j.cej.2020.126265.

Chapter 4

Adsorption studies on Ag(I) using poly(N-phenylglycine) membrane and application in practical silver recycling

4.1. Introduction

Silver is not only widely used in jewelry, coins, and silverware, but also in the electronic industry, which is the dominant consumer of silver owing to its unique properties (e.g., electrical conductivity and corrosion resistance) [1]. Silver is also incorporated into medical products, textiles, and cosmetics as an effective antibacterial agent [2]. Owing to its numerous applications, it is inevitable that silver will find its way into the aquatic system; the threat this poses to the environment and humans has attracted increasing attention [3]. There is evidence that silver, like many other metals, can cause contact allergic reactions in susceptible individuals, deeming it a potential poisoning hazard [2]. Hence, the World Health Organization (WHO) stipulated that the amount of silver in drinking water should less than 0.1 $mg \cdot L^{-1}$ [4, 5]. Moreover, silver scarcity has emerged as a serious global concern; the global demand for silver in 2019 increased to 30,848 tons, whereas the global mine production decreased to 26,019 tons [6]. Sverdrup et al. estimated that half of the recoverable silver reserves have already been consumed, and the remaining will have been exhausted by 2240; therefore, the importance of recycling must be emphasized to make the silver supply more sustainable [7].

Treating Ag(I)-containing wastewater and the subsequent recovery of silver have emerged as focus areas in research because of their environmental and economic advantages [8, 9]. Adsorption is a method commonly used to treat solutions with low Ag(I) concentrations because it is a simple process without secondary pollutants, and has the ability to decontaminate effectively [10, 11].

Conductive polymers are regarded as excellent adsorbents because of their diverse functional groups, large active surfaces, and other properties [12]. Taghizadeh et al.

classified polyaniline (PANI), polypyrrole, polythiophene, and their derivatives as conductive polymers, which are increasingly being used in water treatment individually or as components. PANI and its derivatives rank first among the main conductive polymer-based materials used for water treatment [12]. Poly-N-phenylglycine (PNPG), another type of conducting polymer, has a conjugated skeleton similar to that of PANI, but contains several carboxylic acid groups functioning as adsorption sites, meaning that it also has great potential for water treatment [13, 14]. Upon deprotonation of the –COOH groups of PNPG into $–COO^–$, an ionic interaction occurs between Cu^{2+} and the carboxylate group [14]. Considering the presence of numerous Cu^{2+}, Pb^{2+}, and other metal cations in leaching solutions of waste print circuit boards (PCBs) and other waste water, the selective adsorption of Ag^+ must be studied. To mitigate the undifferentiated attraction of $–COO^–$ to cations, we investigated the adsorption of silver ions using non-deprotonated PNPG which has not been reported so far.

In this study, PNPG was loaded onto a mixed cellulose ester membrane through vacuum filtration. The interaction mechanism between the PNPG membrane and Ag(I) was studied by characterization and adsorption experiments. Silver recovery was also attempted on leaching solutions of waste PCBs and municipal solid waste incineration (MSWI) fly ash.

4.2. Experimental section

4.2.1. Materials

Used materials were N-Phenylglycine (NPG), ammonium peroxodisulfate (APS), thiourea, mixed cellulose ester (MCE) membranes, HNO_3, H_2SO_4, NaOH, Waste PCBs samples, MSWI fly ash, and 1000 $mg·L^{-1}$ standard solutions of Pb(II), Ni(II), Cu(II), Zn(II), Al(III), and Fe(III), Ag(I), Ca(II), Mg(II).

4.2.2. Preparation of PNPG membranes

First, PNPG was synthesized by the polymerization of NPG under acidic conditions, with APS serving as an oxidant [15, 16]. Please refer to Section 2.2.1 for

the synthesis of PNPG and Section 2.2.2 for the detailed preparation procedure of 5 mg PNPG membranes.

4.2.3. Characterization

The ion concentrations were measured using an ICPE-9000 instrument (Shimadzu, Japan). The characterization methods of XRD, FTIR, XPS, SEM, EDS, zeta potential analysis, Barrett–Joyner–Halenda (BJH), and X-ray fluorescence analysis were the same as shown in Section 2.3.2.

4.2.4. Adsorption experiments

In the adsorption experiments of influencing factors, diluting the Ag^+ standard solution to the target working solution and adjusting the pH with NaOH and HNO_3 solutions. To investigate the effect of the pH, PNPG membranes weighing 5 mg were each immersed in 30 mL solutions of 50 $mg \cdot L^{-1}$ Ag(I), with the pH levels ranging from 3 to 7. The PNPG membranes were subjected to oscillating conditions at 120 rpm for 12 h at 25 ℃ and then sealed to prevent evaporation. To determine the effect of time, pH 6 solutions were used, and measurements were conducted from 0.5 h to 14 h, while retaining the rest of the previous conditions. The effect of the concentration was determined by carrying out the experiment using 5, 10, 20, 40, 50, 100, 150, 200, and 250 $mg \cdot L^{-1}$ solutions, while keeping the other conditions unchanged. The adsorption capacity q_t ($mg \cdot g^{-1}$) after time t (h) was determined using eq. (1) [17]:

$$q_t = \frac{(c_0 - c_t)V}{m} \tag{1}$$

where m (g) is the mass of PNPG; V (L), the volume of the Ag(I) solution; c_0 ($mg \cdot L^{-1}$), the initial concentration; and c_t ($mg \cdot L^{-1}$), the residual concentration. When the equilibrium state was reached, the equilibrium adsorption capacity q_e can be calculated from the equilibrium concentration c_e and the adsorption efficiency E_{ad} was calculated using eq. (8) [18]:

$$E_{ad} = \frac{(c_0 - c_e)}{c_0} \times 100\% \quad (2)$$

Both concentrations of metal ions were measured using ICPE-9000. The adsorption capacity was averaged from the results of three equivalent experiments.

4.3. Results and discussion

4.3.1. Characterization

Fig. 4.1a exhibits the FTIR spectrum of raw PNPG, in which six characteristic peaks can be identified within the range of 600–3600 cm^{-1}. The first peak at 1669 cm^{-1} belongs to the C=O of carboxyl groups [15]. The adjacent second and third peaks, at 1574 and 1493 cm^{-1}, are attributed to the stretching vibrations of C=C at the quinonoid ring and benzenoid ring, respectively [15, 19, 20]. The fourth peak at 1303 cm^{-1} is characteristic of the C–N bond in the benzenoid amine [14, 19]. The last two peaks located at 1145 and 807 cm^{-1} are assigned to the quinone ring and 1,4 (para)-substituted phenyl ring structure, respectively, confirming the synthesis of PNPG [14, 21]. Moreover, by comparing the FTIR spectra of NPG monomer and synthesized PNPG (**Fig. 4.1b**), the most obvious change was that there were characteristic peaks of 1,4 (para)-substituted phenyl ring structure (807 cm^{-1}) and quinone ring structure (1145 cm^{-1}) in PNPG, indicating the successful synthesis of PNPG as well.

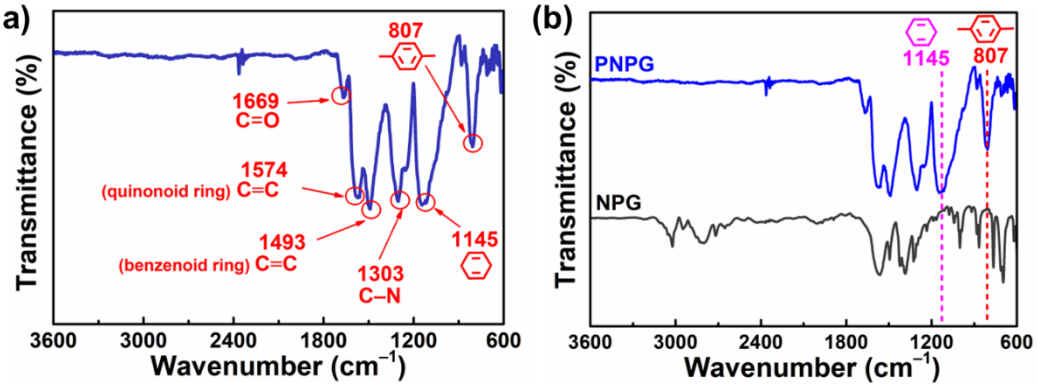

Fig. 4.1. (a) FTIR spectrum of synthesized PNPG. (b) FTIR spectra of NPG monomer and synthesized PNPG.

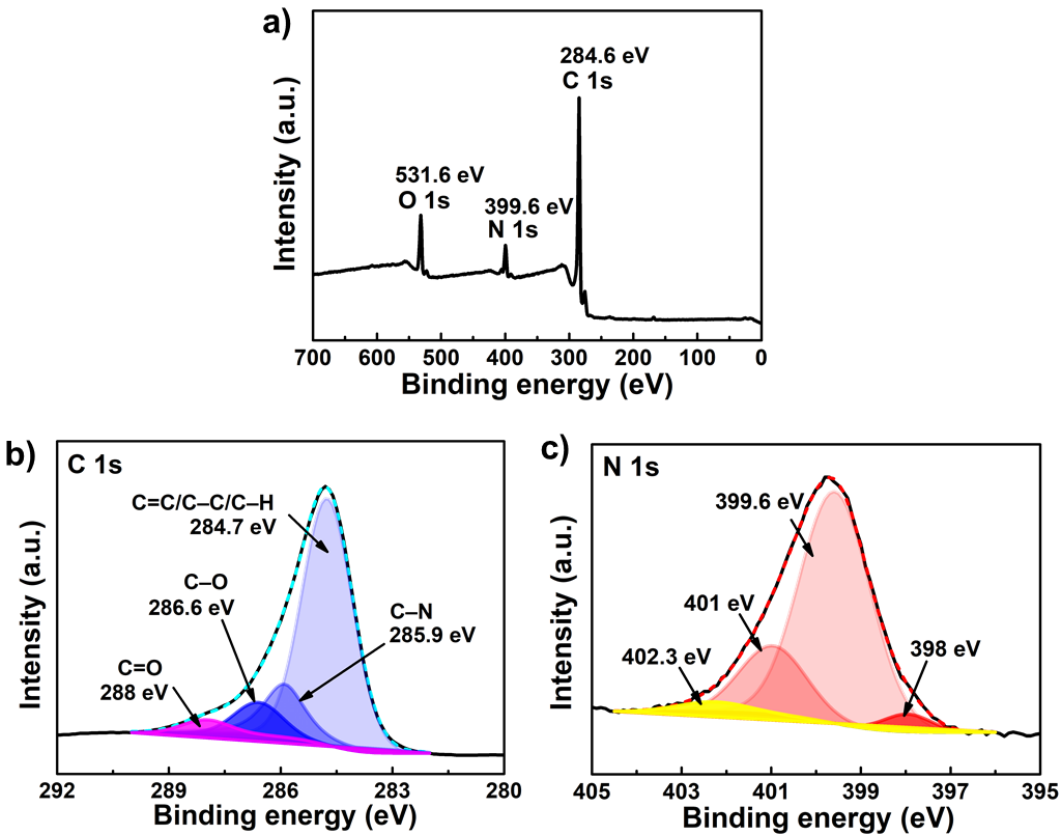

Fig. 4.2. (a) Wide-scan XPS profile of PNPG membrane. XPS profiles of (b) C 1s and (c) N 1s.

Fig. 4.2a shows the XPS wide-scan spectrum of the PNPG membrane. The O 1s, N 1s, and C 1s peaks are easily identifiable at 531.6, 399.6, and 284.6 eV, respectively. As shown in **Fig. 4.2b**, C 1s is divided into four sub-peaks of different sizes: C=C/C–C/C–H at 284.7 eV with the largest area, followed by C−N, C−O, and C=O at 285.9, 286.6 and 288 eV, respectively [22, 23]. **Fig. 4.2c** is the N 1s core-level XPS profile wherein the four peaks cleaved by N 1s are individually assigned to the neutral quinone imine (398 eV), the neutral N of benzenoid diamine (399.6 eV), the conjugative protonated polaron N (401 eV), and the conjugative protonated bipolaron N (402.3 eV) [24, 25].

Fig.4.3 show the morphology of the PNPG membrane. The area of the PNPG region (**Fig. 4.3a**) is equal to the effective filtering area of the funnel (9.6 cm^2). On the microscopic level, the seemingly smooth PNPG membrane contains many folds of different sizes that facilitate sufficient contact by allowing the liquid to penetrate the

interior. Furthermore, the upper PNPG morphology is clearly different from that of the lower support layer (**Fig. 4.3b–c**). The membrane (PNPG and MCE layers), measured in 10 different areas using a digital micrometer, has an average thickness of 126 μm.

The porosity of the membrane, which is the ratio of the pore volume to total membrane volume, was determined according to the following equation:

$$\varepsilon = \frac{V_{pore}}{V_{mem}} = \times 100\% \quad (3)$$

where V_{pore} (cm^3) is the total volume of the pores; V_{mem} (cm^3), the total volume of membrane. V_{pore} can be estimated from the desorption process of the N_2 isotherm using the Barrett-Joyner-Halenda (BJH) method. In the PNPG membrane (area = 9.6 cm^2, thickness = 126 μm, mass = 0.059 g), the measured pore volume at per gram was 0.014 $cm^3 \cdot g^{-1}$, so the total volume of pores V_{pore} was 8.26×10^{-4} cm^3, and the calculation of the equation yielded an approximate porosity of 0.68%.

4.3.2. Interaction mechanism

Conducting polymers adsorb metal ions through the following mechanisms: electrostatic attraction, chelation, and redox reactions. To explore the interaction mechanism between PNPG and Ag(I), SEM, EDS, and XPS characterizations were employed.

The SEM image (**Fig. 4.4a**) shows that many bright and small objects are distributed on the post-adsorption PNPG membrane. Elemental analysis of the yellow-dotted enclosed area **Fig. 4.4b** shows the distribution of Ag (**Fig. 4.4c**) which is consistent with the distribution of bright objects in **Fig. 4.4a,** and a large amount of Ag in this area also has been measured (**Fig. 4.4d**). The XRD results (**Fig. 4.5**) show that the post-adsorption sample has four characteristic peaks at 38.16°, 44.35°, 64.48°, and 77.45°, which correspond to the (1 1 1), (2 0 0), (2 2 0), and (3 1 1) lattice planes of elemental silver (JCPDS No. 04-0783), respectively, indicating the reduction of silver ions to elemental silver [26, 27].

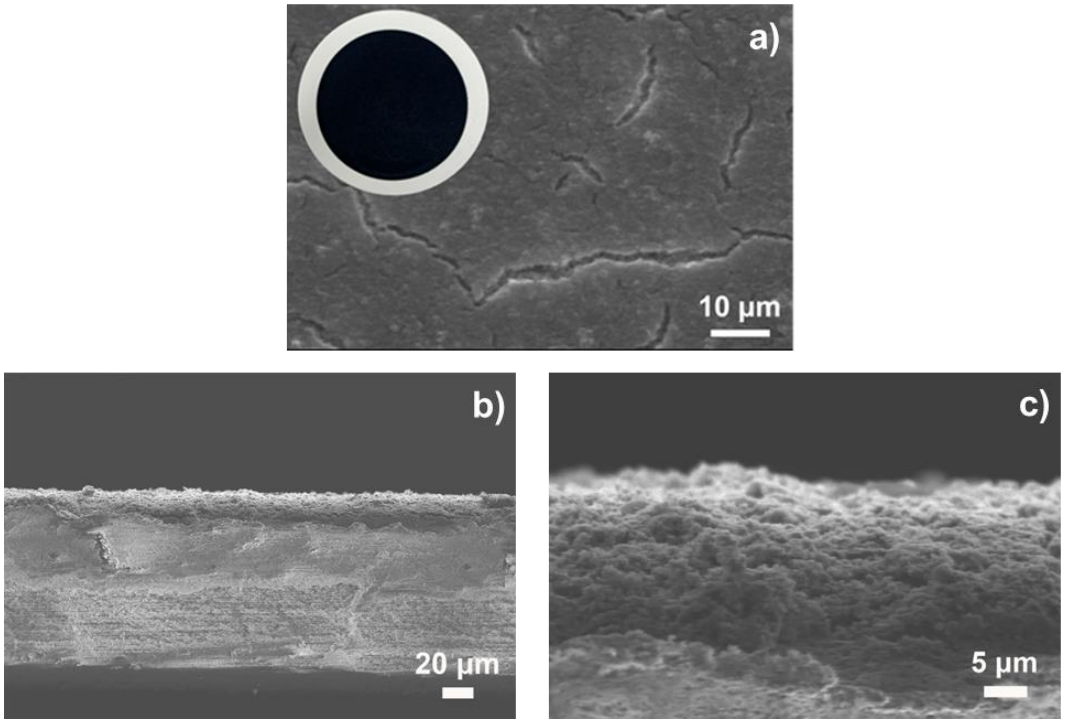

Fig. 4.3. (a) Digital photo of the prepared PNPG membrane and SEM image from top view. (b) SEM image from section view and (b) the local amplification of upper PNPG layer.

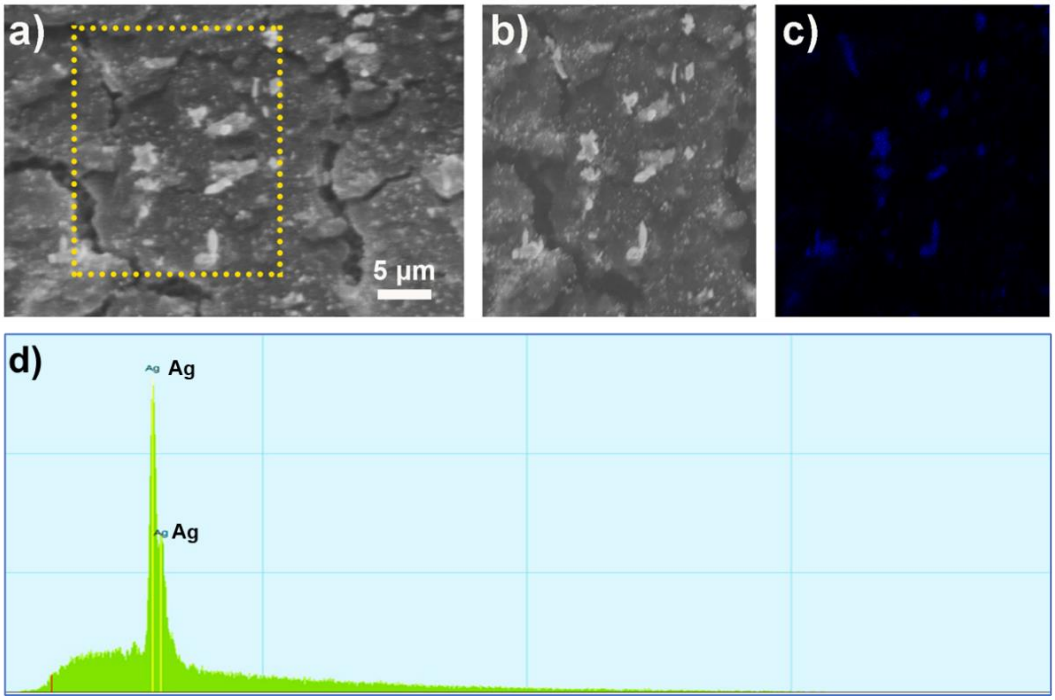

Fig. 4.4. (a) SEM image of the post-adsorption PNPG membrane. (b) Partial view of the yellow box in (a). (c) Elemental mapping image of Ag in post-adsorption PNPG membrane. (d) EDS element composition analysis of PNPG membrane after adsorption.

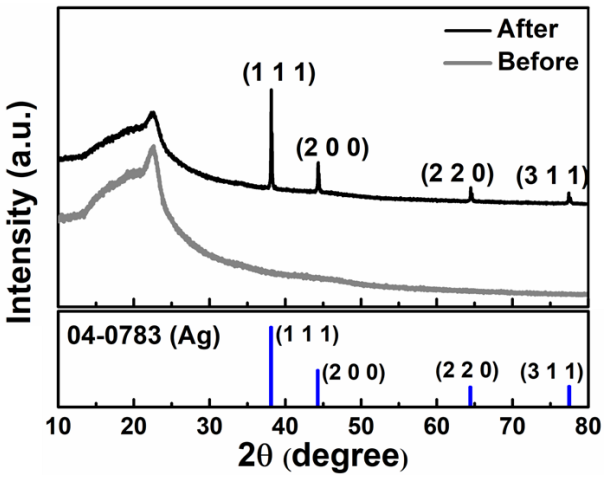

Fig. 4.5. XRD profiles of the PNPG membrane before and after the Ag(I) adsorption.

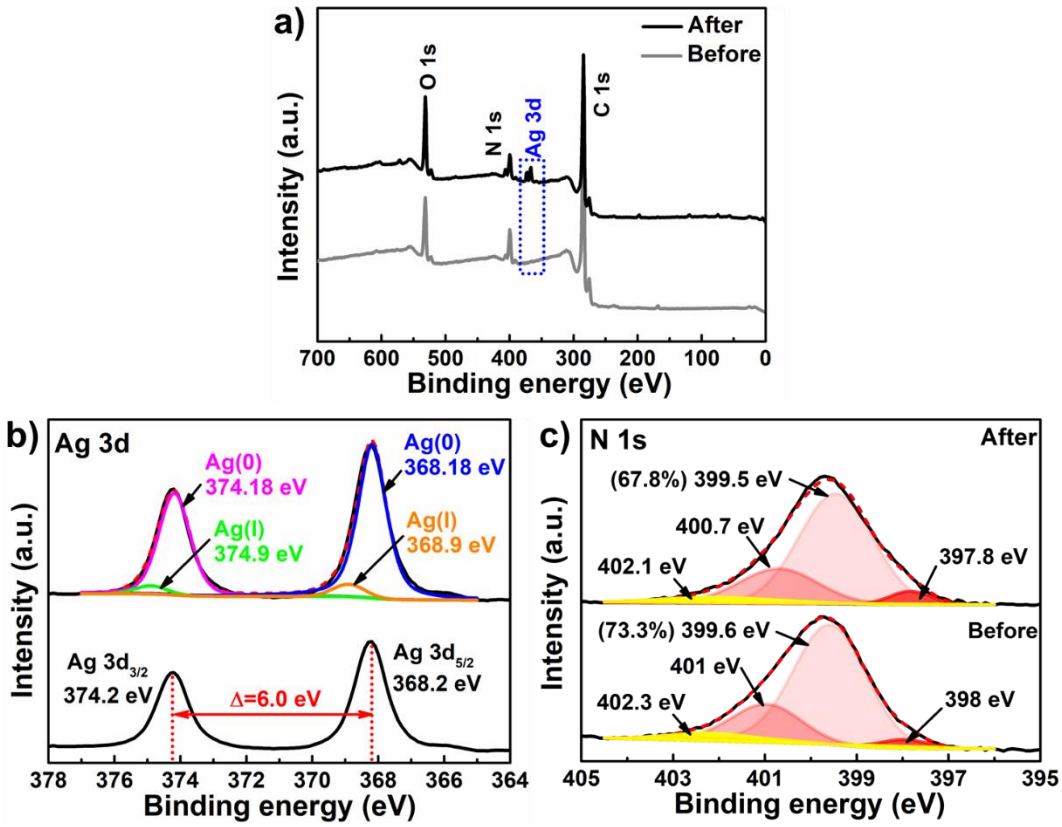

Fig. 4.6. (a) wide-scan XPS, (b) Ag 3d, and (c) N 1s XPS profiles of the PNPG membrane before and after the Ag(I) adsorption.

In the comparison to the XPS wide-scan spectra (**Fig. 4.6a**), Ag 3d peaks were found on the PNPG membrane post adsorption, indicating the successful capture of silver by the PNPG membrane. Further analysis of the Ag 3d spectra (**Fig. 4.6b**) shows that the peaks at 368.2 eV and 374.2 eV are attributed to Ag $3d_{5/2}$ and Ag $3d_{3/2}$,

respectively, and the difference between both is 6.0 eV. Each peak can be fitted with two components, wherein Ag(0) is dominant and Ag(I) occupies a smaller area. This characteristic signal of Ag 3d and the dominant position of Ag (0) indicate that most of the silver ions were reduced to elemental silver during adsorption, whereas a smaller amount was captured through coordination [11, 28].

Table 4.1 Information of N1s XPS spectra before and after adsorption

Assignment	N 1s (Before)			N 1s (After)		
	Peak (eV)	Are	Ratio (%)	Peak (eV)	Are	Ratio (%)
Neutral quinone imine	399.6	25377.5	73.3	399.5	26837.0	67.8
Neutral benzenoid diamine	398.0	1226.7	3.5	397.8	1766.9	4.5
Conjugative protonated-polaron	401.0	6984.8	20.2	400.7	8766.1	22.1
Conjugative protonated-bipolaron	402.3	1056.0	3.0	402.1	2209.7	5.6

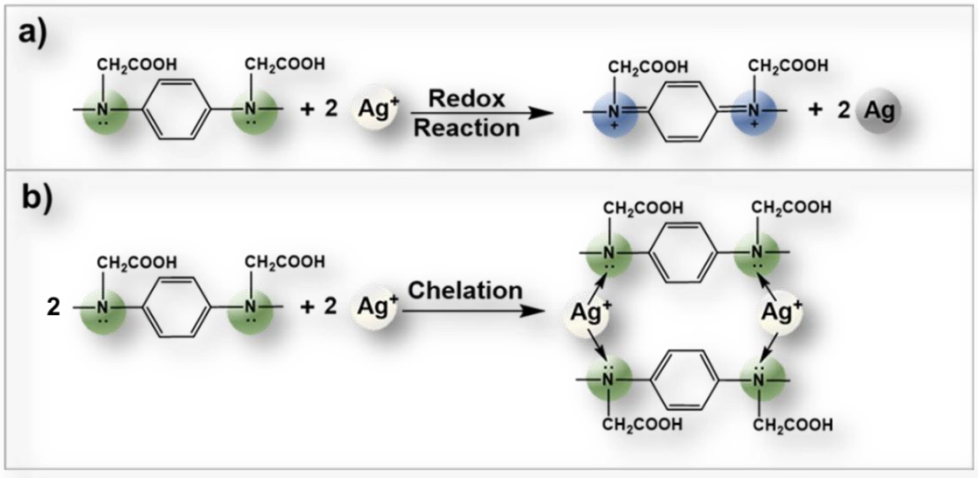

Fig. 4.7. Interaction between PNPG and Ag^+ via (a) redox reaction and (b) chelation reaction.

The N 1s XPS profiles (**Fig. 4.6c**) show that the positions of the four peaks pre- and post-adsorption are similar. However, the amount of post-adsorption neutral benzenoid diamine (399.5 eV) decreased from 73.3% to 67.8%, indicating the involvement of this structure in the reaction with silver ions [11]. This reaction with

silver ions can proceed in two ways to form a conjugative protonated bipolaron (evidenced by its increased content in **Table 4.1**): one, the redox reaction between neutral benzenoid diamine and silver ion (**Fig. 4.7a**) [24] and two, the chelation reaction wherein the lone-pair electrons in the neutral benzenoid diamine bind with silver ions (**Fig. 4.7b**).

4.3.3. Adsorption performance

This section discusses the potential influence of the pH, adsorption time, and Ag(I) concentration on the adsorption performance by the PNPG membranes, and evaluates the Ag(I) adsorption behavior through kinetic and isotherm studies.

Fig. 4.8a shows that q_t gradually increases with an increase in the pH from 3 to 7. This can be explained as follows: Free Ag^+ in the Ag(I) working solution accounts for over 99% of the total amount of silver in solutions with a pH range of 2–7 [29]. The pH point of zero charge (PZC) of PNPG was measured as 7.5 (**Fig. 4.8b**). PNPG becomes positively charged under acidic conditions because of the protonation of functional groups like amine and carboxyl [30, 31]; therefore, Ag^+ cannot be effectively captured due to electrostatic repulsion. Under neutral conditions, some functional groups become electrically neutral [30], resulting in less repulsion and an improvement in the adsorption performance of Ag^+. Based on the above facts, the gradually higher adsorption of Ag(I) on the PNPG membrane with the upward pH can be attributed to: the decrease of positive charge in PNPG makes less repulsion and is beneficial to capture silver ions. A working pH of 6 was chosen for the subsequent two influence-factor experiments because it is safer to handle and has a similar adsorption performance to that obtained with pH 7.

The time-dependent experimental data (**Fig. 4.9**) show that q_t increases from 0.5 h to 14 h. During the first 2 h, the silver ions were adsorbed quickly because of the numerous available adsorption sites. With the progress of time, the available adsorption sites gradually reduced, resulting in a lowered adsorption rate to eventually attain equilibrium (229.5 $mg \cdot g^{-1}$) at 10 h.

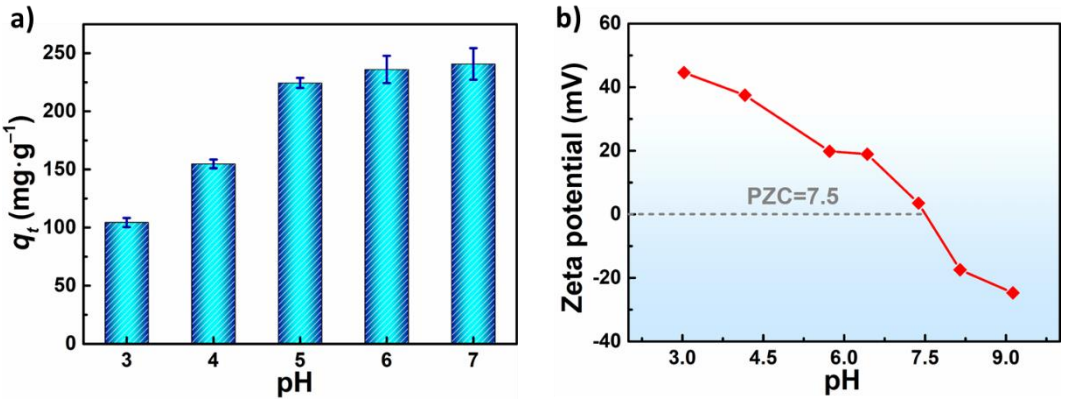

Fig. 4.8. (a) Effect of pH on Ag(I) adsorption by the PNPG membrane. (b) Zeta potentials of PNPG.

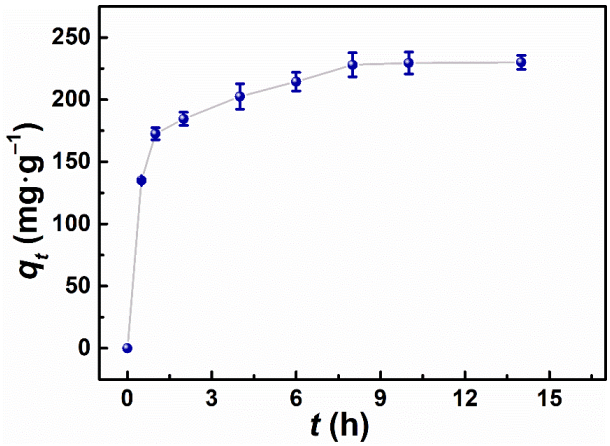

Fig. 4.9. Effect of time on Ag(I) adsorption.

To evaluate the Ag(I) adsorption behavior of the PNPG membrane, the following two kinetic models–Pseudo-first-order model (PFO) and Pseudo-second-order model (PSO) were utilized to fit the experimental data [32]:

$$\text{PFO:}\quad \ln\left(q_e - q_t\right) = \ln q_e - k_1 t \tag{4}$$

$$\text{PSO:}\quad \frac{t}{q_t} = \frac{1}{k_2 q_e^2} + \frac{t}{q_e} \tag{5}$$

where q_e (mg·g^{-1}) denotes the equilibrium adsorption capacity, while k_1 (h^{-1}) and k_2 (g·mg^{-1}·h^{-1}) are the rate constants of the two models. **Fig. 4.10** and **Table 4.2** show the fitting results and analyzed data, respectively. R^2 is a frequently used validation criterion for adsorption kinetics fitting [33]. In Table 1, an $R^2 > 0.8$ for PFO and PSO, but PSO was deemed to be the better-fit model because its R^2 was higher and closer to

1, indicating the dominant role of chemisorption in this process [34]. The equilibrium adsorption capacity obtained from PSO fitting was 238.7 mg·g^{-1}, approximate to the experimental value (229.5 mg·g^{-1}).

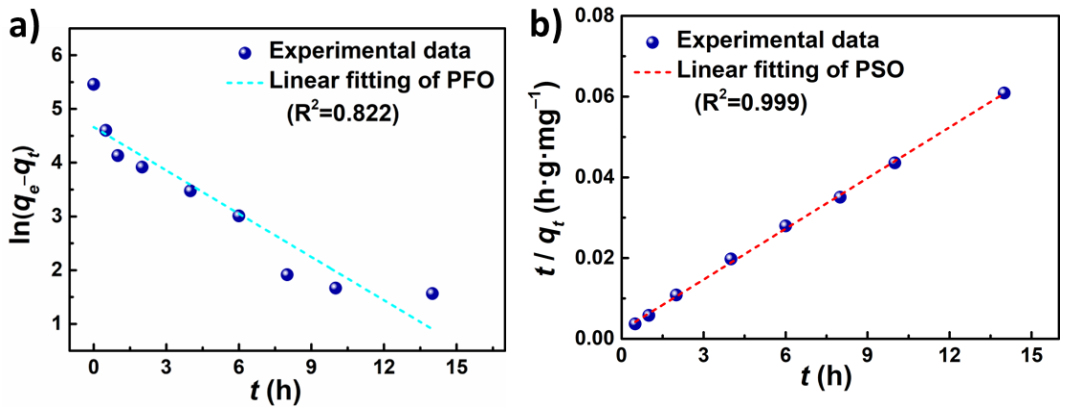

Fig. 4.10. Adsorption kinetics fitting of the (d) PFO and (e) PSO models.

Table 4.2 Parameters of kinetic models

Model	**Parameters**	**Value**
PFO	q_e (mg·g^{-1})	105.8
	k_1 (h^{-1})	0.27
	R^2	0.822
PSO	q_e (mg·g^{-1})	238.7
	k_2 (g·mg^{-1}·h^{-1})	8.3×10^{-3}
	R^2	0.999

Regarding the effect of concentration at 25 ℃, **Fig. 4.11a** shows that the q_e goes up with increasing Ag(I) concentration. For more information on the adsorption, there are three isotherm models to be used. The Langmuir model was applied to represent the equilibrium condition of monolayer homogeneous adsorption; the Freundlich model to describe multilayer adsorption on heterogeneous surfaces; the Temkin model to account for adsorption as a multilayer process. Their linear mathematical equations are expressed as follows [35-37]:

$$\text{Langmuir:}\quad \frac{c_e}{q_e} = \frac{c_e}{q_m} + \frac{1}{K_L \times q_m} \tag{6}$$

$$\text{Freundlich:}\quad \log q_e = \log K_F + \frac{1}{n} \times \log c_e \tag{7}$$

$$\text{Temkin:}\quad q_e = \frac{RT}{b} \ln K_T + \frac{RT}{b} \ln c_e \tag{8}$$

where c_e (mg·L^{-1}) is the equilibrium concentration of the Ag(I) solution; q_e (mg·g^{-1}), the equilibrium adsorption capacity; q_m (mg·g^{-1}), the maximum adsorption capacity. K_L (L·mg^{-1}), K_F (L$^{1/n}$·mg$^{1-1/n}$·g^{-1}), and K_T (L·g^{-1}) represent the isotherm equilibrium binding constants of Langmuir, Freundlich, Temkin model respectively. The $1/n$ term is related to the surface heterogeneity; a smaller $1/n$ corresponds to a stronger heterogeneity of the adsorption sites. The adsorption process is favorable when $0 < 1/n < 1$. The gas constant and temperature are represented by R and T, respectively, and b is a constant [17, 38].

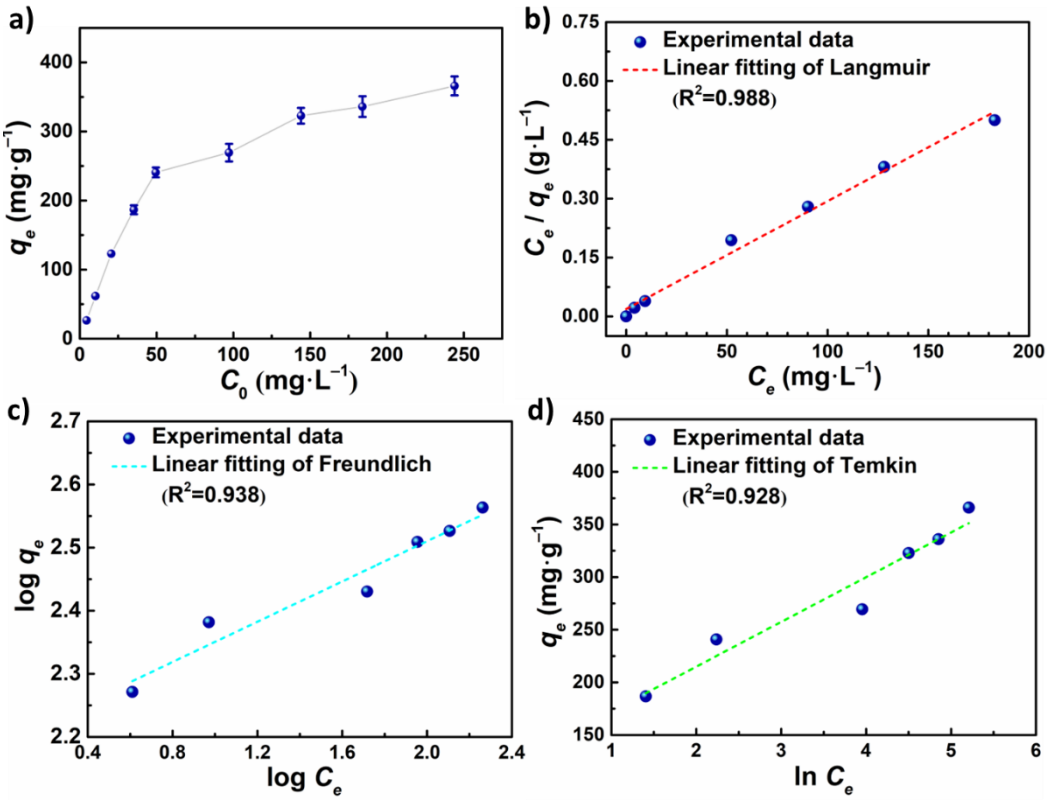

Fig. 4.11. (a) Effect of concentration on Ag(I) adsorption. Adsorption isotherm studies using the (b) Langmuir, (c) Freundlich, and (d) Temkin models.

Table 4.3 Parameters of isotherm models

Model	Parameters	Value
Langmuir	q_m (mg·g^{-1})	363.6
	K_L (L·mg^{-1})	0.15
	R^2	0.988
Freundlich	$1/n$	0.16
	K_F (L$^{1/n}$·mg$^{1-1/n}$·g^{-1})	155.3
	R^2	0.938
Temkin	b	58.3
	K_T (L·g^{-1})	3.06
	R^2	0.928

Table 4.4 Comparison of silver ions adsorption capacity with other adsorbents

Material	q_m (mg·g^{-1})	pH	Reference
PDMTD	127.89	1	[39]
TA-PS nanoparticles	190 ± 5	6	[40]
Thiol-grafted graphene oxide	134.1	5	[6]
TU-PVDF membrane	172.8	6	[41]
Acrylate modified CAB	23.92	3	[42]
2-AMP resin	110.5	4.88	[43]
Fe_3O_4@ microbial extracellular polymeric substances	48	6	[44]
Carboxymethyl functionalized PGMA	157.05	4	[45]
PolyTBAUCH	39.8	2.5	[46]
rSFB	62.50	6	[47]
PNPG membrane	366	6	This work

Among the three models presented in **Figs. 4.11b–d**, the correlation coefficient R^2 of the Langmuir isotherm model was closest to 1 (**Table 4.3**). This implies that

monolayer adsorption promotes Ag(I) adsorption by the PNPG membrane. The theoretical q_m, calculated from the Langmuir model, was 363.6 mg·g^{-1}, which is close to the experimental value of 366 mg·g^{-1}. Additionally, the PNPG membrane exhibits a higher maximum adsorption capacity of silver compared to other reported materials (**Table 4.4**).

4.3.4. Reusability

The study of the potential practical applications of adsorbents for reusability is aligned with the theme of green and environmental protection. Adsorption experiments were carried out in pH 6 Ag(I) solutions at 120 rpm and 25 °C. The membrane was then removed and immersed in a fresh eluting agent (0.5 g thiourea in 50 mL of 0.01 mol·L^{-1} HNO_3) while shaking. Afterwards, the PNPG membrane was washed with deionized water five times to remove the residual eluent, regenerated after drying, and then subjected to the next adsorption experiment.

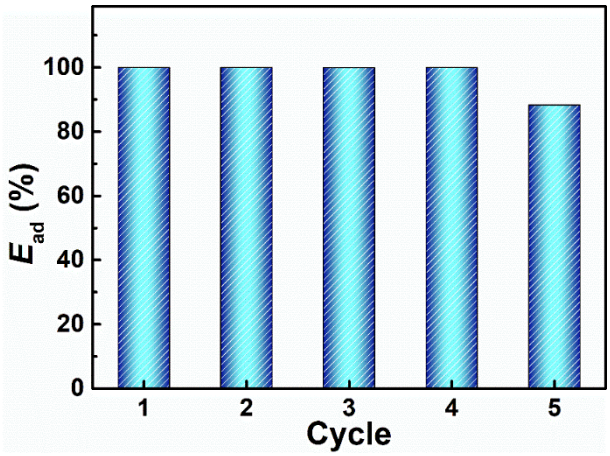

Fig. 4.12. Adsorption efficiencies in the reusability experiment (c_0 = 30 mg·L^{-1}, V =30 mL, t = 12 h)

The results of repeated utilization (**Fig. 4.12**) suggest the good reusability of the PNPG membrane during the first four adsorption-desorption cycles, as evidenced by the nearly 100% adsorption efficiency. By the end of the fifth adsorption process, E_{ad} decreased to approximately 90%, possibly owing to some consumed N sites.

4.3.5. Selectivity

Superior selectivity is necessary because other metal ions (e.g., Pb^{2+}, Cu^{2+}, and Ni^{2+}) coexist with Ag(I) [3]. To ensure the selective adsorption of Ag(I), selective adsorption experiments were conducted using solutions with two different concentration ratios and a pH of 5. The 1 : 5 mixed solution had a Ag(I) concentration of 10 mg·L^{-1}, while the Cu^{2+}, Pb^{2+}, Zn^{2+}, Al^{3+}, Ni^{2+}, and Fe^{3+} concentrations were 50 mg·L^{-1}. Meanwhile, the 1 : 10 mixed solution had a Ag(I) concentration of 5 mg·L^{-1}, while the concentrations of the other components were retained at 50 mg·L^{-1}.

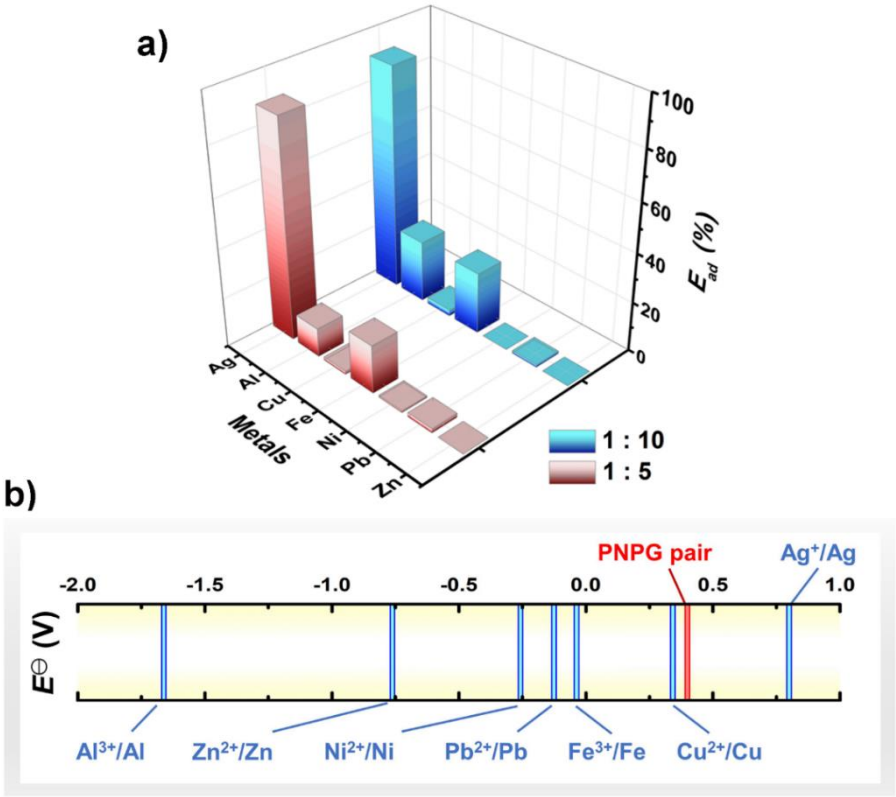

Fig. 4.13. (a) Adsorption efficiency of different metal ions using two types of mixed solutions (V = 20 mL, pH = 5, t = 12 h). (b) Schematic diagram comparing the redox potential.

According to **Fig. 4.13a**, the adsorption efficiency of the PNPG membrane for Ag(I) in these two mixed solutions is approximately 90%, a value greater than those of the other metal ions. The redox potential can give explanation for this high selectivity to Ag(I). The PNPG CV curve obtained by Muniraj et al. showed the redox potential of

PNPG to be approximately 0.4 V [24]. Among the other metal ions present in this experiment, only the Ag^+/Ag pair had a higher redox potential (0.7996 V) than PNPG (**Fig. 4.13b**); thus, PNPG preferentially captures Ag^+ even at low Ag^+ concentrations.

Upon Ag(I) exhaustion, PNPG still have large sums of surplus adsorption sites. **Fig. 4.13a** shows the adsorption efficiency of Al and Fe (approximately 10–25%). This affinity is consistent with the hard acid and base principle, in which Al^{3+} and Fe^{3+} are considered hard acids that bind strongly with the O-reactive groups (–COOH, hard base) of PNPG [29, 48-50]. Pb^{2+}, Cu^{2+}, Ni^{2+}, and Zn^{2+} are generally classified as borderline metals with lower affinity for the hard base [51]; consequently, their adsorption performance is poorer. To summarize the above analysis, the selectivities for metal ions are ranked in descending order as: $Ag^+ > Al^{3+}$, $Fe^{3+} > Pb^{2+}$, Cu^{2+}, Ni^{2+}, and Zn^{2+}.

4.3.6. Recovery of Ag from waste PCBs leaching solution

PCBs are integral components of most electronic waste. The silver content of PCBs is approximately 0.12%, which is higher than that of natural argentiferous ore (~ 0.08% silver) [1]. E-waste is an urban mine, and can be used as a raw material source to extract secondary silver. To investigate the recovery of Ag by the PNPG membrane from two real solutions, the prepared waste PCBs samples were extracted with acid to obtain a leaching solution containing silver ions. The 5 mg PNPG membranes were then immersed in these leaching solutions and shaken for 12 h under the same conditions as before.

The experimental process of preparation waste PCBs leaching solution began with two sequential leaching steps using a H_2SO_4/H_2O_2 solution, followed by a step using a HNO_3 solution (**Fig. 4.14**) [29, 52]. Prepared samples (3.0 g) were firstly leached with H_2SO_4–H_2O_2 mixture (100 mL 2 mol·L^{-1} H_2SO_4, 44 mL 15 % H_2O_2) with heating to 80 ℃ and stirring at 300 rpm for 1 h, and most of the metals such as Cu, Fe, Ni, Al, and Zn were dissolved. After the first reaction, the solid A obtained by filtration was the mixture of gold, silver, lead, and insoluble oxides and salts. And then, the solid A was treated with 50 mL 2 mol·L^{-1} HNO_3 at 80 ℃ with stirring at 300 rpm for 1 h. Since HNO_3 has natural oxidation, it can dissolve Ag, Pb, etc., but does not affect Au and Pt.

After the second reaction and filtration, the liquid was prepared into a 200 mL stock solution which was sampled and adjusted to pH = 7 with NaOH solution before filtration, followed by adsorption experiments. The pH of the leaching solution was then adjusted to the target value (**Fig. 4.14**) before the leaching solution was subjected to silver recovery using a PNPG membrane. While adjusting the pH to neutral, the metal ion concentration decreased due to the increase in the solution volume and the precipitation of Fe, Pb, and Cu. The adjustment of the pH not only provided the optimum pH for Ag adsorption, but also reduced the interference of other metal ions. The initial concentrations of the ions determined using ICPE-9000 were as follows ($mg \cdot L^{-1}$) (**Fig. 4.15a**): Ag, 5.09; Cu, 17.0; Pb, 1.06; Al, 0; Ni, 2.97; Fe, 0; and Zn, 0.801.

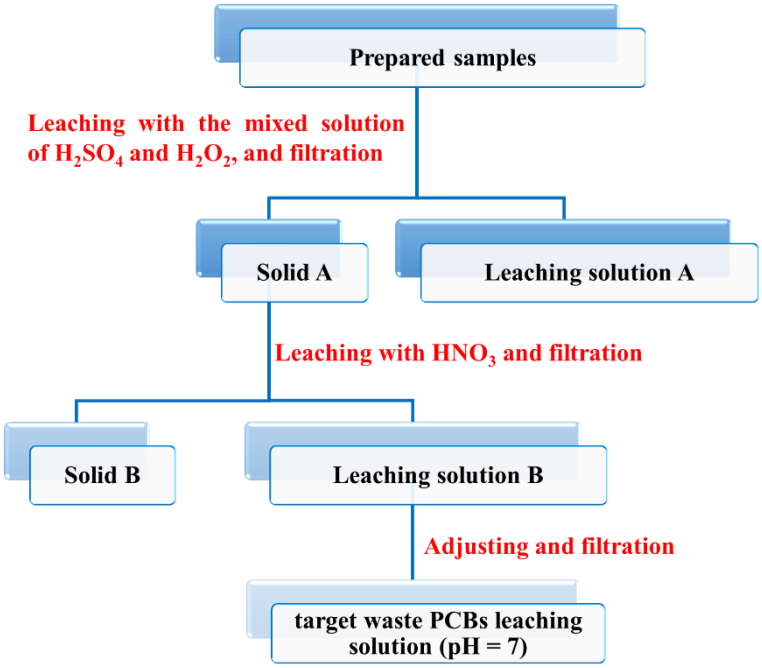

Fig. 4.14. The preparation of target waste PCBs leaching solution which contains Ag(I) with pH = 7.

In heterogeneous multicomponent systems, the adsorption of metal ions relies on several aspects such as the pH, initial metal ion concentration, and competitive binding sites [53]. For the waste PCBs leaching solution with a pH of 7, the adsorption efficiencies decreased in the following order: Ag(93.03%) > Cu(15.88%) > Pb(6.04%) >

Zn(0.5%) (**Fig. 4.15b**). The adsorption of Ag is excellent because the redox potential is higher than that of PNPG (see Section 4.3.5). Wadhawan et al. suggested that the order of adsorption of metal ions was related to the atomic mass, electronegativity, and ion radius [54]. Some studies used a covalent index to measure this correlation and reported that Pb(II), Cu(II), and Zn(II) have covalent index values of 6.41, 2.64, and 2.04, respectively, indicating that Pb(II) has a stronger attraction to the lone-pair electrons of N than the rest do [55, 56]. However, the concentration of Cu(II) is significantly higher than that of Pb(II) in our waste PCBs leaching solution, increasing its probability of being captured, and causing its adsorption efficiency to be higher than that of Pb(II).

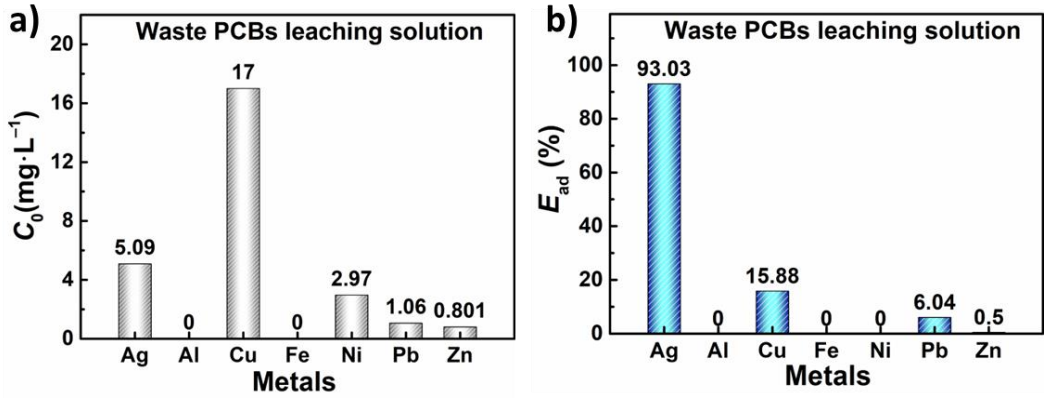

Fig. 4.15. (a) Initial metal concentrations in target waste PCBs leaching solutions and (b) adsorption efficiency of different metals after the experiment (V =30 mL, t = 12 h).

4.3.7. Recovery of Ag from MSWI fly ash leaching solution

MSWI produces large amounts of fly ash. MSWI fly ash contains Ca, Si, Al, Na, K, Mg, Cl, and O (contents >10000 mg·kg^{-1}); other metal elements such as Zn, Pb, Cu, Cr; and several other components. Recently, rather than landfill disposal, many regions have been progressively encouraging rational waste disposal by reuse and recovery of heavy metals from MSWI fly ash [57]. To investigate the silver recovery from MSWI fly ash, the leaching solution of MSWI fly ash samples was prepared, and then performing the adsorption experiments.

To remove the soluble salt and improve the metal grade as much as possible, the MSWI fly ash was initially washed with deionized water. Mix 20 g fly ash with 400 mL water and stir thoroughly at 800 rpm for 5 minutes. The solids obtained by

centrifugation are dried at 60°C. Collect the dried samples for subsequent experiments.

Zhang et al. reported that the concentration of leached elements increases as the pH decreases during the digestion of MSWI fly ash. They observed that leaching was most effective at pH 2 [58]. To obtain leaching solutions containing more silver ions and fewer other elements, pre-treated fly ash was digested stepwise prior to adjusting the pH to 6. Dried pre-treated MSWI fly ashes samples (2.0 g) went through two steps of leaching: leaching at pH = 2 condition and leaching with 2 mol·L^{-1} acid (**Fig. 4.16**). It is important to note that in the first step, the mixture needs to be maintained at pH = 2 by dropping a higher-concentration HNO_3 while stirring. After every centrifugation, wash the solids and then centrifuge again, and this process needs to be repeated 3 times.

The results from the quantitative elemental analysis of dried pre-treated MSWI fly ash (**Fig. 4.17**) show that CaO accounted for the largest proportion (37.87%), followed by Zn (10.02%) and Ag (0.08%) in the sample. Other substances not listed amounted to 45.02%.

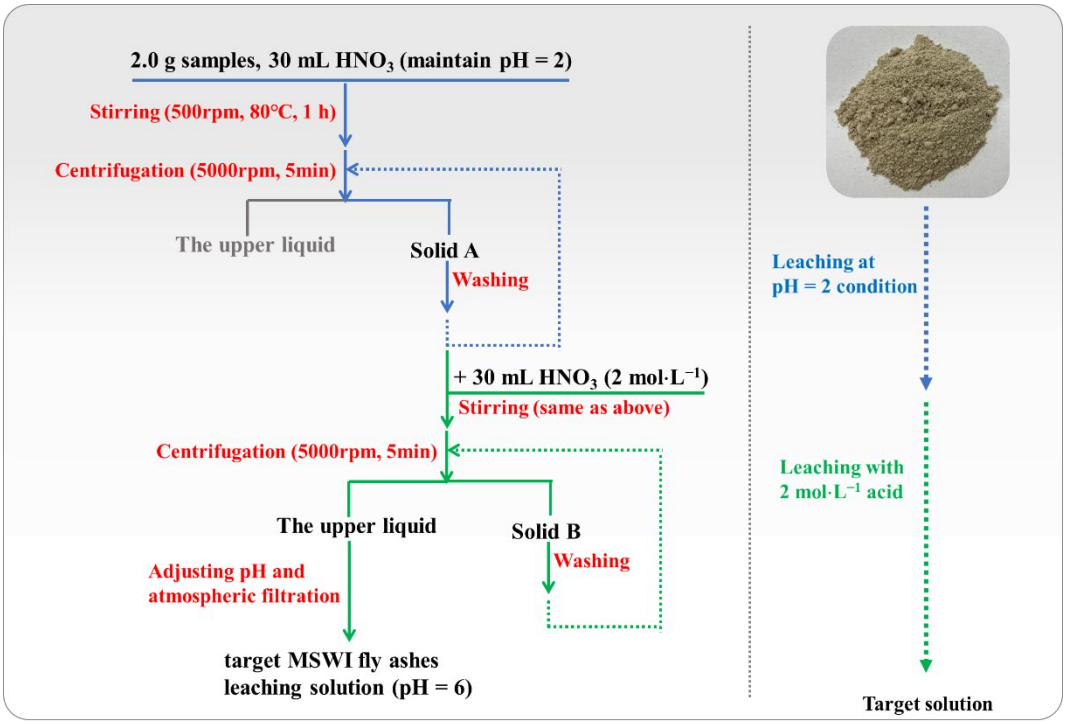

Fig. 4.16. The preparation of target MSWI fly ashes leaching solution containing Ag(I) with pH=6.

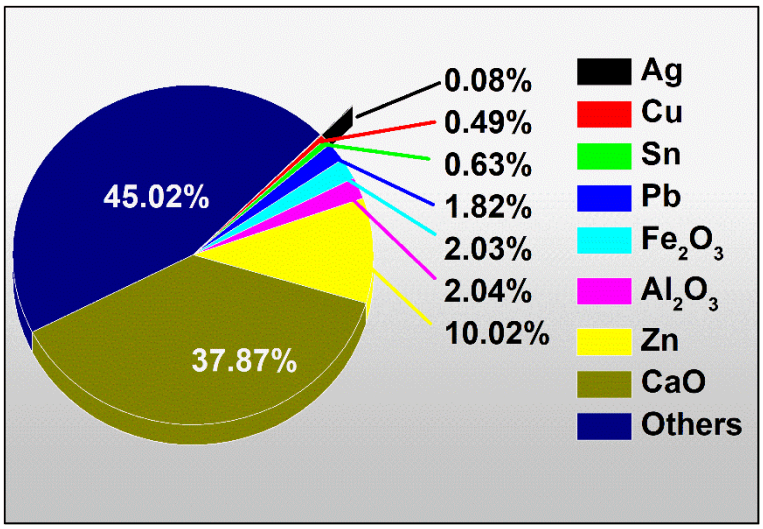

Fig. 4.17. Elemental analysis of pre-treated fly ash (measured by the portable X-ray fluorescence analyzer).

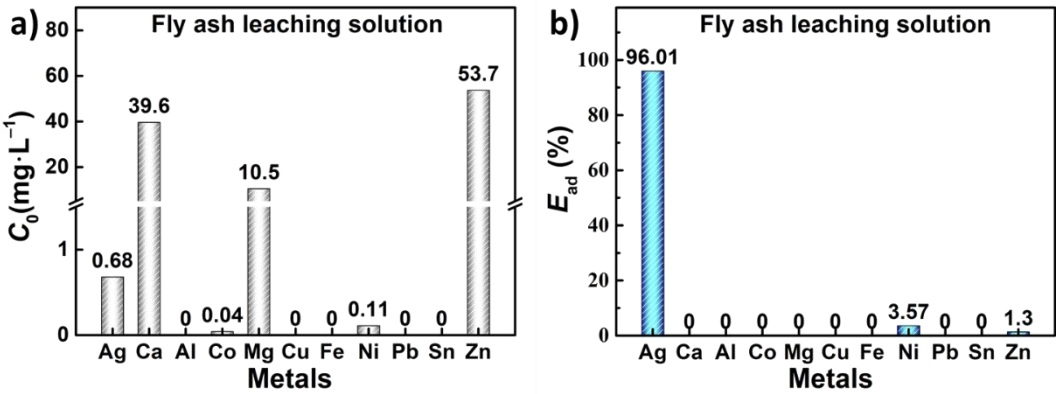

Fig. 4.18. (a) Initial metal concentrations in target MSWI fly ash leaching solution and (b) adsorption efficiency of different metals after the experiment (V =20 mL, t = 12 h).

Analysis (**Fig. 4.18a**) shows that the concentrations of Ca, Mg, and Zn were very high; those of Ag, Co, and Ni were less than 1%; and those of Al, Cu, Fe, Pb, and Sn were zero. Such could results arise from the leaching during the previous step or filtering by precipitation during pH adjustment. Despite the harsh environment of real solutions, the sensitivity of PNPG enabled the adsorption of approximately 96% of Ag (**Fig. 4.18b**). Combining this property with the selective adsorption of silver in real waste PCBs leaching solution, it can be deduced that the PNPG membrane is promising for the recovery of silver.

4.4. Conclusion

In this study, a PNPG membrane was successfully prepared via vacuum filtration after forming PNPG by the polymerization of the NPG monomer. The PNPG membrane could adsorb silver ions. The characterization results obtained from SEM, EDS, XRD, and XPS analyses revealed the reaction mechanism of the PNPG membrane with Ag(I): (1) most of the redox reactions occurred between the neutral benzenoid diamine of PNPG and Ag(I) to generate a positively charged conjugative bipolaron and elemental silver; (2) coordination reactions occurred between Ag(I) and the lone-pair electrons of benzenoid diamine, to a lesser extent. This discovery of the interaction mechanism between the PNPG membrane and silver ions has broadened the scope of this specific conductive polymer in adsorption studies. Based on the adsorption experiments, the performance of Ag adsorption was highly dependent on the pH and was optimal under neutral conditions. The kinetic results showed that the adsorption process agreed well with the PSO model, indicating chemical adsorption. The adsorption isotherm results displayed good consistency with the Langmuir model, indicating monolayer adsorption. The experimental q_m value (366 $mg \cdot g^{-1}$) was also close to the theoretically calculated value. After selectivity and reusability studies, adsorption experiments were carried out on two leaching solutions from waste PCBs and MSWI fly ash, in which more than 90% Ag ions can be adsorbed by PNPG membrane. The results indicate that the PNPG membrane has practical potential for silver recycling.

Reference

[1] G. Mishra, R. Jha, M.D. Rao, et al., Recovery of silver from waste printed circuit boards (WPCBs) through hydrometallurgical route: A review, Environmental Challenges, 4 (2021) 100073-100081. https://doi.org/10.1016/j.envc.2021.100073.

[2] A.B.G. Lansdown, A pharmacological and toxicological profile of silver as an antimicrobial agent in medical devices, Advances in Pharmacological Sciences, 2010 (2010) 910686-910701. https://doi.org/10.1155/2010/910686.

[3] X. Yin, P. Shao, L. Ding, et al., Protonation of rhodanine polymers for enhancing the capture and recovery of Ag^{+} from highly acidic wastewater, Environ. Sci. Nano, 6 (2019) 3307-3315. http://dx.doi.org/10.1039/C9EN00833K.

[4] M. Hosoba, K. Oshita, R.K. Katarina, et al., Synthesis of novel chitosan resin possessing histidine moiety and its application to the determination of trace silver by ICP-AES coupled with triplet automated-pretreatment system, Anal. Chim. Acta, 639 (2009) 51-56. https://doi.org/10.1016/j.aca.2009.02.050.

[5] X. Song, P. Gunawan, R. Jiang, et al., Surface activated carbon nanospheres for fast adsorption of silver ions from aqueous solutions, J. Hazard. Mater., 194 (2011) 162-168. https://doi.org/10.1016/j.jhazmat.2011.07.076.

[6] Z. Zhang, Y. Kuang, Y. Lin, et al., A closed-loop sustainable scheme for silver recovery from water by reusable thiol-grafted graphene oxide, J. Clean. Prod., 305 (2021) 127146-127158. https://doi.org/10.1016/j.jclepro.2021.127146.

[7] H. Sverdrup, D. Koca, K.V. Ragnarsdottir, Investigating the sustainability of the global silver supply, reserves, stocks in society and market price using different approaches, Resour. Conserv. Recycl., 83 (2014) 121-140. https://doi.org/10.1016/j.resconrec.2013.12.008.

[8] T.W. Purcell, J.J. Peters, Sources of silver in the environment, Environ. Toxicol. Chem., 17 (1998) 539-546. https://doi.org/10.1002/etc.5620170404.

[9] S.H. Mousavi, M. Manoochehri, F. Afshar Taromi, Fabrication of a novel magnetic metal–organic framework functionalized with 2-aminothiophenol for preconcentration of trace silver amounts in water and wastewater, RSC Advances,

11 (2021) 13867-13875. http://dx.doi.org/10.1039/D1RA00420D.

[10] A. Nasar, F. Mashkoor, Application of polyaniline-based adsorbents for dye removal from water and wastewater—A review, Environ. Sci. Pollut. Res., 26 (2019) 5333-5356. https://doi.org/10.1007/s11356-018-3990-y.

[11] L. Zhang, L. Chai, J. Liu, et al., Ph manipulation: A facile method for lowering oxidation state and keeping good yield of poly(*m*-phenylenediamine) and its powerful Ag^{+} adsorption ability, Langmuir, 27 (2011) 13729-13738. https://doi.org/10.1021/la203162y.

[12] A. Taghizadeh, M. Taghizadeh, M. Jouyandeh, et al., Conductive polymers in water treatment: A review, J. Mol. Liq., 312 (2020) 113447. https://doi.org/10.1016/j.molliq.2020.113447.

[13] B.-P. Jiang, L. Zhang, X.-L. Guo, et al., Poly(N-phenylglycine)-based nanoparticles as highly effective and targeted near-infrared photothermal therapy/photodynamic therapeutic agents for malignant melanoma, Small, 13 (2017) 1602496-1602510. https://doi.org/10.1002/smll.201602496.

[14] J.H. Doh, J.H. Kim, H.J. Kim, et al., Enhanced adsorption of aqueous copper(II) ions using dedoped poly-N-phenylglycine nanofibers, Chem. Eng. J., 277 (2015) 352-359. http://dx.doi.org/10.1016/j.cej.2015.04.120.

[15] Z. Lin, T. Wu, J. Shi, et al., Poly(N-phenylglycine)-based bioinspired system for stably and efficiently enhancing solar evaporation, ACS Sustainable Chem. Eng., 9 (2021) 448-457. https://doi.org/10.1021/acssuschemeng.0c07608.

[16] Z. Lin, T. Wu, Y.-F. Feng, et al., Poly(N-phenylglycine)/MoS_2 nanohybrid with synergistic solar-thermal conversion for efficient water purification and thermoelectric power generation, ACS Appl. Mater. Interfaces, 14 (2022) 1034-1044. https://doi.org/10.1021/acsami.1c20393.

[17] X. Chen, Y. Xiang, L. Xu, et al., Recovery and reduction of Au(III) from mixed metal solution by thiourea-resorcinol-formaldehyde microspheres, J. Hazard. Mater., 397 (2020) 122812-122820. https://doi.org/10.1016/j.jhazmat.2020.122812.

[18] T.H. Bui, S. Jeon, Y. Lee, Facile recovery of gold from e-waste by integrating

chlorate leaching and selective adsorption using chitosan-based bioadsorbent, J. Environ. Chem. Eng., (2020) 104661-104669. https://doi.org/10.1016/j.jece.2020.104661.

[19] M. Ben Ali, F. Wang, R. Boukherroub, et al., High performance of phytic acid-functionalized spherical poly-phenylglycine particles for removal of heavy metal ions, Appl. Surf. Sci., 518 (2020) 146206-146213. https://doi.org/10.1016/j.apsusc.2020.146206.

[20] C. Lei, C. Wang, W. Chen, et al., Polyaniline@magnetic chitosan nanomaterials for highly efficient simultaneous adsorption and in-situ chemical reduction of hexavalent chromium: Removal efficacy and mechanisms, Sci. Total Environ., 733 (2020) 139316-139328. https://doi.org/10.1016/j.scitotenv.2020.139316.

[21] M.R. Nabid, S.S. Taheri, R. Sedghi, et al., Chemical synthesis and characterization of water-soluble, conducting poly(N-phenylglycine), Iran. Polym. J., 17 (2008) 365-371. https://www.sid.ir/en/Journal/ViewPaper.aspx?ID=107888.

[22] H.J. Kim, S. Im, J.C. Kim, et al., Phytic acid doped polyaniline nanofibers for enhanced aqueous copper(II) adsorption capability, ACS Sustainable Chem. Eng., 5 (2017) 6654-6664. https://doi.org/10.1021/acssuschemeng.7b00898.

[23] R. Li, C. Zhou, L. Yang, et al., Multifunctional cotton with PANI-Ag NPs heterojunction for solar-driven water evaporation, J. Hazard. Mater., 424 (2022) 127367. https://doi.org/10.1016/j.jhazmat.2021.127367.

[24] V.K.A. Muniraj, R. Boukherroub, M.V. Shelke, Flexible energy storage device based on poly(N-phenylglycine), an incentive-energy pseudocapacitive conducting polymer, and electrochemically exfoliated graphite sheets, ACS Sustainable Chem. Eng., 8 (2020) 6433-6441. https://doi.org/10.1021/acssuschemeng.0c00880.

[25] S.N. Kumar, F. Gaillard, G. Bouyssoux, et al., High-resolution XPS studies of electrochemically synthesized conducting polyaniline films, Synth. Met., 36 (1990) 111-127. https://doi.org/10.1016/0379-6779(90)90240-L.

[26] X. Zhang, L. Song, F. Bi, et al., Catalytic oxidation of toluene using a facile synthesized Ag nanoparticle supported on UiO-66 derivative, J. Colloid Interface

Sci., 571 (2020) 38-47. https://doi.org/10.1016/j.jcis.2020.03.031.

[27] M. Xie, T. Zhang, A novel efficient visible-light-driven double Z-scheme PANI/Ag_3Po_4/CNO heterojunction photocatalyst mediated by PANI and in situ grown agnps, J. Mater. Sci., 55 (2020) 3974-3990. https://doi.org/10.1007/s10853-019-04252-7.

[28] W. Pei, J. Zhang, H. Tong, et al., Removal and reutilization of metal ions on ZIF-67/GO membrane via synergistic photocatalytic-photothermal route, Applied Catalysis B: Environmental, 282 (2021) 119575-119584. https://doi.org/10.1016/j.apcatb.2020.119575.

[29] K.Z. Elwakeel, A.S. Al-Bogami, E. Guibal, 2-mercaptobenzimidazole derivative of chitosan for silver sorption – contribution of magnetite incorporation and sonication effects on enhanced metal recovery, Chem. Eng. J., 403 (2021) 126265. https://doi.org/10.1016/j.cej.2020.126265.

[30] H.J. Kim, H. Choi, A.K. Sharma, et al., Recyclable aqueous metal adsorbent: Synthesis and Cu(II) sorption characteristics of ternary nanocomposites of Fe_3O_4 nanoparticles@graphene-poly-N-phenylglycine nanofibers, J. Hazard. Mater., 401 (2021) 123283. https://doi.org/10.1016/j.jhazmat.2020.123283.

[31] S. Bhattarai, J.S. Kim, Y.-S. Yun, et al., Preparation of polyaniline-coated polystyrene nanoparticles for the sorption of silver ions, React. Funct. Polym., 105 (2016) 52-59. https://doi.org/10.1016/j.reactfunctpolym.2016.05.013.

[32] Q. Wang, Y. Tian, L. Kong, et al., A novel 3D superelastic polyethyleneimine functionalized chitosan aerogels for selective removal of Cr(VI) from aqueous solution: Performance and mechanisms, Chem. Eng. J., 425 (2021) 131722-131733. https://doi.org/10.1016/j.cej.2021.131722.

[33] E.D. Revellame, D.L. Fortela, W. Sharp, et al., Adsorption kinetic modeling using pseudo-first order and pseudo-second order rate laws: A review, Clean. Eng. Technol., 1 (2020) 100032. https://doi.org/10.1016/j.clet.2020.100032.

[34] J.-P. Simonin, On the comparison of pseudo-first order and pseudo-second order rate laws in the modeling of adsorption kinetics, Chem. Eng. J., 300 (2016) 254-263. https://doi.org/10.1016/j.cej.2016.04.079.

[35] J. Wang, X. Guo, Adsorption isotherm models: Classification, physical meaning, application and solving method, Chemosphere, 258 (2020) 127279-127303. https://doi.org/10.1016/j.chemosphere.2020.127279.

[36] B. Feng, C. Yao, S. Chen, et al., Highly efficient and selective recovery of Au(III) from a complex system by molybdenum disulfide nanoflakes, Chem. Eng. J., 350 (2018) 692-702. https://doi.org/10.1016/j.cej.2018.05.130.

[37] P. Samaddar, S. Kumar, K.-H. Kim, Polymer hydrogels and their applications toward sorptive removal of potential aqueous pollutants, Polym. Rev. (Philadelphia, PA, U. S.), 59 (2019) 418-464. https://doi.org/10.1080/15583724.2018.1548477.

[38] M.A. Al-Ghouti, D.A. Da'ana, Guidelines for the use and interpretation of adsorption isotherm models: A review, J. Hazard. Mater., 393 (2020) 122383-122404. https://doi.org/10.1016/j.jhazmat.2020.122383.

[39] B. Zhang, S. Wang, L. Fu, et al., Selective adsorption of silver ions from highly acidic aqueous solutions by polymers containing multiple sulfur groups, Water, Air, Soil Pollut., 229 (2018) 199-210. https://doi.org/10.1007/s11270-018-3849-3.

[40] J.-I. Yun, S. Bhattarai, Y.-S. Yun, et al., Synthesis of thiourea-immobilized polystyrene nanoparticles and their sorption behavior with respect to silver ions in aqueous phase, J. Hazard. Mater., 344 (2018) 398-407. https://doi.org/10.1016/j.jhazmat.2017.10.050.

[41] P. Liu, X. Wang, L. Tian, et al., Adsorption of silver ion from the aqueous solution using a polyvinylidene fluoride functional membrane bearing thiourea groups, J. Water Process. Eng., 34 (2020) 101184-101194. https://doi.org/10.1016/j.jwpe.2020.101184.

[42] A. Beyler Çiğil, O. Aydın Urucu, H. Birtane, et al., Cellulose/cysteine based thiol-ene UV cured adsorbent: Removal of silver (I) ions from aqueous solution, Cellulose, 28 (2021) 6439-6448. https://doi.org/10.1007/s10570-021-03932-5.

[43] X. Yang, Z. Dong, M. Zhang, et al., Selective recovery of Ag(I) using a cellulose-based adsorbent in high saline solution, J. Chem. Eng. Data, 65 (2020) 1919-1926. https://doi.org/10.1021/acs.jced.9b01107.

[44] W. Wei, A. Li, S. Pi, et al., Synthesis of core–shell magnetic nanocomposite

Fe_3O_4@ microbial extracellular polymeric substances for simultaneous redox sorption and recovery of silver ions as silver nanoparticles, ACS Sustainable Chem. Eng., 6 (2018) 749-756. https://doi.org/10.1021/acssuschemeng.7b03075.

[45] J. Zhao, S. Wang, L. Zhang, et al., Kinetic, isotherm, and thermodynamic studies for Ag(I) adsorption using carboxymethyl functionalized poly(glycidyl methacrylate), Polymers, 10 (2018) 1090-1109. https://doi.org/10.3390/polym10101090.

[46] Y. Sun, Y. Matsumura, B. Ochiai, Selective Ag^+ adsorption of ureido polymer prepared by cyclopolymerization giving large ring repeating units, ACS Appl. Polym. Mater., 2 (2020) 1417-1421. https://doi.org/10.1021/acsapm.9b01138.

[47] W. Nitayaphat, T. Jintakosol, Adsorption of Ag(I) from aqueous solutions using regenerated silk fibroin adsorbent beads, J. Nat. Fibers, (2020) 1-13. https://doi.org/10.1080/15440478.2020.1848697.

[48] Y. Yang, S.D. Alexandratos, Affinity of polymer-supported reagents for lanthanides as a function of donor atom polarizability, Ind. Eng. Chem. Res., 48 (2009) 6173-6187. https://doi.org/10.1021/ie900074t.

[49] J.-b. Huo, G. Yu, J. Wang, Adsorptive removal of Sr(II) from aqueous solution by polyvinyl alcohol/graphene oxide aerogel, Chemosphere, (2021) 130492-130502. https://doi.org/10.1016/j.chemosphere.2021.130492.

[50] M.N. Ahamad, M.S. Khan, M. Shahid, et al., Metal organic frameworks decorated with free carboxylic acid groups: Topology, metal capture and dye adsorption properties, Dalton Trans., 49 (2020) 14690-14705. http://dx.doi.org/10.1039/D0DT02949A.

[51] M.F. Hamza, Y. Wei, H.I. Mira, et al., Synthesis and adsorption characteristics of grafted hydrazinyl amine magnetite-chitosan for Ni(II) and Pb(II) recovery, Chem. Eng. J., 362 (2019) 310-324. https://doi.org/10.1016/j.cej.2018.11.225.

[52] E.A. Elshehy, M.A. Shenashen, M.O. Abd El-Magied, et al., Selective recovery of silver(I) ions from e-waste using cubically multithiolated cage mesoporous monoliths, Eur. J. Inorg. Chem., 2017 (2017) 4823-4833. https://doi.org/10.1002/ejic.201700644.

[53] İ.A. Şengil, M. Özacar, Competitive biosorption of Pb^{2+}, Cu^{2+} and Zn^{2+} ions from aqueous solutions onto valonia tannin resin, J. Hazard. Mater., 166 (2009) 1488-1494. https://doi.org/10.1016/j.jhazmat.2008.12.071.

[54] S. Wadhawan, A. Jain, J. Nayyar, et al., Role of nanomaterials as adsorbents in heavy metal ion removal from waste water: A review, J. Water Process. Eng., 33 (2020) 101038-101054. https://doi.org/10.1016/j.jwpe.2019.101038.

[55] Y. Zhu, J. Hu, J. Wang, Competitive adsorption of Pb(II), Cu(II) and Zn(II) onto xanthate-modified magnetic chitosan, J. Hazard. Mater., 221-222 (2012) 155-161. https://doi.org/10.1016/j.jhazmat.2012.04.026.

[56] M.A.H. Badsha, M. Khan, B. Wu, et al., Role of surface functional groups of hydrogels in metal adsorption: From performance to mechanism, J. Hazard. Mater., 408 (2021) 124463-124485. https://doi.org/10.1016/j.jhazmat.2020.124463.

[57] S. Han, T. Ju, Y. Meng, et al., Evaluation of various microwave-assisted acid digestion procedures for the determination of major and heavy metal elements in municipal solid waste incineration fly ash, J. Clean. Prod., 321 (2021) 128922-128931. https://doi.org/10.1016/j.jclepro.2021.128922.

[58] Y. Zhang, B. Cetin, W.J. Likos, et al., Impacts of ph on leaching potential of elements from msw incineration fly ash, Fuel, 184 (2016) 815-825. https://doi.org/10.1016/j.fuel.2016.07.089.

Chapter 5

Poly-N-phenylglycine@multi-walled carbon nanotubes composite membrane for improvement of Au(III) adsorption

5.1. Introduction

Sustainable development goals (SDGs) aim to ensure the availability and sustainable management of water and other natural resources [1]. To avoid the waste of metal resources and environmental pollution caused by heavy metal ions or organic pollutants [2], emerging methods, such as artificial intelligence [3], bio-chemical strategy [4], and photocatalysis [5, 6], have been used to treat waste products containing metal ions, wastewater, and landfill leachate.

Metal resources, particularly precious metals, are very limited but extensively researched and widely used in many fields, such as jewelry, biomedicine, catalysts, and electronics, owing to their unique physicochemical properties [7-9]. Electronic waste (e-waste) components, particularly printed circuit boards, contain higher grades of precious metals compared to primary ores; therefore, it is economically attractive to recover precious metals from e-waste leachates or waste fluids [10]. Although several research efforts are being invested in the aforementioned emerging methods, metallurgical approaches, including pyro- and hydrometallurgy are the most practical and mature processes for extracting metals from solid e-waste. Hydrometallurgy involves metal dissolution and leaching for extracting metals and offers advantages of less environmental impact and high metal recovery. In the final step of hydrometallurgy, metals can be recovered from aqueous solutions by various processes, including adsorption, membrane filtration, chemical precipitation, cementation, and ion exchange [11].

Adsorption methods have attracted significant attention because they are suitable for enrichment or recovery at very low concentrations, are simple to operate, and do

not produce secondary pollutants [12]. For example, the commonly used activated carbon shows tremendous potential in the adsorption of metal ions. However, it still needs to be improved, such as selectivity [11]. Recently, conjugated polymers have been recognized as excellent adsorbents owing to their numerous sites for adsorbing active functional groups, unique redox chemistry, and reversible ion (especially cationic) adsorption/desorption capabilities [13]. Conjugated polymers, such as polyaniline, polypyrrole, polydopamine, and their composites, have been widely studied as noble metal adsorbents [14-16].

Poly-N-phenylglycine (PNPG), another conjugated polymer with a skeleton similar to that of polyaniline, is a promising adsorbent containing several functional groups that can provide numerous adsorption sites. Previous studies reported the recovery of gold and silver using a conjugated polymeric PNPG [17, 18]. Conjugated polymers are increasingly being used for precious metal recovery. However, challenging problems remain despite significant progress in using membranes to reduce the separation burden of nanoparticles after adsorption. For example, owing to intermolecular and intramolecular interactions, bare PNPG particles easily aggregate, which significantly reduces the surface area and reduces the adsorption capacity. The use of membranes for metal recovery faces some challenges, such as the instability of the membrane and the inadequate exposure of adsorption sites [19]. The composite adsorbents of conjugated polymers and organic/inorganic materials may combine the special advantages of both components to enhance the purification and adsorption effects [20]. Considering graphdiyne, which can anchor nanoparticles [21], we used carbon nanotubes, another commonly used carbon material, to improve membrane stability without compromising adsorption performance. Carbon nanotubes are rich in delocalized π electrons, act as good electron donors, and show non-covalent functionalization [22]. Moreover, it will be an important development if the combination of PNPG and carbon nanotubes has an effect of $1 + 1 > 2$.

This study reports the design and preparation of a PNPG@multi-walled carbon

nanotube (MWCNT) composite membrane, in which MWCNT are uniformly distributed in the PNPG matrix, inhibiting the aggregation of PNPG, and enhancing the stability and overall mechanical properties of the membrane. Moreover, the effects of pH, time, and concentration on the adsorption behavior of Au, as well as the kinetics, isotherms, and adsorption mechanism, were studied. Further, gold recovery from the leaching solution of e-waste was attempted. The results demonstrated the potential of the PNPG@MWCNT composite membrane for practical applications.

5.2. Experimental details

5.2.1. Materials and equipment

Used materials were multi-walled carbon nanotubes (MWCNT), N-phenylglycine (NPG), ammonium peroxodisulfate (APS), mixed cellulose ester (MCE) membrane, thiourea, NaOH, HCl, H_2SO_4, Na_2SO_4, NaCl, $NaNO_3$, waste printed circuit boards (PCBs) samples, and standard solutions (1000 $mg \cdot L^{-1}$) of Al(III), Au(III), Cd(II), Co(II), Cu(II), Fe(III), Ni(II), Pb(II), Pt(IV), Sn(II), and Zn(II).

5.2.2. Preparation of the PNPG suspension

PNPG can be synthesized by polymerization of the NPG monomer, where APS acts as an oxidant and dilute sulfuric acid provides the necessary acidic environment [23]. The procedure is almost consistent with that described in Section 2.2. In short, the APS–H_2SO_4 mixture (6.4 g APS; 100 mL 0.1 $mol \cdot L^{-1}$ H_2SO_4) was added dropwise to the NPG–H_2SO_4 mixture (4.0 g NPG; 200 mL 0.1 $mol \cdot L^{-1}$ H_2SO_4) in a beaker with stirring in an ice-water bath (about 0 °C) for 24 h. The products were separated by filtration and washed with DI water until the filtrate was colorless. The collected no-impurities PNPG was redispersed in DI water to form a suspension whose concentration was calculated by carefully filtering 1.0 mL dispersion and weighing the dried solid.

5.2.3. Preparation of the PNPG@MWCNT membrane

The preparation procedure of 4 mg PNPG membranes and PNPG@MWCNT

membrane (**Scheme 5.1**) was described above in Sections 2.2.2 and 2.2.3, respectively. Please refer to the corresponding section for detail.

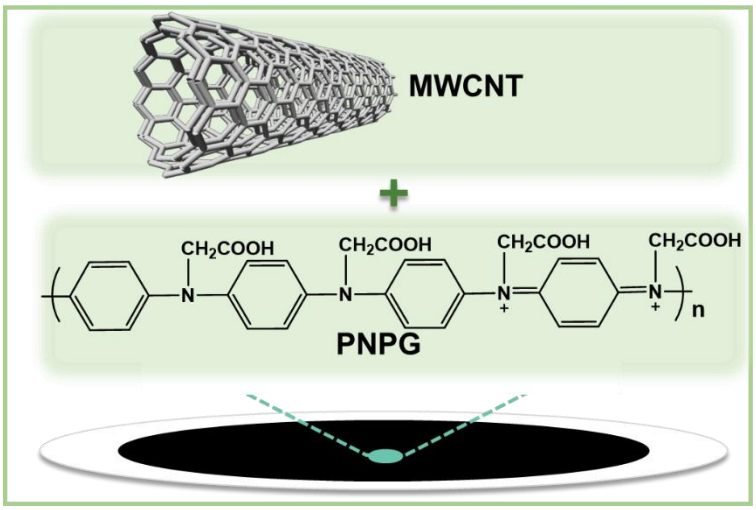

Scheme 5.1. Schematic diagram of the PNPG@MWCNT composite membrane

5.2.4. Characterization

The concentrations of the metal ions were determined using a plasma atomic emission spectrometer (ICPE-9820, Shimadzu, Japan). The characterization methods of FTIR, XRD, XPS, SEM, EDS, zeta potential analysis, Brunauer–Emmett–Teller (BET) and Barrett–Joyner–Halenda (BJH) were the same as shown in Section 2.3.2.

5.2.5. Adsorption experiment

Au(III) solutions with the desired concentrations and pH were prepared by diluting the standard solution and adjusting pH using 0.1 mol·L^{-1} NaOH or HCl solution. The total mass of the sorbent (i.e. PNPG and MWCNT) in the composite membrane was 4 mg.

In the adsorption experiment to determine the influence of composition, each of the as-prepared membranes with different PNPG-MWCNT compositions was immersed in 50 mL of Au(III) solution (100 mg·L^{-1}, pH = 1) for 24 h. To examine the influence of pH on adsorption, composite membranes in four proportions (P4M0, P3.5M0.5, P2M2, and P0M4) were separately soaked in Au(III) solutions (50 mL, 100

mg·L^{-1}) of pH 1, 3, and 5 for 24 h. The effect of anions (Cl^-, SO_4^{2-}, and NO_3^-) on adsorption was investigated by soaking P3.5M0.5 composite membranes in 50 mL anion-containing Au (III) solutions for 24 h, where the concentration of Au(III) was 100 mg·L^{-1}, the pH of the solutions was 1, and the anion concentrations were set to 0.001, 0.01, and 0.1 mol·L^{-1}.

In the adsorption experiment to determine the influence of time, P3.5M0.5 composite membranes were soaked in 16 beakers containing 80 mL of Au(III) solutions (100 mg·L^{-1}, pH = 1), and the membranes were then removed from the corresponding beakers at 0.5, 1, 2, 4, 6, 8, 10, 12, 15, 18, 21, 24, 30, 36, 42, and 48 h. To study the effect of concentration on adsorption, serial Au(III) solutions (pH = 1) with concentrations of 20, 40, 60, 80, 100, 120, 140, and 160 mg·L^{-1} were prepared before the adsorption experiment, where P3.5M0.5 composite membranes were individually soaked in 80 mL of Au(III) solution for 24 h.

The competition among several metal ions was evaluated by immersing the P3.5M0.5 membrane into three types of mixed solutions (pH = 1, 50 mL): 50 mg·L^{-1} for other metal ions, whereas gold ions were 5, 10, and 25 mg·L^{-1} in sequence, for 24 h.

In the reusability experiment, the prepared P3.5M0.5 membrane was dipped into 50 mg·L^{-1} Au(III) solution for 24 h, and the post-adsorption membrane underwent for desorption 24 h by bathing in the acidic thiourea solution (containing 1.0 mol·L^{-1} $CS(NH_2)_2$, 1.0 mol·L^{-1} HCl) [24]. The next reusability round began after the membrane was cleaned with DI water three times and dried at 60 ℃ for 12 h.

Recovery capacity experiments were conducted in an actual leaching solution of waste PCBs. After processing the original samples, the solid residue "concentrate" with a high gold content was obtained. The concentrate (3.5 g) was first treated with 40 mL concentrated HNO_3 (magnetic stirring at 300 rpm, heating at approximately 100 ℃, 3 h), and the residual solid was then treated with 20 mL of freshly prepared aqua regia under the same process conditions and covered with a watch glass to prevent water

from evaporating. After the reaction, the filtrate was collected and adjusted to pH 1 using 1 mol·L^{-1} NaOH and stored as the leaching solution (**Scheme 5.2**). The P3.5M0.5 membrane was dipped into 50 mL of the leaching solution for 24 h adsorption.

These experiments were performed in triplicate under constant shaking at 120 rpm and 25 °C room temperature, and each beaker was covered with sealing film to keep the water from evaporating. The adsorption capacities were expressed as mean ± standard deviation.

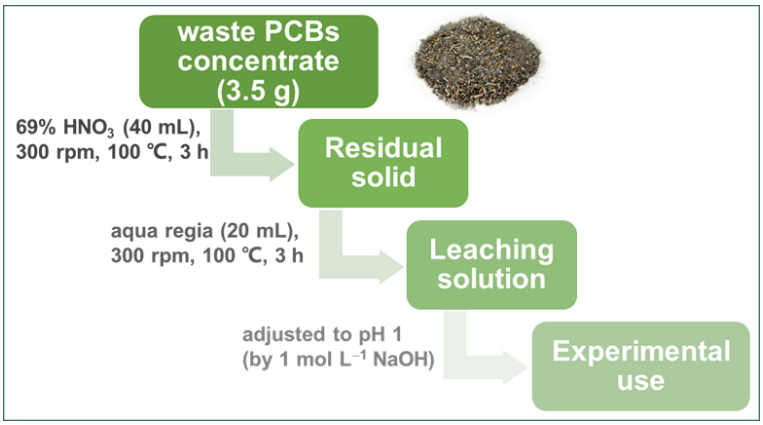

Scheme 5.2. Schematic diagram of the preparation of leaching solution containing Au.

5.3. Results and discussion

5.3.1. Preparation and Characterization of PNPG@MWCNT membrane

The XRD patterns of membranes with different proportions are shown in **Fig. 5.1a**. Because only MWCNT are present in the P0M4 membrane, its XRD pattern has a distinct characteristic peak at $2\theta \approx 26.2°$, representing the (002) reflection planes of the MWCNT. The presence of this peak is due to the effect of several overlapping graphene sheets in the concentric circles mode, indicating the features of multi-walled carbon nanotubes [25]. This characteristic peak of MWCNT can also be observed in the P2M2 membrane, but it seems that the peak is not well displayed in the P3.5M0.5 membrane, which may be due to the small amount of MWCNT compared with PNPG.

FTIR spectroscopy was used to further characterize the composite materials. Three samples, pristine MWCNT, dried as-prepared PNPG, and collected P3.5M0.5, were

separately pressed by KBr for FTIR measurements from 600 to 3600 cm^{-1}, and their spectra are shown in **Fig. 5.1b**. The FTIR spectrum of the pristine MWCNT exhibits a relatively intense peak at approximately 1540 cm^{-1}, representing the double bonds of C=C [26]. There are six characteristic peaks in the spectrum of PNPG: 815 and 1152 cm^{-1} are assigned to the 1,4 (para)-substituted phenyl ring structure and the N=Q=N vibration in the quinone ring, respectively; 1309 cm^{-1} is the characteristic peak of C–N at benzenoid amine; 1497 and 1585 cm^{-1} belong to the stretching deformation of C=C at the benzenoid and quinonoid rings, respectively; and 1673 cm^{-1} is attributed to the C=O of carboxyl groups [27-29]. In the P3.5M0.5 spectrum, no new peak can be observed, compared with that of PNPG, but a change in absorption intensity (1497 cm^{-1}) is observed, which may be influenced by the C=C double bond in the MWCNT, indicating the successful combination of both substances [30].

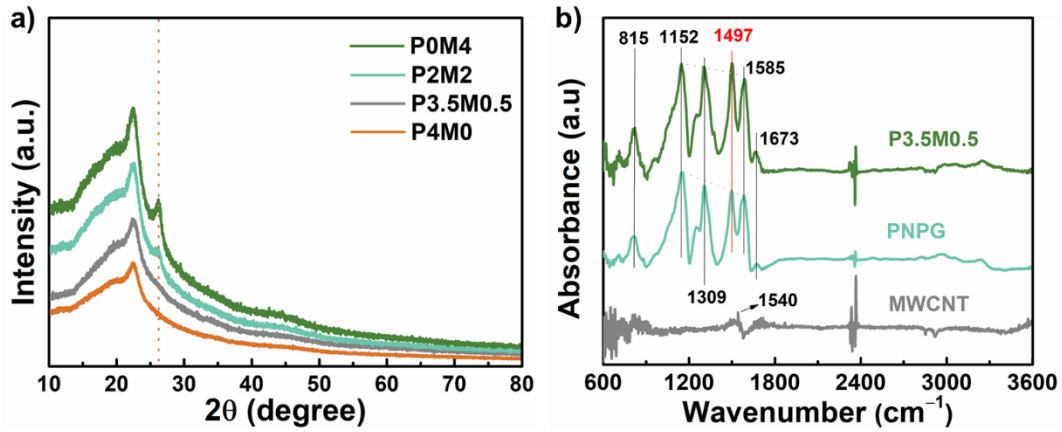

Fig. 5.1. (a) XRD spectra of P0M4, P2M2, P3.5M0.5, and P4M0 membranes. (b) FTIR spectra of MWCNT, PNPG, and P3.5M0.5.

The combination of PNPG and MWCNT can be clearly observed in the SEM images (**Figs. 5.2a–b**), which shows that the PNPG particles gathered to form a rough surface and a porous structure on the as-prepared P4M0 (**Fig. 5.2a**), whereas the surface of P3.5M0.5 is densely crisscrossed with fiber-shaped MWCNT that spread among the PNPG particles (**Fig. 5.2c**). In addition, there are obvious large cracks whose average gap is up to ten microns on the PNPG surface in P4M0 (**Fig. 5.2b**), whereas on the

surface of P3.5M0.5, the large cracks are not observed, only tiny cracks (**Fig. 5.2d**).

Concerning membrane stability, similar results are observed for other equally proportional composite membranes of different masses (**Fig. 5.3**). The pure PNPG membranes (**Fig. 5.3a**–**c**) are prone to break, and micrometer-sized cracks appear after 24 h of drying, which is attributed to desiccation-related membrane shrinkage [31]. In this case, the higher loading on the supporting layer leads to significantly visible cracks (**Fig. 5.3c**), which may reduce the stability of the membrane in solutions. The addition of MWCNT (**Figs. 5.3d**–**f**) has an obvious effect on alleviating the cracks caused by drying, which greatly improves the stability of the membranes. The consolidation effect of MWCNT on PNPG is similar to that of plant roots on loose soil particles.

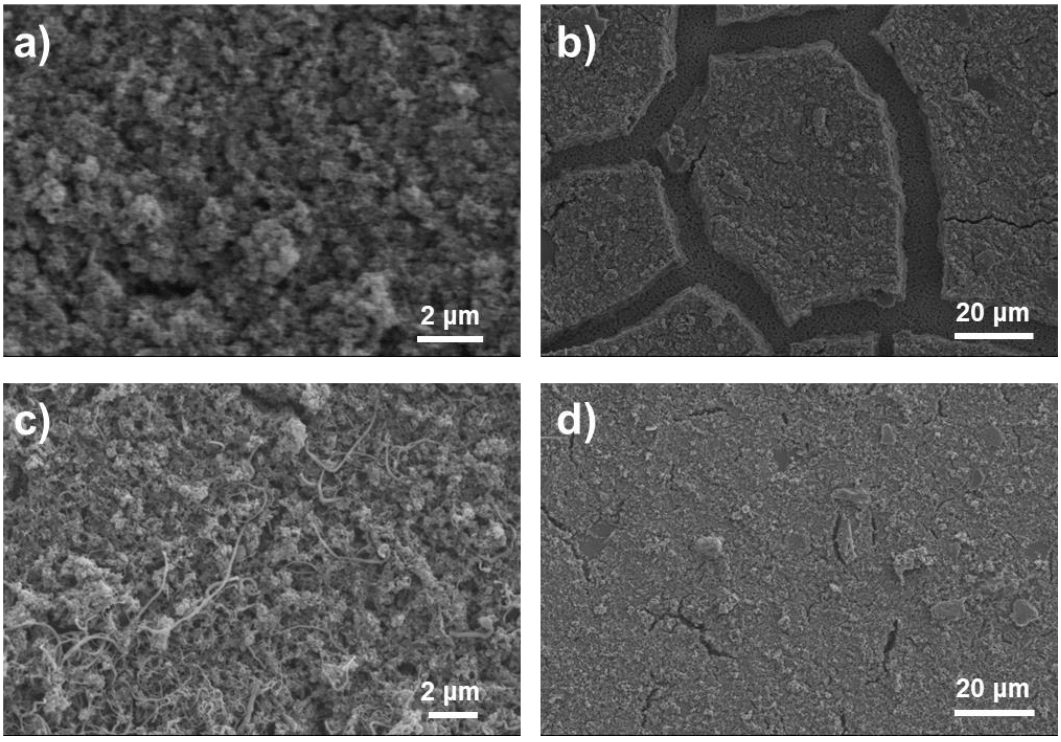

Fig. 5.2. SEM images of (a) (b) P4M0 and (c) (d) P3.5M0.5. (g) Schematic diagram of the PNPG@MWCNT composite membrane.

XPS was used to further explore why the cracks in the composite membrane were repaired after adding MWCNT and the interaction between MWCNT and PNPG. The XPS spectrum of the P3.5M0.5 membrane (**Fig. 5.4a**) shows three peaks: C 1s, N 1s, and O 1s, at 284.8, 399.9, and 531.9 eV, respectively. **Fig. 5.4b** displays the

deconvolution of the C 1s spectrum, which is split into six sub-peaks. From right to left, the peaks at 284.5, 284.8, 285.5, 286.3, and 288.0 eV are assigned to sp^2 C, sp^3 C, C−N, C−O, and C=O, respectively [32, 33]. The peak at 290.8 eV is due to the π−π structure of conjugate PNPG and MWCNTs [34, 35].

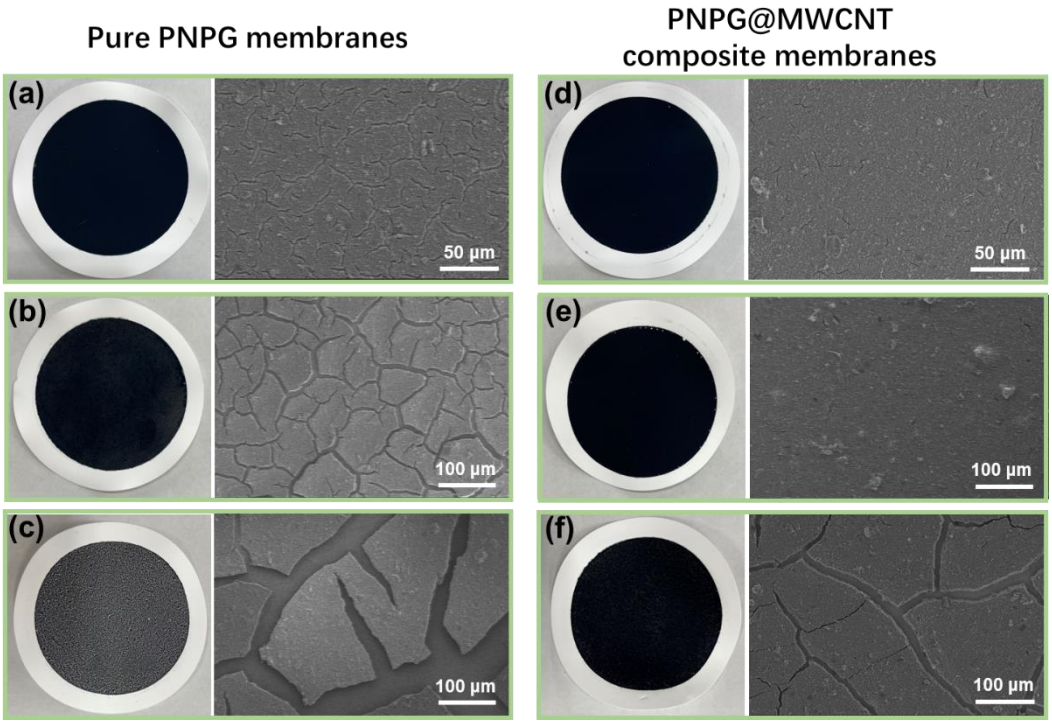

Fig. 5.3. Digital photograph and SEM image of pure PNPG membranes containing (a) 1.75 mg, (b) 3.5 mg, (c) 7 mg, and those of PNPG@MWCNT composite membrane with the addition of MWCNT of (d) 0.25 mg, (e) 0.5 mg, and (f) 1 mg, correspondingly.

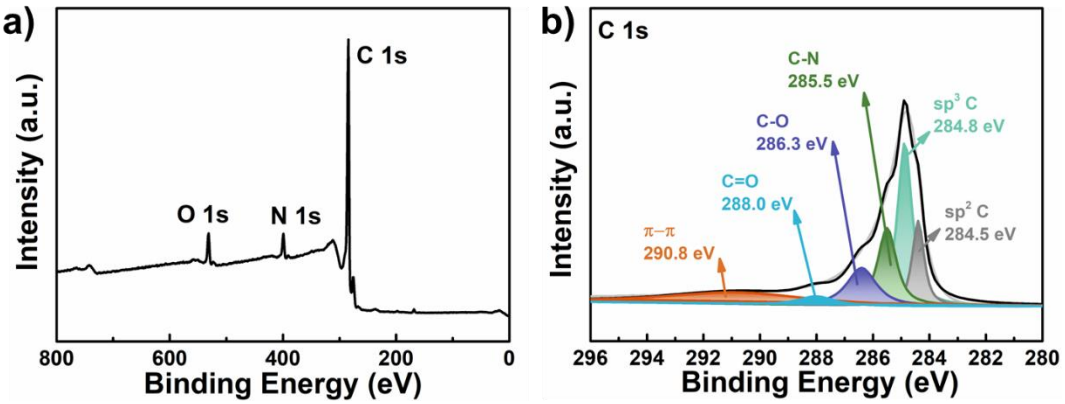

Fig. 5.4. (a) XPS spectrum of the P3.5M0.5 membrane. (b) C 1s XPS-spectrum of P3.5M0.5 membrane.

In addition, the results of the characterization of the zeta potential can also explain the interaction between MWCNT and PNPG. As shown in **Fig. 5.5**, the PNPG dispersed in DI water is positively charged with a zeta potential of 40.51 mV. At the same time, a zeta potential of −36.18 mV is determined for MWCNT which were uniformly distributed in DI water after ultrasonic dispersion. After the liquid-phase mixing of PNPG and MWCNT (PNPG: 3.5 mg; MWCNT: 0.5 mg), the zeta potential shifts to 35.36 mV. This is because of the Coulombic interactions between the negative MWCNT and the positive PNPG, which screen the surface charges of PNPG.

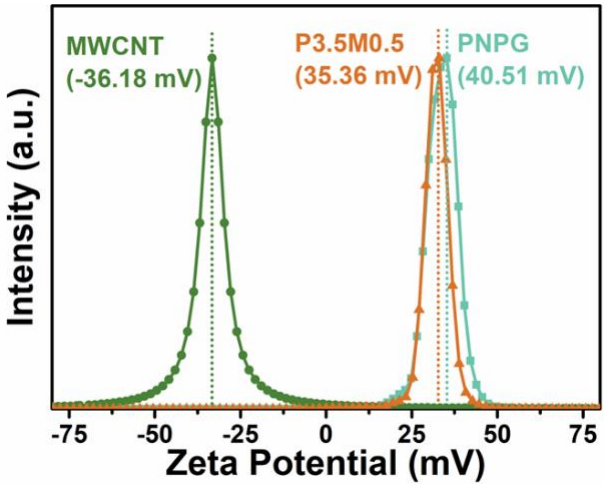

Fig. 5.5. Zeta potential of PNPG, MWCNT, and P3.5M0.5.

5.3.2. Adsorption performance at different PNPG@MWCNT membrane compositions and solution pH values

To understand the effect of the ratio of PNPG and MWCNT on Au(III) adsorption, different PNPG@MWCNT membranes were prepared and used for the adsorption experiment. The adsorption capacity q_t (mg·g^{-1}) was calculated using Eq. (1) [36]:

$$q_t = \frac{(c_0 - c_t)V}{m} \quad (1)$$

where V (L) is the volume of the Au(III) solution and m (g) is the sum of the mass of PNPG and MWCNT. c_0 (mg·L^{-1}) and c_t (mg·L^{-1}) represent the initial and residual

concentrations at time *t* (h), respectively.

As shown in **Fig. 5.6a**, the two ends of the curve represent the pure PNPG membrane and MWCNT membrane, and their adsorption capacities are approximately 980.9 and 54.5 mg·g^{-1}, respectively. It can be seen that untreated MWCNT (P0M4) displays very low adsorption of gold ions compared to PNPG (P4M0), and the adsorption capacity of the composite membranes mainly depends on PNPG. Under the constant condition that the total mass of PNPG and MWCNT is constant at 4 mg, the adsorption capacity gradually increases from 980.9 to 1191.6 mg·g^{-1} when the content of MWCNT increases from 0 to 0.5 mg. The growth rate of the adsorption capacity is 21.48%. Beyond this point (PNPG = 3.5 mg, MWCNT = 0.5 mg), the adsorption capacity decreases with decreasing PNPG content. The P3.5M0.5 composite membrane shows the highest adsorption capacity for Au(III).

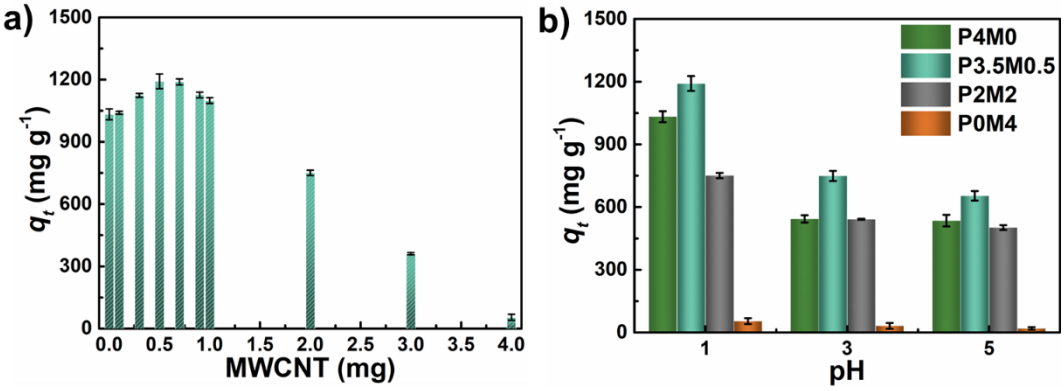

Fig. 5.6. (a) Comparison of adsorption capacity among different PNPG@MWCNT membranes for 24 h adsorption. The *x*-axis represents the mass change in MWCNT, and the corresponding mass of PNPG in the composite membrane is (4−*x*) mg. (b) Au(III) adsorption capacity of the four membranes at different pH.

The pH range was not higher than 7 because most of the real leaching solutions were acidic. To examine the influence of pH on adsorption, several membranes of representative proportions were selected for the experiments at pH of 1, 3, and 5. As demonstrated in **Fig. 5.6b**, with increasing pH, the adsorption capacity of these membranes shows a downward trend: P3.5M0.5 is the most significant, whereas P4M0

and P2M2 are the least. In addition, the adsorption capacity of the P3.5M0.5 composite membrane is the highest among all membranes, regardless of the pH of the Au(III) solution.

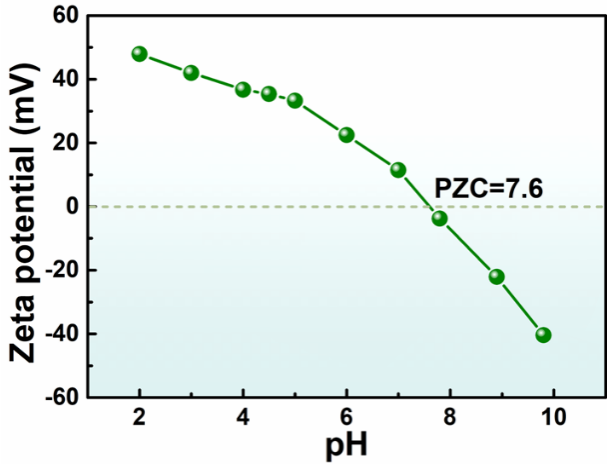

Fig. 5.7. Zeta potential of P3.5M0.5 mixture at different pH.

The pH of the solution is an important factor that affects the adsorption capacity because it affects not only the form of the gold ions in the solution but also the binding site of the adsorbent. It can be seen from the species distribution of Au(III) at varied pH that the major existing form of Au(III) is $[AuCl_4]^-$ in a strongly acidic solution, such as pH = 1, whereas a small fraction of $[AuCl_4]^-$ gradually becomes $[AuCl_3(OH)]^-$ at a pH of 5 [37]. Thus, in the studied pH range of 1–5, Au(III) always exists as a negative monovalent ligand in solutions, regardless of the configuration. As shown in **Fig. 5.7**, the point of zero charge (PZC) of the P3.5M0.5 composite adsorbent is at pH 7.6, which means that it is easy for P3.5M0.5 to capture negatively charged Au(III) species by electrostatic interactions below this pH. In addition, with a decrease in pH, the potential of P3.5M0.5 increases, inducing an increase in Au(III) adsorption capacity, which is consistent with the results shown in **Fig. 5.6b**. Therefore, pH of 1 was considered beneficial for Au(III) adsorption.

5.3.3. Adsorption performance of P3.5M0.5 at different anions

The effect of coexisting anions on Au(III) adsorption was investigated by soaking

P3.5M0.5 composite membranes in different Au (III) solutions separately containing Cl^-, SO_4^{2-}, and NO_3^- at concentrations of 0.001, 0.01, and 0.1 mol·L^{-1}, respectively, and the results are shown in **Fig. 5.8**. Owing to the increase in anion concentrations from 0.001 to 0.1 mol·L^{-1}, Cl^-, SO_4^{2-}, and NO_3^- cause the decline in Au(III) adsorption capacity. This is due to the anions competing with $[AuCl_4]^-$ to occupy some adsorption sites through electrostatic interaction. Although the anion concentration (0.1 mol·L^{-1}) is significantly higher than that of Au(III) (100 mg·L^{-1} = 5.08 × 10^{-4} mol·L^{-1}), the Au(III) adsorption capacity was still over 900 mg·g^{-1}, implying that electrostatic interaction was not the main or only interaction force.

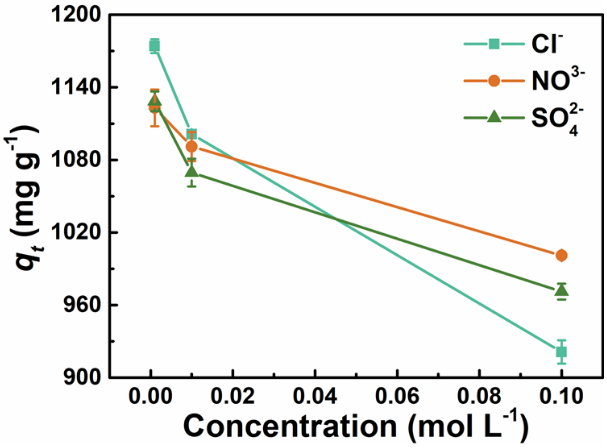

Fig. 5.8. Au(III) adsorption capacity of the P3.5M0.5 composite membrane in the presence of different anions.

5.3.4. Adsorption kinetics study of P3.5M0.5

The time-influenced results of Au(III) adsorption by the P3.5M0.5 composite membrane are shown in **Fig. 5.9**. The adsorption capacity increases sharply to approximately 550 mg·g^{-1} in a short time (0.5 h) and then gradually increases because abundant active sites are involved in the adsorption process. After 24 h, q_t reaches equilibrium because the adsorption sites are exhausted.

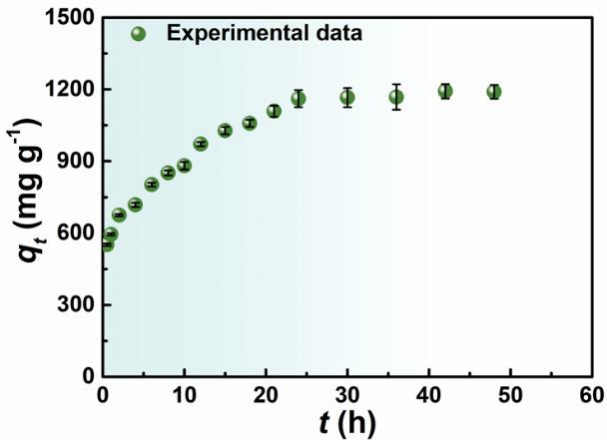

Fig. 5.9. Adsorption capacity of P3.5M0.5 composite membrane at different times.

The adsorption process of Au(III) by the P3.5M0.5 composite membrane was studied using the pseudo-first-order (PFO), pseudo-second-order (PSO), and intra-particle diffusion (IPD) models. The PFO kinetic model presupposes that the adsorption process is limited by physical adsorption, and a diffusion step restricts the movement of the adsorbed substance (Au(III) in our study) from the liquid to the surface of the adsorbent material (P3.5M0.5 composite membrane in our study). The PSO kinetic model assumes that the adsorption process is controlled by chemisorption, involving the sharing or transfer of electrons between the adsorbed substances and adsorbent materials. The IPD model illustrates the multistep adsorption process, including the transport of adsorbate from liquid to the adsorbent surface and the transfer of adsorbate from the adsorbent surface to its interior [38] Their linear formulae are as follows [39, 40]:

$$\text{PFO: } \ln\left(q_e - q_t\right) = \ln q_e - k_1 t \tag{2}$$

$$\text{PSO: } \frac{t}{q_t} = \frac{1}{k_2 q_e^2} + \frac{t}{q_e} \tag{3}$$

$$\text{IPD: } q_t = k_i t^{1/2} + C_i \tag{4}$$

where q_e (mg·g^{-1}) and q_t (mg·g^{-1}) are the equilibrium adsorption capacity and the instantaneous adsorption capacity at time t (h), respectively; k_1 (h^{-1}), k_2 (g·mg^{-1}·h^{-1}),

and k_i (mg·g^{-1}·h$^{-1/2}$) are the rate constants of the PFO, PSO, and IPD models, respectively. C_i is an ordinary constant that reflects the boundary–layer effect [39].

The kinetic parameters of the PFO and PSO models are listed in **Table 5.1**, and the relevant fitting curves are presented in **Fig. 5.10**, respectively. The correlation coefficient (R^2) is mostly used to measure the fitting degree between the model and experimental data [41]. From **Table 5.1** and **Fig. 5.10**, the observed correlation coefficient of the PSO kinetic model is 0.9956, which is closer to 1 than that of the PFO kinetic model (R^2 = 0.9570). Thus, the PSO kinetic model is fitted well with the experimental data, indicating that the adsorption of Au(III) using the P3.5M0.5 composite membranes is primarily controlled by chemisorption.

Table 5.1 Parameters of gold ions adsorption by the P3.5M0.5 membrane

Model	**Parameters**	**Value**
PFO kinetic model	q_e (mg·g^{-1})	716.38
	k_1 (h^{-1})	0.106
	R^2	0.9570
PSO kinetic model	q_e (mg·g^{-1})	1250.32
	k_2 (g·mg^{-1}·h^{-1})	3.09×10^{-4}
	R^2	0.9956
IPD model (Stage 1)	k_i (mg·g^{-1}·h$^{-1/2}$)	144.84
	C_i (mg·g^{-1})	448.91
	R^2	0.9942
IPD model (Stage 2)	k_i (mg·g^{-1}·h$^{-1/2}$)	16.41
	C_i (mg·g^{-1})	1077.64
	R^2	0.7711

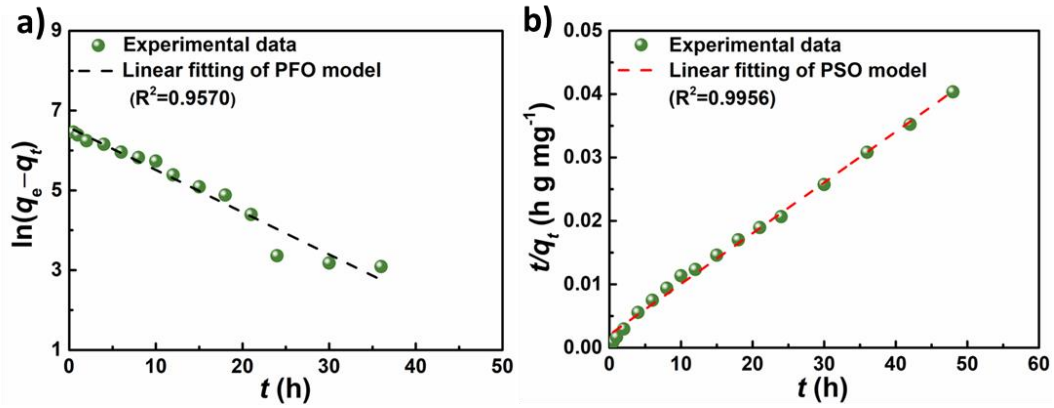

Fig. 5.10. Linear fitting of the (a) PFO kinetics model, (b) PSO kinetics model.

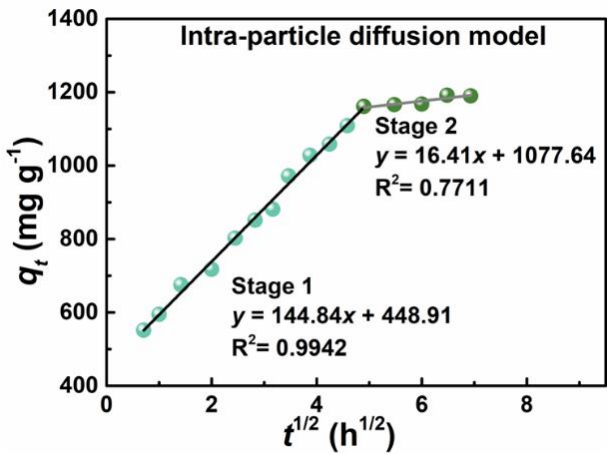

Fig. 5.11. The linear fitting of the intra-particle diffusion model.

Moreover, the fitting results of IPD model are shown in **Table 5.1** and **Fig. 5.11**. Multilinearity in the q_t vs. $t^{1/2}$ plot can be observed in **Fig. 5.11**, indicating that two stages are involved in the Au(III) adsorption by the P3.5M0.5 composite membrane. Stage 1 involves surface adsorption of Au(III) by the P3.5M0.5 composite membranes and shows a slope of 144.84 and an intercept of 448.91. The second stage has a smaller slope (16.41), indicating the diffusion of Au(III) through the surface to the interior of the P3.5M0.5 composite membrane until the adsorption achieves equilibrium. The C_i of Stage 2 (1077.64 mg·g^{-1}) is significantly larger than that of the first stage; therefore, the boundary–layer effect in Stage 2 is much greater. Besides, the entire adsorption process is not rate-limited as no value of C_i in the fitted curves is equal to 0 [42].

5.3.5. Adsorption isotherm study of P3.5M0.5

The trend in the adsorption capacity of gold ions with the initial concentration was studied, and **Fig. 5.12** shows that the adsorption capacity increases with increasing initial concentration and gradually reaches equilibrium. At low concentrations (20–80 $mg \cdot L^{-1}$), there are abundant unoccupied active sites for adsorption; therefore, the adsorption capacity increases as the initial concentration increases. Subsequently, owing to the saturation of the adsorption sites, equilibrium is reached. The maximum Au(III) adsorption capacity of the P3.5M0.5 composite membrane was 1262.6 $mg \cdot g^{-1}$.

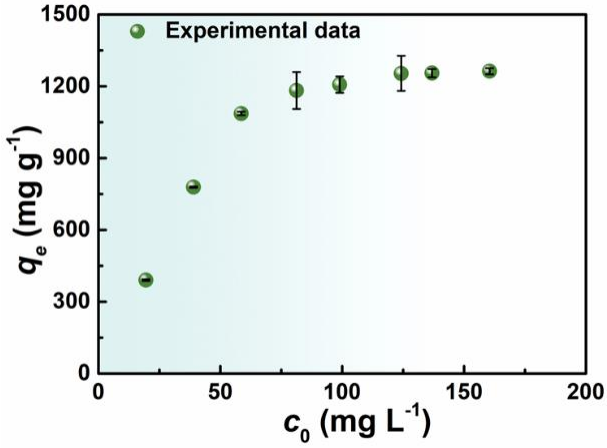

Fig. 5.12. Adsorption capacity of the P3.5M0.5 composite membrane at different initial concentrations.

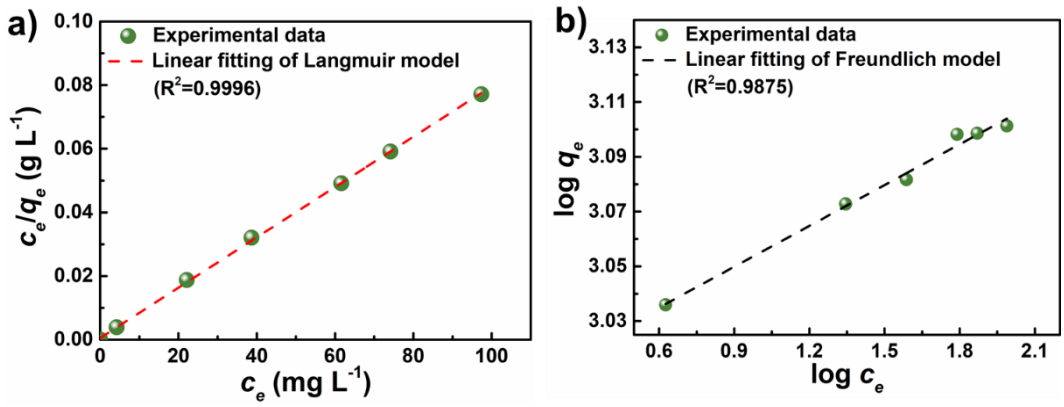

Fig. 5.13. The fitting results of (a) Langmuir and (b) Freundlich isotherm models.

Table 5.2 Isotherm parameters of gold ions adsorption by P3.5M0.5 membrane

Model	**Parameters**	**Value**
Langmuir model	q_m (mg·g^{-1})	1264.6
	K_L (L·mg^{-1})	1.495
	R^2	0.9996
Freundlich model	$1/n$	0.0497
	K_F (L$^{1/n}$·mg$^{1-1/n}$·g^{-1})	1011.9
	R^2	0.9875

The interaction between the P3.5M0.5 composite membrane and Au(III) can be interpreted and analyzed using adsorption isotherm models. Here, two isotherm models are used to fit the experimental data, and the correlation coefficient (R^2) indicated the degree of fitting. One model is the Langmuir isothermal model, which assumes monolayer adsorption and that the accessible adsorption sites on the adsorbent surface are homogeneously distributed. The second model is the Freundlich isotherm model, which is suitable for multilayer adsorption on heterogeneous surfaces. The linear formulae are listed in Eqs. (5) and (6), respectively [39, 40]:

$$\text{Langmuir: } \frac{c_e}{q_e} = \frac{c_e}{q_m} + \frac{1}{K_L \times q_m} \tag{5}$$

$$\text{Freundlich: } \log q_e = \log K_F + \frac{1}{n} \times \log c_e \tag{6}$$

where c_e (mg·L^{-1}) is the equilibrium concentration. q_e (mg·g^{-1}) and q_m (mg·g^{-1}) are the equilibrium and maximum adsorption capacities, respectively; K_L (L·mg^{-1}) and K_F (L$^{1/n}$·mg$^{1-1/n}$·g^{-1}) are the isotherm equilibrium binding constants of the Langmuir and Freundlich isotherm models, respectively. The value of $1/n$ determines the availability of the adsorption process.

Table 5.2 and **Fig. 5.13** show the fitting results of the experimental data using the linear equations of the Langmuir and Freundlich isotherm models. According to the

data in **Table 5.2**, the $R^2 = 0.999$ of the Langmuir isotherm model is significantly larger and closer to 1 than that of the Freundlich isotherm model ($R^2 = 0.9875$). These values indicate that the Langmuir isotherm model can better describe the Au(III) adsorption process of the P3.5M0.5 composite membrane, in which monolayer adsorption is the main adsorption process. In addition, the theoretical maximum adsorption capacity (q_m = 1264.6 mg g^{-1}) calculated from the Langmuir isothermal model was very close to the experimental data (1262.6 mg·g^{-1}). Furthermore, our P3.5M0.5 composite membrane, which was prepared by ultrasound-aided vacuum-assisted filtration, showed a higher adsorption capacity for gold ions at pH 1 than that of the previously reported membrane adsorbents (**Table 5.3)**

Table 5.3 Comparison with other membrane adsorbents during the adsorption of gold ions

Material	**Membrane assembly method**	**kinetics**	**Isotherm**	q_m **(mg·g^{-1})**	**pH**	**Temp. (K)**	**Ref.**
Poly-thiosemicarbazide membrane	Non-solvent induced phase separation	PSO	−	5.4 mmol·g^{-1} (=1063.6 mg·g^{-1})	10% HCl	298	[43]
PVDF membrane functionalized with thiosemicarbazide	Non-solvent induced phase separation	PSO	−	17.2	3	298	[44]
Cellulose acetate-polyaniline membranes	Phase inversion	−	Langmuir	1.2394	−	298	[45]
Thiourea grafted PVDF affinity membrane	Non-solvent induced phase separation	PSO	Langmuir	20.1	3	298	[46]
ADH@BC hybrid membrane	Schiff base reaction strategy	PSO	Langmuir	1149	3	298	[47]
AONFA membrane	Electrospinning	PSO	Langmuir	509.3	5	298	[48]
P3.5M0.5 composite membrane	Vacuum-assisted filtration	PSO	Langmuir	1262.6	1	298	This work

5.3.6. Adsorption thermodynamic study of P3.5M0.5

Several composite membranes P3.5M0.5 were soaked into 80 mL Au(III) solutions and constantly stirred at different temperatures (298, 303, 308, 313, and 318 K) for 24 h to attain equilibrium. The thermodynamic study of P3.5M0.5 toward Au(III) is conducted by calculating the change in Gibbs free energy (ΔG, kJ·mol^{-1}), enthalpy (ΔH, kJ·mol^{-1}), and entropy (ΔS, J·mol^{-1}·K^{-1}) using the following Eqs. (7−10) [49-52]:

$$\Delta G = \Delta H - T\Delta S \tag{7}$$

$$\Delta G = -RT \ln K_c \tag{8}$$

$$\ln K_c = \frac{\Delta S}{R} - \frac{\Delta H}{RT} \tag{9}$$

$$K_c = \frac{C_0 - C_e}{C_e} \tag{10}$$

where K_c is the dimensionless equilibrium constant, R is the ideal gas constant (8.314 J·K^{-1}·mol^{-1}), and T (K) is the absolute temperature.

From the Van't Hoff equation (Eq. 9), plotting $\ln K_c$ with $1/T$ yields a straight line (**Fig. 5.14**), in which the intercept and slope values predict ΔH and ΔS, respectively. As shown in **Table 5.4**, positive ΔH (23.35 kJ·mol^{-1}) suggests the endothermic adsorption process, whereas the positive ΔS (78.92 J·mol^{-1}·K^{-1}) reflects an increased randomness of gold ions adsorption on the surface of P3.5M0.5 composite membranes [24]. In addition, ΔG is negative in the temperature range 298–313 K according to Eq. 7, indicating spontaneous adsorption; decrease in ΔG with increasing temperature indicates the increasing spontaneity of adsorption. High spontaneity at high temperature can be explained in two ways: one is assigned to the swelling of the adsorbent, thereby making it easier for gold ions to enter, and the other can be attributed to the enhanced protonation of carboxyl groups and amine groups, improving the affinity between the adsorbent and gold ions [52].

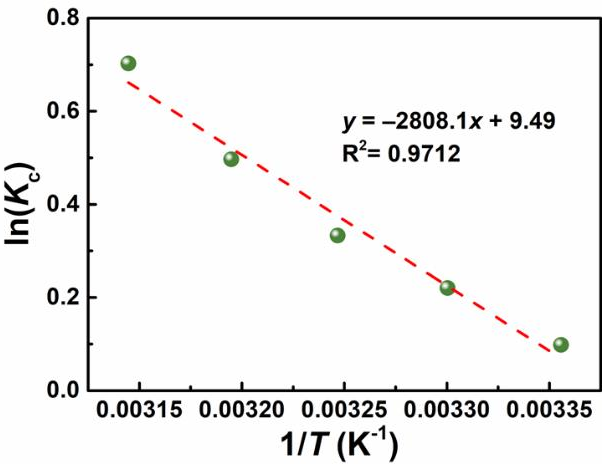

Fig. 5.14. Relationship curve between $1/T$ and $\ln K_c$.

Table 5.4 Thermodynamics parameters of gold ions adsorption by P3.5M0.5 membrane

T (K)	ΔG (kJ·mol^{-1})	ΔH (kJ·mol^{-1})	ΔS (J·mol^{-1}·K^{-1})
298	−0.17		
303	−0.57		
308	−0.96	23.35	78.92
313	−1.35		
318	−1.75		

5.3.7. Adsorption mechanism

Based on the SEM, EDS, XRD, and XPS characterizations, the Au(III) adsorption mechanism of the PNPG@MWCNT membrane was determined.

The SEM images of the post-adsorption P3.5M0.5 composite membrane show the presence of gold particles (**Fig. 5.15a**). Further analysis of the partial area is performed using EDS, and the elemental mappings of Cl and Au (**Figs. 5.15e–g**) show their presence with atomic percentages of 53.68% and 46.32%, respectively (**Fig. 5.15c**). Cl is homogeneously dispersed because of the capture of the $[AuCl_4]^-$ ligands by P3.5M0.5 through electrostatic interactions. Depending on the ratio of atoms in the $[AuCl_4]^-$ ligand, the extra atomic percentage of Au represents the elemental gold. In addition, **Fig. 5.15b** and **Figs. 5.15f–g** show that the distribution of the centrally distributed Au

is very consistent with the position of the particles in the SEM images, indicating the existence of elemental gold in the P3.5M0.5 composite membrane after adsorption, which provides a powerful support for chemisorption.

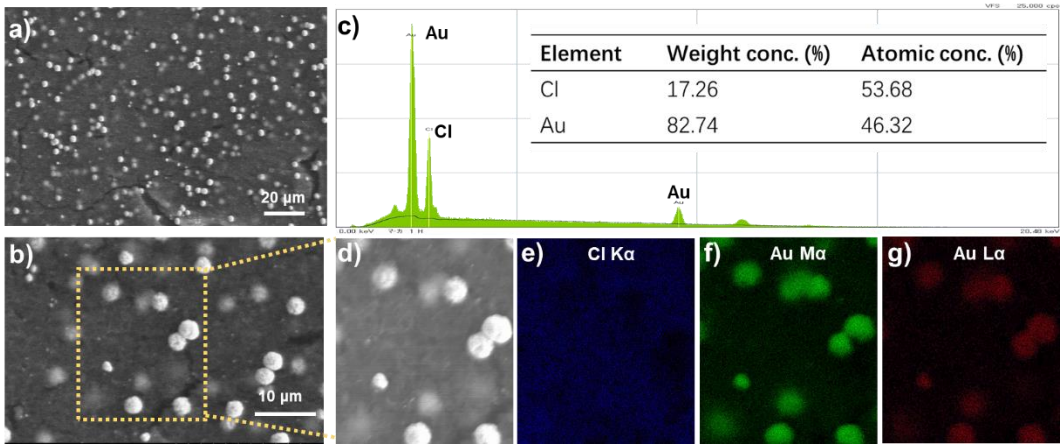

Fig. 5.15. (a) (b) SEM images of P3.5M0.5 composite membrane after Au(III) adsorption. (c) Energy dispersive X-ray spectra of the yellow-box area of (b). The corresponding elemental maps of (e) Cl Kα, (f) Au Mα, and (g) Au Lα in the SEM image shown in (d).

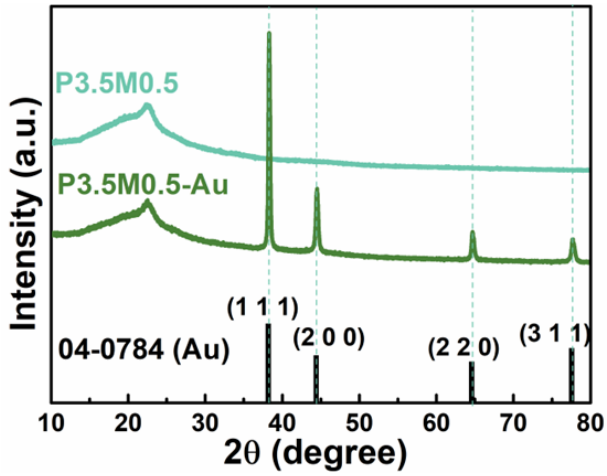

Fig. 5.16. XRD spectra of P3.5M0.5 membrane before and after Au(III) adsorption.

The chemisorption of Au(III) by the composite membrane can also be demonstrated by XRD characterization. The XRD spectrum in **Fig. 5.16** shows four peaks at 2θ = 38.3, 44.5, 64.7, and 77.6° for the P3.5M0.5 membrane after Au(III) adsorption (line P3.5M0.5-Au), which is consistent with those described in the gold

standard card (JCPDS No. 04−0784). These peaks correspond to the crystal faces of elemental gold: (1 1 1), (2 0 0), (2 2 0), and (3 1 1) [53]. The average crystallite size of the Au particles from the XRD patterns can be calculated from the Debye–Scherrer equation: $d = (k\lambda/\beta\cos\theta)$, where d is the average crystallite size, λ is the wavelength of the Cu-Kα radiation (0.154 nm), β is the Full width at half maximum (FWHM) width of the diffraction peak, *and k* is the Scherrer constant, which depends on the broadening parameter, crystal shape, and symmetry and is generally considered to be equal to 0.94 [54]. Using the Debye-Scherrer equation and the four peaks at 2θ, the average crystallite size of the Au particles was calculated to be approximately 27.5 nm.

The full XPS profiles of the P3.5M0.5 membrane before and after Au(III) adsorption are shown in **Fig. 5.17**. Compared with spectrum of P3.5M0.5 (before adsorption), that of P3.5M0.5-Au exhibits dominant peaks of O 1s, N 1s, and C 1s, which are also characteristic of Au 4d, Cl 1p, and Au 4f, suggesting the adsorption of gold ions on the P3.5M0.5 membrane. The Au 4f spectrum has two adjacent peaks representing Au $4f_{7/2}$ and Au $4f_{5/2}$, and each of them can be well fitted by two other sub-peaks (**Fig. 5.17b**). The Au $4f_{7/2}$ peak is split into Au(0) (83.9 eV) and Au(III) (84.5 eV), whereas the Au $4f_{5/2}$ peak is split into Au(0) (87.6 eV) and Au(III) (88.3 eV). However, the Au(0) curves show a stronger intensity than the Au(III) curves. Combined with the characteristic peaks of Cl observed in the broad spectrum, it is confirmed that some gold ions are reduced to elemental gold and the others are captured in the $[AuCl_4]^-$ form. As reported, the N on PNPG was the main group for the redox reaction [35]. In **Fig. 5.17c**, the three sub-peaks of N 1s at 399.7, 400.9, and 402.3 eV are ascribed to the neutral benzenoid amine, conjugative protonated polaron, and bipolaron with a proportion of 76.65%, 19.56%, and 3.78%, respectively [35]. After Au(III) adsorption (**Fig. 5.17d**), the proportion of N in the benzenoid amine structure sharply decreases to 49.75%; however, that of the conjugative protonated polaron N increases to 46.94%. The content loss, which was approximately equal to the increment of the polaron, suggested that the N in the benzene ring units underwent oxidation to form the

conjugated polaron. In addition, these protonated polarons or bipolarons of N mainly combine with $[AuCl_4]^-$ through electrostatic interactions [55, 56].

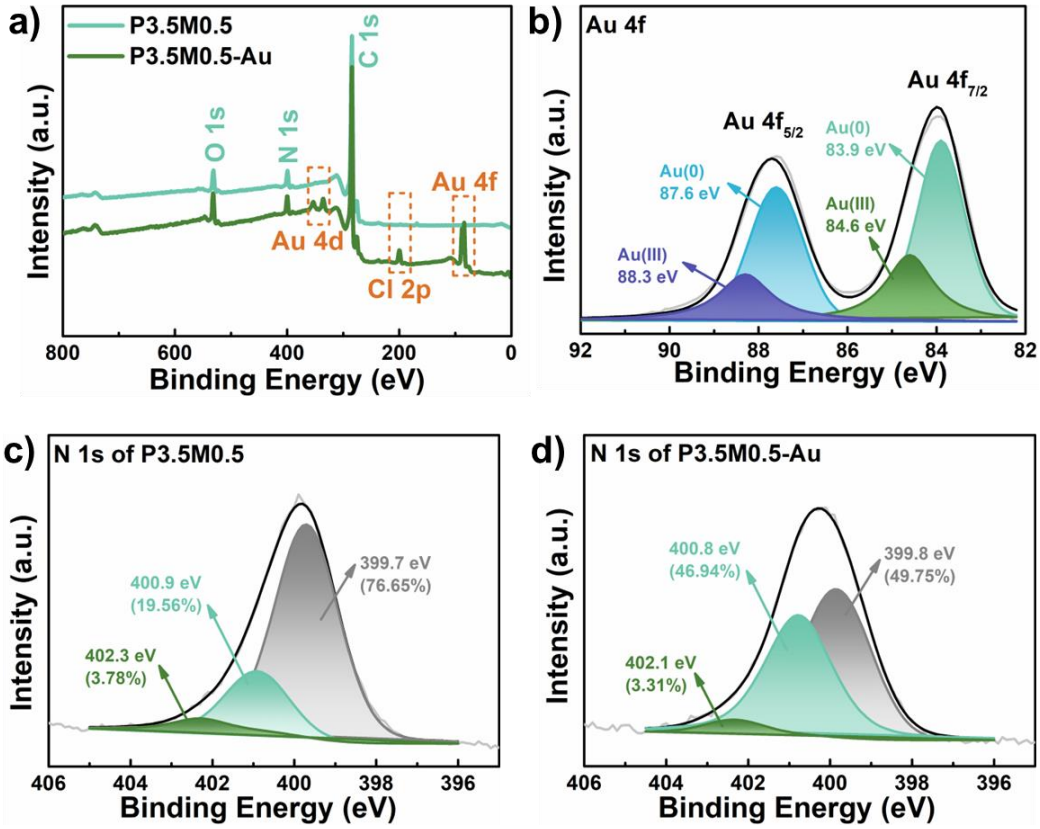

Fig. 5.17. (a) XPS profiles and the core-level spectra of the (b) Au 4f in P3.5M0.5-Au, (c) N 1s in P3.5M0.5, (d) N 1s in P3.5M0.5-Au.

Two main factors affect the adsorption performance of adsorbents: the physical properties (surface area, pore volume, and pore size) and surface chemical properties (functional groups and surface charge). **Table 5.5** lists information on the physical properties of the pure PNPG and P3.5M0.5 composite membranes. No significant changes are observed in the composite membrane, and thus the physical properties are not suitable to show the relationship between the adsorbent composition and corresponding improvement in adsorption capacity. Moreover, because of electrostatic interactions, PNPG and MWCNT combines more closely as the surface area decreases. From the aspect of chemical properties, PNPG is a conductive polymer with a structure similar to that of polyaniline, which can form more polarons and bipolarons when

functionalized by MWCNT through π-π interactions, thereby enhancing the electrical conductivity [30, 57]. The proportion of polarons in P3.5M0.5 (19.56%) is slightly higher than in the pure PNPG membrane (17.47%) (**Fig. 5.18a**). Besides, it has been reported that the addition of a small amount of MWCNT, making MWCNT randomly distributed, can play the role of a "conductive bridge", which may be caused by electron transfer from the conductive polymer to the carbon nanotubes [57]. In our study, SEM images and BET results prove that the distributed MWCNT made PNPG connect closer to each other, which ensures a more favorable electron transport, that is, the electrons on the internal adsorption site can be better transferred to the exterior to enable the reduction of Au(III). Even if the inner N of benzenoid amine is oxidized to quinone N due to the loss of electrons, the positively charged conjugated polaron can still be used as the active site for secondary adsorption by electrostatic interaction because the volume size of the ligand $[AuCl_4]^-$ is much smaller than that of the gold nanoparticles; otherwise, the adsorption is hindered as the Au particles had a larger crystallite size (calculated as 27.5 nm) than the pore diameter of the membranes (**Table 5.4**). However, this "conductive bridge" plays a promoting role rather than a decisive role in the adsorption; therefore, the Au(III) adsorption capacity decreases with increasing MWCNT proportion because adsorption mainly depends on PNPG.

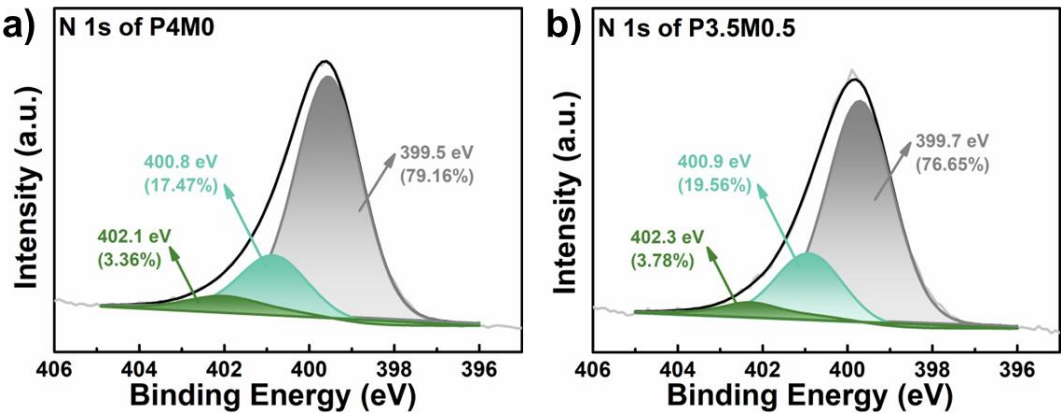

Fig. 5.18. XPS profiles of N 1s in (a) P4M0 and (b) P3.5M0.5 samples.

Table 5.5 Physical parameters of the P4M0 and P3.5M0.5 membranes.

Parameters	**P4M0**	**P3.5M0.5**
Surface area ($m^2\ g^{-1}$)	17.88	15.14
Pore Volume ($cm^3\ g^{-1}$)	0.026	0.021
Pore Diameter (nm)	15.08	15.21

5.3.8. Competition study

Index–selectivity is very important for evaluating the adsorption performance of adsorbent materials in multi-metal liquids, where the concentrations of ions are diverse. To study whether the P3.5M0.5 composite membrane has a selectivity for Au(III), the adsorption experiment of the competition study was carried out using three mixed solutions with different concentrations. The adsorption efficiency *E* of each metal was calculated using Eq. (11) [36]:

$$E = \frac{(c_0 - c_e)}{c_0} \times 100\% \tag{11}$$

In a binary mixture of the precious metals Au and Pt, the gold ions concentration was 5, 10, or 25 $mg{\cdot}L^{-1}$, and the platinum ion concentration was set at 50 $mg{\cdot}L^{-1}$. **Fig. 5.19a** shows that the adsorption efficiency of gold is 100%, whereas that of Pt is 30–35% for all Au–Pt mixtures with different concentrations. In another binary mixed solution of Au–Sn (**Fig. 5.19b**), whose initial concentrations were the same as those of the Au–Pt mixture, the P3.5M0.5 composite membrane also exhibits 100% adsorption of gold ions, but 6–11% Sn(II) is adsorbed. In the multi-metal mixed solutions (**Fig. 5.19c**), the adsorption efficiency of Au(III) is always the highest (100%), regardless of the harsh conditions, where the gold ions concentration was 5, 10, or 25 $mg{\cdot}L^{-1}$, when other base metal ions were controlled at 50 $mg{\cdot}L^{-1}$. It can be said that the P3.5M0.5 composite membrane is extremely selective for gold ions and displayed very little or no adsorption for coexisting metal ions of Al, Cd, Co, Cu, Fe, Ni, Pb, and Zn.

The relatively high selectivity of P3.5M0.5 for Au(III) can be explained in two ways. The first one is based on electrostatic interactions. In a solution of HCl with pH

1, Al, Cd, Co, Cu, Fe, Ni, Pb, and Zn mainly exist in the form of positive valence ions, while the main chemical forms of Au(III) and Pt(IV) are $[AuCl_4]^-$ and $[PtCl_6]^{2-}$, and Sn(II) can also form anionic complexes with Cl^- in such a strongly acidic solution [58, 59]. As shown in **Fig. 5.7**, the zeta potential of P3.5M0.5 at pH 1 is higher than 50 mV, which strongly repels the positively charged ions, but generates an electrostatic attraction toward the negatively charged species.

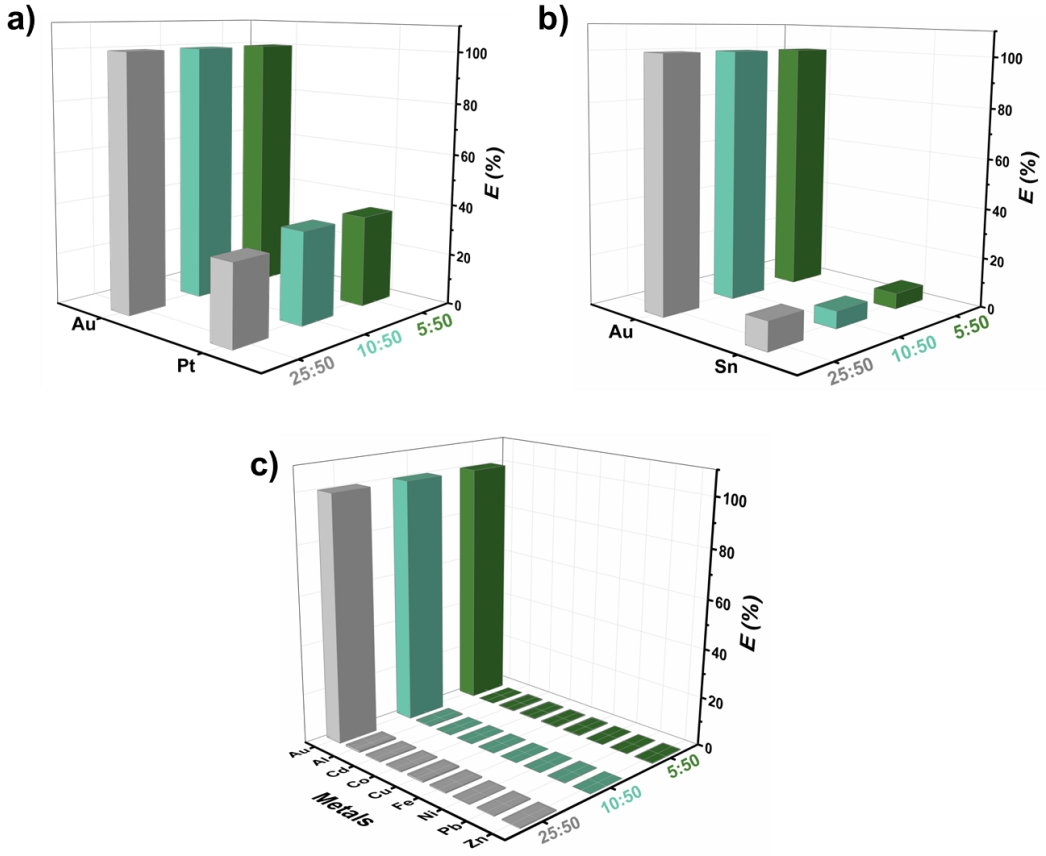

Fig. 5.19. Adsorption efficiency of metal ions in the (a) Au-Pt mixed solution, (b) Au-Sn mixed solution, and (c) multi-metal mixed solution. (x:50 signifies x $mg{\cdot}L^{-1}$ for Au versus 50 $mg{\cdot}L^{-1}$ for others)

Another explanation is the redox reaction. The standard electrode potential of $[AuCl_4]^-$ | Au (1.002 V) is much higher than that of Al^{3+} | Al (−1.662 V), Cd^{2+} | Cd (−0.403 V), Co^{2+} | Co (−0.28 V), Cu^{2+} | Cu (0.342 V), Fe^{3+} | Fe (−0.037 V), Ni^{2+} | Ni (−0.257 V), Pb^{2+} | Pb (−0.1263 V), Zn^{2+} | Zn (−0.7618 V), $[SnCl_4]^{2-}$ | Sn (−0.19 V), $[PtCl_6]^{2-}$ | $[PtCl_4]^{2-}$ (0.726 V), and $[PtCl_4]^{2-}$ | Pt (0.758 V), indicating that Au(III) is

more prone to undergo redox reactions with P3.5M0.5 than other metals ions. Although the standard electrode potential of $[PtCl_6]^{2-}$ | Pt has not been listed directly, there is a possibility for $[PtCl_6]^{2-}$ to become Pt(0) based on a previous study on a similar-structured adsorbent, poly(*m*-aminobenzoic acid), that captured Pt (IV) only through ionic interactions at pH < 3.5 [58]. Consequently, the P3.5M0.5 composite membrane demonstrates a good selectivity for the adsorption of Au(III).

5.3.9. Stability and Reusability study

Good stability indicates a potential practical application. A self-made device was prepared to test the stability of pure PNPG membrane (P4M0) and P3.5M0.5 composite membrane by making 100 mL DI water fall freely from the separatory funnel to scour the membrane surface at a height of 40 cm (**Fig. 5.20**). From the photographs taken before and after observation, it is obvious that the loaded adsorbent in the P4M0 membrane detached, while the P3.5M0.5 composite membrane is still in perfect condition. Considering that the purpose of converting nano-adsorbents into films is to reduce the separation burden of the adsorbent after adsorption, it can be achieved if the adsorbent is firmly attached to the supporting layer without shedding. Therefore, the P3.5M0.5 composite membrane is more stable and exhibits greater practical application value than the pure PNPG membrane.

The desirable property of reusability means that the adsorbent material can be used in multiple adsorption cycles to reduce the treatment cost [60]. As shown in **Fig. 5.21**, although the adsorption efficiency slightly decreases after the first three cycles, it remains above 95%. The adsorption efficiency in the fourth round decreased to 90.5%. The main reason for this downward trend is that the occupied adsorption sites are not released. The P3.5M0.5 composite membrane can be recycled for at least four rounds, and the adsorption efficiency generally remained above 90%, indicating that the P3.5M0.5 composite membrane possessed good reusability.

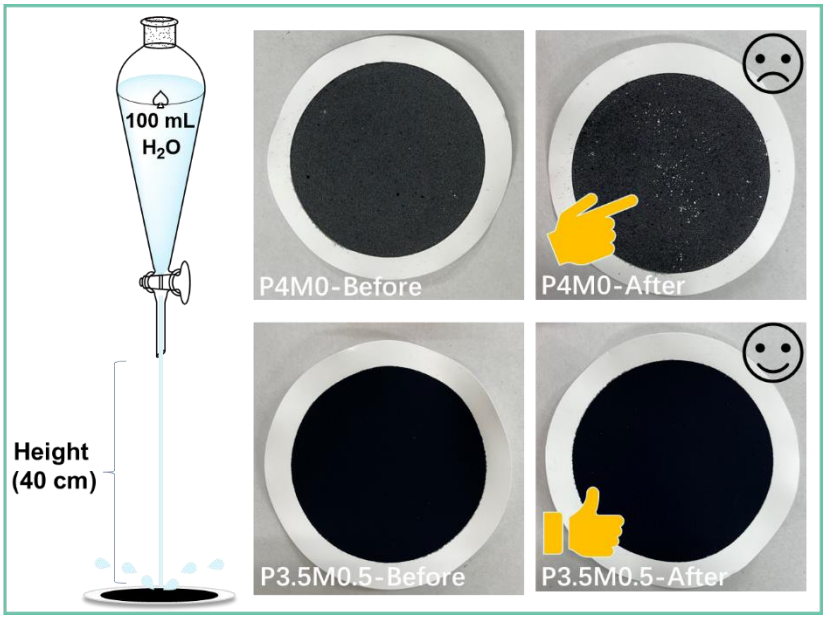

Fig. 5.20. Schematic diagram of membrane stability test and digital photos of membranes before and after washing.

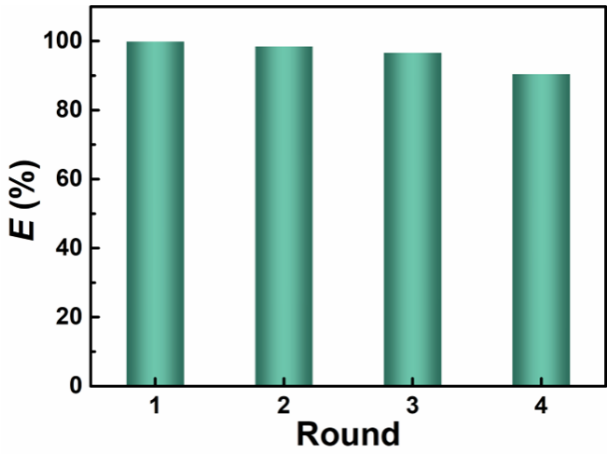

Fig. 5.21. Adsorption efficiency of Au(III) in consecutive rounds.

5.3.10. Recovery of Au from the actual solution

To further evaluate the practical application of the P3.5M0.5 composite membrane for gold recovery, a leaching solution of PCBs of waste computers was selected as a representative. The leaching solution was prepared as described in Section 5.2.5. The initial and residual concentrations of the metal ions in the leaching solution are shown in **Fig. 5.22**, along with the calculated adsorption efficiencies. The adsorption efficiency of Au(III) is the highest, up to 100%. This result indicates that the P3.5M0.5 composite

membrane can efficiently capture Au(III) from the e-waste leaching solution, showing good practical application prospects. Because the gold ions content is very low, the P3.5M0.5 composite membrane captures all the Au(III) and still has numerous adsorption sites available for the adsorption of 5% Sn. This suggests that Sn and other base metal ions should first be removed as much as possible from the leachate to maximize the utilization of the P3.5M0.5 composite membrane for Au(III).

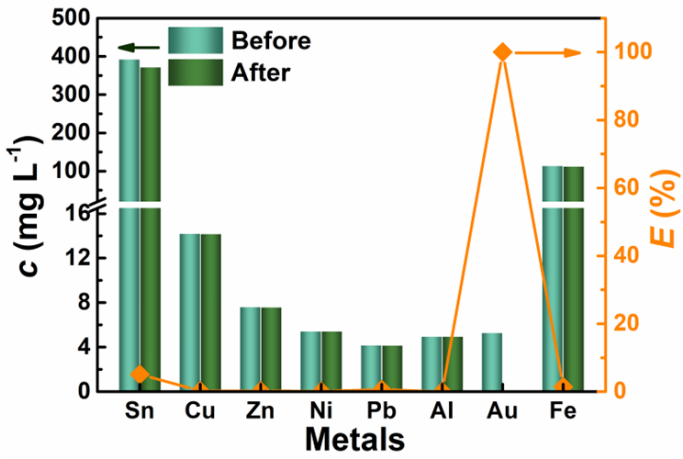

Fig. 5.22. Concentration of metal ions in actual leaching solution before and after adsorption, and the corresponding adsorption efficiency.

5.4. Conclusion

In summary, XRD, FTIR, and SEM characterization confirmed the synthesis of the PNPG@MWCNT composite membrane. The Au(III) adsorption capacity of the as-prepared composite membrane varied with the change in the compositions of PNPG and MWCNT; the P3.5M0.5 composite membrane showed the highest adsorption capacity of 1262.6 $mg \cdot g^{-1}$ at pH 1, which was approximately 20% higher than that of the pure PNPG membrane. The Au(III) adsorption process was well fitted by the PSO kinetic model and Langmuir isotherm model, suggesting that it was mainly chemisorption and monolayer adsorption. The adsorption proceeded spontaneously and endothermically, as confirmed by the negative ΔG and positive ΔH values. The SEM, FTIR, XPS, and other characterization results showed that the Au(III) adsorption mechanism of the composite membrane included redox reactions as well as electrostatic

interactions. Moreover, the P3.5M0.5 composite membrane was extremely selective for gold ions in the solution of multi-metal ions, exhibited good stability and reusability, and could efficiently capture Au(III) from the e-waste leaching solution. The combination of MWCNT and PNPG via non-covalent interactions not only alleviated the PNPG cracks and enhanced the stability of the membrane but also improved the Au(III) adsorption performance by fully utilizing the inner adsorption sites through the transfer of electrons from PNPG to MWCNT. The PNPG@MWCNT composite membrane showed good prospects for practical application in gold recovery.

Reference

[1] UN, Department of economic and social affairs sustainable development, (2015). https://sdgs.un.org/goals/goal6 and https://sdgs.un.org/goals/goal12.

[2] Y. Zhou, W.B. Li, V. Kumar, et al., Synthetic organic antibiotics residues as emerging contaminants waste-to-resources processing for a circular economy in china: Challenges and perspective, Environ. Res., 211 (2022) 113075. https://doi.org/10.1016/j.envres.2022.113075.

[3] G. Alam, I. Ihsanullah, M. Naushad, et al., Applications of artificial intelligence in water treatment for optimization and automation of adsorption processes: Recent advances and prospects, Chem. Eng. J., 427 (2022) 130011. https://doi.org/10.1016/j.cej.2021.130011.

[4] Y. Yuan, J. Liu, B. Gao, et al., Landfill leachate treatment in-depth by bio-chemical strategy: Microbial activation and catalytic ozonation mechanism, Chem. Eng. J., 444 (2022) 136464. https://doi.org/10.1016/j.cej.2022.136464.

[5] Y. Naciri, A. Hsini, A. Ahdour, et al., Recent advances of bismuth titanate based photocatalysts engineering for enhanced organic contaminates oxidation in water: A review, Chemosphere, 300 (2022) 134622. https://doi.org/10.1016/j.chemosphere.2022.134622.

[6] R. Vinayagam, N. Dave, T. Varadavenkatesan, et al., Artificial neural network and statistical modelling of biosorptive removal of hexavalent chromium using macroalgal spent biomass, Chemosphere, 296 (2022) 133965. https://doi.org/10.1016/j.chemosphere.2022.133965.

[7] R. Ciriminna, E. Falletta, C. Della Pina, et al., Industrial applications of gold catalysis, Angew. Chem. Int. Ed., 55 (2016) 14210-14217. https://doi.org/10.1002/anie.201604656.

[8] X. Yang, M. Yang, B. Pang, et al., Gold nanomaterials at work in biomedicine, Chem. Rev., 115 (2015) 10410-10488. https://doi.org/10.1021/acs.chemrev.5b00193.

[9] H.W. Tan, J. An, C.K. Chua, et al., Metallic nanoparticle inks for 3D printing

of electronics, Adv. Electron. Mater., 5 (2019) 1800831. https://doi.org/10.1002/aelm.201800831.

[10] A. Kumar, M. Holuszko, D.C.R. Espinosa, E-waste: An overview on generation, collection, legislation and recycling practices, Resour. Conserv. Recycl., 122 (2017) 32-42. https://doi.org/10.1016/j.resconrec.2017.01.018.

[11] S. Krishnan, N.S. Zulkapli, H. Kamyab, et al., Current technologies for recovery of metals from industrial wastes: An overview, Environ. Technol. Innov., 22 (2021) 101525. https://doi.org/10.1016/j.eti.2021.101525.

[12] F. Fu, Q. Wang, Removal of heavy metal ions from wastewaters: A review, J. Environ. Manage., 92 (2011) 407-418. https://doi.org/10.1016/j.jenvman.2010.11.011.

[13] A. Taghizadeh, M. Taghizadeh, M. Jouyandeh, et al., Conductive polymers in water treatment: A review, J. Mol. Liq., 312 (2020) 113447. https://doi.org/10.1016/j.molliq.2020.113447.

[14] T. Mahlangu, R. Das, L.K. Abia, et al., Thiol-modified magnetic polypyrrole nanocomposite: An effective adsorbent for the adsorption of silver ions from aqueous solution and subsequent water disinfection by silver-laden nanocomposite, Chem. Eng. J., 360 (2019) 423-434. https://doi.org/10.1016/j.cej.2018.11.231.

[15] C. Wang, J. Zhao, S. Wang, et al., Efficient and selective adsorption of gold ions from wastewater with polyaniline modified by trimethyl phosphate: Adsorption mechanism and application, Polymers, 11 (2019) 652. https://doi.org/10.3390/polym11040652.

[16] C. Mu, L. Zhang, X. Zhang, et al., Selective adsorption of Ag (I) from aqueous solutions using Chitosan/polydopamine@C@magnetic fly ash adsorbent beads, J. Hazard. Mater., 381 (2020) 120943. https://doi.org/10.1016/j.jhazmat.2019.120943.

[17] T. Wu, Z. Lin, H. Wu, et al., Adsorption studies on Ag(I) using poly(N-phenylglycine) membrane and application in practical silver recycling, ACS Appl.

Polym. Mater., 4 (2022) 3333-3342. https://doi.org/10.1021/acsapm.1c01901.

[18] T. Wu, Z. Lin, H. Wu, et al., Selective and sensitive adsorption of Au(III) by poly-N-phenylglycine, Sep. Purif. Technol., 287 (2022) 120604. https://doi.org/10.1016/j.seppur.2022.120604.

[19] M.B. Asif, S. Iftekhar, T. Maqbool, et al., Two-dimensional nanoporous and lamellar membranes for water purification: Reality or a myth?, Chem. Eng. J., 432 (2022) 134335. https://doi.org/10.1016/j.cej.2021.134335.

[20] M.R. Ardani, A.L. Pang, U. Pal, et al., Ultrasonic-assisted polyaniline-multiwall carbon nanotube photocatalyst for efficient photodegradation of organic pollutants, J. Water Process. Eng., 46 (2022) 102557. https://doi.org/10.1016/j.jwpe.2021.102557.

[21] P. Shandilya, P. Mandyal, V. Kumar, et al., Properties, synthesis, and recent advancement in photocatalytic applications of graphdiyne: A review, Sep. Purif. Technol., 281 (2022) 119825. https://doi.org/10.1016/j.seppur.2021.119825.

[22] R. Benda, G. Zucchi, E. Cancès, et al., Insights into the $\pi - \pi$ interaction driven non-covalent functionalization of carbon nanotubes of various diameters by conjugated fluorene and carbazole copolymers, J. Chem. Phys., 152 (2020) 064708. https://doi.org/10.1063/1.5133634.

[23] Z. Lin, T. Wu, Y.-F. Feng, et al., Poly(N-phenylglycine)/MoS_2 nanohybrid with synergistic solar-thermal conversion for efficient water purification and thermoelectric power generation, ACS Appl. Mater. Interfaces, 14 (2022) 1034-1044. https://doi.org/10.1021/acsami.1c20393.

[24] M. Zhao, Z. Huang, S. Wang, et al., Ultrahigh efficient and selective adsorption of Au(III) from water by novel chitosan-coated mos2 biosorbents: Performance and mechanisms, Chem. Eng. J., 401 (2020) 126006. https://doi.org/10.1016/j.cej.2020.126006.

[25] C.E. Kozonoe, R. Giudici, M. Schmal, Ruthenium catalyst supported on multi-walled carbon nanotubes for co oxidation, Modern Research in Catalysis, 10 (2021)

73-91. https://doi.org/10.4236/mrc.2021.103005.

[26] D. Calle, V. Negri, C. Munuera, et al., Magnetic anisotropy of functionalized multi-walled carbon nanotube suspensions, Carbon, 131 (2018) 229-237. https://doi.org/10.1016/j.carbon.2018.01.104.

[27] Z. Lin, T. Wu, J. Shi, et al., Poly(N-phenylglycine)-based bioinspired system for stably and efficiently enhancing solar evaporation, ACS Sustainable Chem. Eng., 9 (2021) 448-457. https://doi.org/10.1021/acssuschemeng.0c07608.

[28] M. Ben Ali, F. Wang, R. Boukherroub, et al., High performance of phytic acid-functionalized spherical poly-phenylglycine particles for removal of heavy metal ions, Appl. Surf. Sci., 518 (2020) 146206-146213. https://doi.org/10.1016/j.apsusc.2020.146206.

[29] J.H. Doh, J.H. Kim, H.J. Kim, et al., Enhanced adsorption of aqueous copper(II) ions using dedoped poly-N-phenylglycine nanofibers, Chem. Eng. J., 277 (2015) 352-359. http://dx.doi.org/10.1016/j.cej.2015.04.120.

[30] H.K. Rasheed, A.A. Kareem, Effect of multiwalled carbon nanotube reinforcement on the opto-electronic properties of polyaniline/c-si heterojunction, J. Opt. Commun., 42 (2021) 25-29. https://doi.org/10.1515/joc-2018-0024.

[31] W.P. Lee, A.F. Routh, Why do drying films crack?, Langmuir, 20 (2004) 9885-9888. https://doi.org/10.1021/la049020v.

[32] H.J. Kim, S. Im, J.C. Kim, et al., Phytic acid doped polyaniline nanofibers for enhanced aqueous copper(II) adsorption capability, ACS Sustainable Chem. Eng., 5 (2017) 6654-6664. https://doi.org/10.1021/acssuschemeng.7b00898.

[33] R. Li, C. Zhou, L. Yang, et al., Multifunctional cotton with PANI-Ag NPs heterojunction for solar-driven water evaporation, J. Hazard. Mater., 424 (2022) 127367. https://doi.org/10.1016/j.jhazmat.2021.127367.

[34] M. Dong, J. Guo, Y. Wang, et al., Humic acid non-covalent functionalized multi-walled carbon nanotubes composite membrane and its application for the removal of organic dyes, J. Environ. Chem. Eng., 10 (2022) 107320. https://doi.org/1

0.1016/j.jece.2022.107320.

[35] V.K.A. Muniraj, R. Boukherroub, M.V. Shelke, Flexible energy storage device based on poly(N-phenylglycine), an incentive-energy pseudocapacitive conducting polymer, and electrochemically exfoliated graphite sheets, ACS Sustainable Chem. Eng., 8 (2020) 6433-6441. https://doi.org/10.1021/acssuschemeng.0c00880.

[36] Y. Geng, J. Li, W. Lu, et al., Au(III), Pd(II) and Pt(IV) adsorption on amino-functionalized magnetic sorbents: Behaviors and cycling separation routines, Chem. Eng. J., 381 (2020) 122627. https://doi.org/10.1016/j.cej.2019.122627.

[37] F. Liu, Z. Zhou, G. Li, Persimmon tannin functionalized polyacrylonitrile fiber for highly efficient and selective recovery of Au(III) from aqueous solution, Chemosphere, 264 (2021) 128469. https://doi.org/10.1016/j.chemosphere.2020.128469.

[38] S. Wadhawan, A. Jain, J. Nayyar, et al., Role of nanomaterials as adsorbents in heavy metal ion removal from waste water: A review, J. Water Process. Eng., 33 (2020) 101038-101054. https://doi.org/10.1016/j.jwpe.2019.101038.

[39] F.-C. Wu, R.-L. Tseng, R.-S. Juang, Initial behavior of intraparticle diffusion model used in the description of adsorption kinetics, Chem. Eng. J., 153 (2009) 1-8. https://doi.org/10.1016/j.cej.2009.04.042.

[40] L. Wang, K. Wang, R. Huang, et al., Hierarchically flower-like WS_2 microcrystals for capture and recovery of Au(III), Ag(I) and Pd(II), Chemosphere, 252 (2020) 126578. https://doi.org/10.1016/j.chemosphere.2020.126578.

[41] E.D. Revellame, D.L. Fortela, W. Sharp, et al., Adsorption kinetic modeling using pseudo-first order and pseudo-second order rate laws: A review, Clean. Eng. Technol., 1 (2020) 100032. https://doi.org/10.1016/j.clet.2020.100032.

[42] B. Zhang, S. Wang, L. Fu, et al., Selective high capacity adsorption of Au(III) from aqueous solution by poly(glycidyl methacrylate) functionalized with 2,6-diaminopyridine, Polym. Bull., 76 (2019) 4017-4033. https://doi.org/10.1007/s00

289-018-2594-5.

[43] L.F. Villalobos, T. Yapici, K.-V. Peinemann, Poly-thiosemicarbazide membrane for gold recovery, Sep. Purif. Technol., 136 (2014) 94-104. https://doi.org/10.1016/j.seppur.2014.08.027.

[44] H. Li, X. Wang, L. Cao, et al., Gold-recovery pvdf membrane functionalized with thiosemicarbazide, Chem. Eng. J., 280 (2015) 399-408. https://doi.org/10.1016/j.cej.2015.06.021.

[45] F. Rodríguez, M.M. Castillo-Ortega, J.C. Encinas, et al., Adsorption of a gold -iodide complex (AuI_2^-) onto cellulose acetate-polyaniline membranes: Equilibrium experiments, J. Appl. Polym. Sci., 113 (2009) 2670-2674. https://doi.org/10.1002/app.30337.

[46] X. Wang, J. Xu, L. Li, et al., Thiourea grafted pvdf affinity membrane with narrow pore size distribution for Au(III) adsorption: Preparation, characterization, performance investigation and modeling, Chem. Eng. J., 314 (2017) 700-713. https://doi.org/10.1016/j.cej.2016.12.035.

[47] X. Zhang, H. Li, M. Ye, et al., Bacterial cellulose hybrid membrane grafted with high ratio of adipic dihydrazide for highly efficient and selective recovery of gold from e-waste, Sep. Purif. Technol., 292 (2022) 121021. https://doi.org/10.1016/j.seppur.2022.121021.

[48] Y. Chen, L. Jiang, A core–shell amidoxime electrospun nanofiber affinity membrane for rapid recovery Au(III) from water, Chin. J. Chem. Eng., 42 (2022) 424-436. https://doi.org/10.1016/j.cjche.2021.08.021.

[49] T. Chen, T. Da, Y. Ma, Reasonable calculation of the thermodynamic parameters from adsorption equilibrium constant, J. Mol. Liq., 322 (2021) 114980. https://doi.org/10.1016/j.molliq.2020.114980.

[50] P.B. Vilela, C.A. Matias, A. Dalalibera, et al., Polyacrylic acid-based and chitosan-based hydrogels for adsorption of cadmium: Equilibrium isotherm, kinetic and thermodynamic studies, J. Environ. Chem. Eng., 7 (2019) 103327. https://doi.

org/10.1016/j.jece.2019.103327.

[51] N.F. Abd Razak, M. Shamsuddin, S.L. Lee, Adsorption kinetics and thermodynamics studies of gold(III) ions using thioctic acid functionalized silica coated magnetite nanoparticles, Chem. Eng. Res. Des., 130 (2018) 18-28. https://doi.org/10.1016/j.cherd.2017.12.004.

[52] Y. Chen, Z. Li, R. Ding, et al., Construction of porphyrin and viologen-linked cationic porous organic polymer for efficient and selective gold recovery, J. Hazard. Mater., 426 (2022) 128073. https://doi.org/10.1016/j.jhazmat.2021.128073.

[53] C. Wang, R. Cheng, P.-X. Hou, et al., Mxene-carbon nanotube hybrid membrane for robust recovery of Au from trace-level solution, ACS Appl. Mater. Interfaces, 12 (2020) 43032-43041. https://doi.org/10.1021/acsami.0c09310.

[54] K. Nitta, K. Ishizumi, Y. Shimizu, et al., One-step gold line fabrication from particle-free inorganic salt-based ink via atmospheric pressure nonequilibrium plasma-assisted inkjet printing, Mater. Chem. Phys., 258 (2021) 123836. https://doi.org/10.1016/j.matchemphys.2020.123836.

[55] S. Bhattarai, J.S. Kim, Y.-S. Yun, et al., Preparation of polyaniline-coated polystyrene nanoparticles for the sorption of silver ions, React. Funct. Polym., 105 (2016) 52-59. https://doi.org/10.1016/j.reactfunctpolym.2016.05.013.

[56] K.Z. Elwakeel, A.S. Al-Bogami, E. Guibal, 2-mercaptobenzimidazole derivative of chitosan for silver sorption – Contribution of magnetite incorporation and sonication effects on enhanced metal recovery, Chem. Eng. J., 403 (2021) 126265. https://doi.org/10.1016/j.cej.2020.126265.

[57] C. Oueiny, S. Berlioz, F.-X. Perrin, Carbon nanotube–polyaniline composites, Prog. Polym. Sci., 39 (2014) 707-748. https://doi.org/10.1016/j.progpolymsci.2013.08.009.

[58] T. Öztürk, M. Gülfen, A. Özdemir, Sorption of Pt(IV) ions on poly(*m*-aminobenzoic acid) chelating polymer: Equilibrium, kinetic and thermodynamic

studies, SN Appl. Sci., 2 (2020) 1886. https://doi.org/10.1007/s42452-020-03692-0.

[59] E. Lakay, S. Hermans, K. Koch, et al., The efficient recovery of Au(III) ions from acidic solutions by a novel scavenger based on functionalized poly(styrene-co-maleimide) nanoparticles, Chem. Eng. J., 414 (2021) 128761. https://doi.org/10.1016/j.cej.2021.128761.

[60] M.A.H. Badsha, M. Khan, B. Wu, et al., Role of surface functional groups of hydrogels in metal adsorption: From performance to mechanism, J. Hazard. Mater., 408 (2021) 124463-124485. https://doi.org/10.1016/j.jhazmat.2020.124463.

Chapter 6

General Conclusion and Outlook

As non-renewable resources, demand and consumption of precious metals (PMs) are increasing year by year, drawing more and more attention to the recovery from secondary resources. Compared with primary metal resources such as ores, secondary metal resources such as e-waste contain various fractions of metals with high grades. Industrially, pyrometallurgy, hydrometallurgy, or a combination of all routes are used for recovering PMs from e-waste. Appropriate hydrometallurgical techniques/methods can lead to an excellent future for gold and silver recovery with decreased environmental pollution. Adsorption is an effective and promising method to isolate and separate PMs ions from aqueous solution, and the development and utilization of nanomaterials for PMs recycling are consequently attracting tremendous interest.

In this research, the latest developments in PNPG-based adsorbents for PMs recovery have been presented. Firstly, it has been demonstrated that the nanoscale PNPG particles have a good adsorption ability towards gold ions, but their nanoscale structure complicate the separation of PNPG after adsorption. To address this issue, we proposed a strategy method based on the PNPG membrane, which can facilitate rapid adsorbent separation after adsorption. Subsequently, the adsorption mechanism towards gold and silver ions were elaborated with the aid of a series of characterization methods. The PNPG-based adsorbents have a good adsorption effect on gold ions and silver ions, and the adsorption process were well-fitted with the PSO and Langmuir model which means the chemisorption and monolayer adsorption were dominant. Mechanisms of Au(III) and Ag(I) adsorption by PNPG-based materials included physical adsorption (i.e. electrostatic interaction), and chemical adsorption (i.e. coordination and reduction) which mainly occurs in N-containing groups. Furthermore, we developed PNPG@MWCNT composite membranes for solving the crack problem of pure PNPG membrane when PNPG load increases. The experimental results showed that the cracks were repaired and the stability of PNPG@MWCNT composite membranes were better,

thus improving its practical application possibility. Moreover, the composite membrane with optimal mass ratio can improve the adsorption capacity of gold ions, compared with pure PNPG membrane. These PNPG-based adsorbents also showed good adsorption effects of gold and silver ions in both experimental mixed solutions and real leaching solutions of waste PCBs and MSWI fly ash, indicating the possibility of practical application in metals recovery.

In most cases, the adsorption process is complicated, and so is the actual metal recovery work. Conclusively, more efforts still need to be put into promoting the large-scale and industrial-scale utilization of PNPG-based adsorbents in the field of PMs recovery.

List of publication

1. Periodical papers

[1] **Tingting Wu**, Zhaoxing Lin, Hongyi Wu, Chunhong Zhu, Takao Komiyama, Jian Shi, Ruilu Liang, Selective and sensitive adsorption of Au(III) by poly-N-phenylglycine, Separation and Purification Technology, 287 (2022) 120604. https://doi.org/10.1016/j.seppur.2022.120604 (IF=9.136)

[2] **Tingting Wu**, Zhaoxing Lin, Hongyi Wu, Mingxu Wang, Chunhong Zhu, Nobuhiro Kanazawa, Jian Shi, Ruilu Liang, Adsorption studies on Ag(I) using poly(N-phenylglycine) membrane and application in practical silver recycling, ACS Applied Polymer Materials, 4 (2022) 3333-3342. https://doi.org/10.1021/acsapm.1c01901 (IF=4.855)

[3] **Tingting Wu**, Zhaoxing Lin, Yi Zhang, Nobuhiro Kanazawa, Takao Komiyama, Chunhong Zhu, Eiji Kikuchi, Jian Shi, Ruilu Liang, Poly-N-phenylglycine@ multi-walled carbon nanotubes composite membrane for improvement of Au(III) adsorption, Separation and Purification Technology, 304 (2023) 122404. https://doi.org/10.1016/j.seppur.2022.122404 (IF=9.136)

[4] Zhaoxing Lin, **Tingting Wu**, Jian Shi, Bo Zhou, Chunhong Zhu, Yiyu Wang, Ruilu Liang, Mamoru Mizuno, Poly(N-phenylglycine)-based bioinspired system for stably and efficiently enhancing solar evaporation, ACS Sustainable Chemistry & Engineering, 9 (2021) 448-457. https://doi.org/10.1021/acssuschemeng.0c07608 (IF=9.224)

[5] Zhaoxing Lin, **Tingting Wu**, Yan-Fang Feng, Jian Shi, Bo Zhou, Chunhong Zhu, Yiyu Wang, Ruilu Liang, Mamoru Mizuno, Poly(N-phenylglycine)/MoS_2 nanohybrid with synergistic solar-thermal conversion for efficient water purification and thermoelectric power generation, ACS Applied Materials and Interfaces, 14 (2022) 1034-1044. https://doi.org/10.1021/acsami.1c20393 (IF=10.383)

[6] Zhaoxing Lin, **Tingting Wu**, Benxu Jia, Jian Shi, Bo Zhou, Chunhong Zhu, Yiyu Wang, Ruilu Liang, Mamoru Mizuno, Nature-inspired poly(N-phenylglycine)/wood solar evaporation system for high-efficiency desalination and water purification, Colloids and Surfaces A: Physicochemical and Engine ering Aspects, 637 (2022) 128272-128280. https://doi.org/10.1016/j.colsurfa.2022.128272 (IF=5.518)

Note: Doctoral dissertation related: 3 papers ([1]–[3]), others: 3 papers ([4] ~ [6])

2. Conference

[1] **呉 婷婷**, 林 肇星, 梁 瑞録: The Adsorption Mechanism between Conductive Polymer Poly-N-phenylglycine on Ag ions and Recovery of Silver (導電性高分子ポリ-N-フェニルグリシンへの Ag イオン吸着機構と銀の回収), 一般社団法人資源・素材学会(2022 年 3 月), オンライン

[2] **呉 婷婷**, 林 肇星, 梁 瑞録: Poly-N-phenylglycine Membrane for Recovery of Au from Trace-Level Solution (ポリ-N-フェニルグリシン（PNPG）吸着剤の開発), 一般社団法人資源・素材学会(2021 年 3 月), オンライン

[3] 梁 瑞録, **呉 婷婷**: Effect of Ultrasonication on Leaching of Metal (超音波援用による浸出への影響), 一般社団法人資源・素材学会(2022 年 3 月), オンライン

[4] 劉 怡萱, 倉嶌 佑之介, **呉 婷婷**, 梁 瑞録: Study on ultrasound-assisted leaching (超音波を援用した浸出に関する研究), 一般社団法人資源・素材学会(2021 年 3 月), オンライン

[5] 林 肇星, **呉 婷婷**, 施 建, 水野 衛: Poly(N-phenylglycine)-based photothermal membrane system for stably solar evaporation, 日本繊維学会秋季研究発表会(2021 年 11 月), オンライン

Acknowledgments

I have had a wonderful time doing my Ph.D. at Akita Prefectural University (APU) and I would therefore like to give my heartfelt thanks to everyone who helped make it such an exciting experience that I will never forget.

First and foremost, I would like to thank the following people for their support in my research.

I would like to thank my supervisor, Prof. Ruilu Liang, for giving me this incredible opportunity, for supporting me throughout the whole process, and for having faith in my abilities and ideas. Considering that I majored in chemistry for both my undergraduate and master's degrees and have little knowledge about the field of recycling, Prof. Liang often spent hours patiently teaching me and broadening my knowledge of this field. I also want to thank Prof. Jian Shi, who played the same role as my supervisor and trained my logical thinking in writing, summarizing, and so on. Both teachers are like my friends comforting me when I was upset and giving me the courage to overcome difficulties in my study. They are constant cheerleaders, mentors, and motivators, and they continually teach me how to be a better researcher. I am thankful to them from the bottom of my heart. In addition, I would also like to express my heartfelt gratitude to my deputy supervisor, Prof. Eiji Kikuchi. He not only gave me the opportunity to pursue a Ph.D. at APU but also selflessly provided me with experimental resources and reviewed my articles.

The completion of this research is also inseparable from the generous help of Prof. Nobuhiro Kanazawa, Assistant Prof. Takao Komiyama, Prof. Teruo Bitoh, Prof. Hiroto Kawashima, and Prof. Chunhong Zhu (Shinshu University), Prof. Atsushi Shibayama (Akita University). I am deeply grateful for their equipment, resources, and technical assistance. I am also thankful to my master's supervisor, Prof. Shichen Ji (Guangxi Normal University), who recommended me to apply for a Ph.D. at APU. Although I have not continued the research of theoretical simulation of polymer, I still benefit from the ability and knowledge I have learned from him.

In addition, I am also thankful to everyone who helped me during my Ph.D., either

through direct collaboration, ideas inspiration, or providing useful advice and teaching me experimental methods. On that note, I would like to thank Dr. Hongyi Wu (Shinshu University), Dr. Mingxu Wang (Shinshu University), Dr. Yi Zhang (Shinshu University), Dr. Zhaoxing Lin, Dr. Qifan Liu, Dr. Chunyin Lu, Dr. Manxi Sun, Dr. Hongjian Huang, Dr. Haodao Mo, and Dr. Wei Zhao. I am also deeply indebted to the Japan Society for the Promotion of Science (Grant No. 19 K12402) for funding this Ph.D. project, and the Editage group for proofreading three research articles.

Secondly, I would like to thank those people who have stood behind me and raised me up all the time.

I am very grateful to my parents, younger brother, and uncle, who resisted the opposition from relatives and supported me to study for a Ph.D. in Japan which is thousands of miles away from my hometown. How fortunate I am to have such a family supporting me to do what I want to do. When my parents were at the hospital or my family was in difficulties, I was very sad because I could not go back to help them, as it became costlier, more difficult, and more time-consuming to return home in the past three years. Thanks to the care and help from my brother and uncle, my parents were healed and my family overcome the difficulties, so that I could focus on my study. I am extremely grateful for everything they do for me. I also want to thank my boyfriend Zhaoxing Lin for giving me company, support, and encouragement over the years from our master to doctorate.

I wish to express my gratitude to those friends for their kindness and assistance: Xin Fang, Cheng Hang, Qifan Liu, Chunyin Lu, Manxi Sun, Hongjian Huang, Haodao Mo, Wei Zhao, Andong Pan, Haonan Wu, and other fellow international students in APU. Besides, I would like to thank Japan Educational Exchanges and Services for the scholarship support, which has reduced my financial burden and mental burden, allowing me to focus on study. I am also very grateful for the inspiration of JJ Lin's songs, and the warm company of two lovely dogs – Haki and Woody.

Thirdly, I want to thank the people and things I met in Japan during these three years. There are not only experiments or research, but also many interesting activities and cultural events which enrich my life and heart. I am really thankful for their

kindness and help with language and life when I'm in a foreign country, and I will miss Ms. Miwa Sasaki, Mrs. Eiko Fujishima, Mrs. Shuku Miya, Mrs. Chika Furukawa, Mr. Masumi Hashimoto, Ms. Saki Tanaka, all members of the Liang group, all the Japanese teachers in Yurihonjo City Culture Center KADARE, and all teachers and staff members in Akita Prefectural University.

Last but not least, I would like to express my gratitude to all the members of the Thesis Defense Committee for their valuable time and generous constructive suggestions for the completion of this thesis.

Sincerely

Tingting Wu

Yurihonjo, Akita, Japan

2023.03